# Rapid Cell Growth Regulation in Arabidopsis

by

**Lanxin Li**

Oct, 2021

*A thesis submitted to the*
*Graduate School*
*Institute of Science and Technology Austria*
*in partial fulfillment of the requirements*
*for the degree of*
*Doctor of Philosophy*

The thesis of Lanxin Li, titled *Rapid Cell Growth Regulation in Arabidopsis*, is approved by:

**Supervisor**: Jiří Friml, IST Austria, Klosterneuburg, Austria

Signature: _____

**Committee Member**: Eva Benková, IST Austria, Klosterneuburg, Austria

Signature: _____

**Committee Member**: Stefan Kepinski, University of Leeds, Leeds, England

Signature: _____

**Exam Chair**: Martin Loose, IST Austria, Klosterneuburg, Austria

Signature: _____

Signed page is on file

IST Austria Thesis, ISSN: 2663-337X

I hereby declare that this dissertation is my own work and that it does not contain other people's work without this being so stated; this thesis does not contain my previous work without this being stated, and the bibliography contains all the literature that I used in writing the dissertation.

I declare that this is a true copy of my thesis, including any final revisions, as approved by my thesis committee, and that this thesis has not been submitted for a higher degree to any other university or institution.

I certify that any republication of materials presented in this thesis has been approved by the relevant publishers and co-authors.

Signature: _____

Lanxin Li

October 14, 2021

Signed page is on file

# Abstract

Plant motions occur across a wide spectrum of timescales, ranging from seed dispersal through bursting (milliseconds) and stomatal opening (minutes) to long-term adaptation of gross architecture. Relatively fast motions include water-driven growth as exemplified by root cell expansion under abiotic/biotic stresses or during gravitropism. A showcase is a root growth inhibition in 30 seconds triggered by the phytohormone auxin. However, the cellular and molecular mechanisms are still largely unknown. This thesis covers the studies about this topic as follows.

By taking advantage of microfluidics combined withs live imaging, pharmaceutical tools, and transgenic lines, we examined the kinetics of and causal relationship among various auxin-induced rapid cellular changes in root growth, apoplastic pH, cytosolic $Ca^{2+}$, cortical microtubule (CMT) orientation, and vacuolar morphology. We revealed that CMT reorientation and vacuolar constriction are the consequence of growth itself instead of responding directly to auxin. In contrast, auxin induces apoplast alkalinization to rapidly inhibit root growth in 30 seconds. This auxin-triggered apoplast alkalinization results from rapid $H^+$-influx that is contributed by $Ca^{2+}$ inward channel CYCLIC NUCLEOTIDE-GATED CHANNEL 14 (CNGC14)-dependent $Ca^{2+}$ signaling.

To dissect which auxin signaling mediates the rapid apoplast alkalinization, we combined microfluidics and genetic engineering to verify that TIR1/AFB receptors conduct a non-transcriptional regulation on $Ca^{2+}$ and $H^+$-influx. This non-canonical pathway is mostly mediated by the cytosolic portion of TIR1/AFB. On the other hand, we uncovered, using biochemical and phospho-proteomic analysis, that auxin cell surface signaling component TRANSMEMBRANE KINASE 1 (TMK1) plays a negative role during auxin-trigger apoplast alkalinization and root growth inhibition through directly activating PM $H^+$-ATPases. Therefore, we discovered that PM $H^+$-ATPases counteract instead of mediate the auxin-triggered rapid $H^+$-influx, and that TIR1/AFB and TMK1 regulate root growth antagonistically.

This opposite effect of TIR1/AFB and TMK1 is consistent during auxin-induced hypocotyl elongation, leading us to explore the relation of two signaling pathways. Assisted with biochemistry and fluorescent imaging, we verified for the first time that TIR1/AFB and TMK1 can interact with each other. The ability of TIR1/AFB binding to membrane lipid provides a basis for the interaction of plasma membrane- and cytosol-localized proteins. Besides, transgenic analysis combined with genetic engineering and biochemistry showed that

they do function in the same pathway. Particularly, auxin-induced TMK1 increase is TIR1/AFB dependent, suggesting TIR1/AFB regulation on TMK1. Conversely, TMK1 also regulates TIR1/AFB protein levels and thus auxin canonical signaling.

To follow the study of rapid growth regulation, we analyzed another rapid growth regulator, signaling peptide RALF1. We showed that RALF1 also triggers a rapid and reversible growth inhibition caused by $H^+$ influx, highly resembling but not dependent on auxin. Besides, RALF1 promotes auxin biosynthesis by increasing expression of auxin biosynthesis enzyme YUCCAs and thus induces auxin signaling in ca. 1 hour, contributing to the sustained RALF1-triggered growth inhibition.

These studies collectively contribute to understanding rapid regulation on plant cell growth, novel auxin signaling pathway as well as auxin-peptide crosstalk.

# Acknowledgments

My Ph.D. journey started with the first meeting with my supervisor Jiri. His passion, intelligence, and dedication as the light bestowed on me, opened a door for my scientific research. Since then, I started to explore things with great freedom, which I am truly grateful for.

Ph.D. is said to be extremely hard but I never imagined it until it came. It came with troubleshooting days and nights on technical difficulties, fighting for a good habit dealing with long-term and multiple tasks, and confronting being lost in direction. Especially, being lost in direction is like diving in a dark sea for the first time, and time pressure makes it even worse. Luckily, the light afterwards re-bore a person to be hard and persistent. This circle completes the Ph.D. and makes me very lucky.

The journey cannot be started and achieved without my supervisor Jiri. Let alone his great ability and talent, the presence of himself as a charming scientist model encourages me. Like the phytohormone auxin we studied, Jiri is the auxin, and we can make our own organ following his guidance. Specifically, I thank him for giving me the most interesting projects and the most excellent working environments both technically and culturally. Besides science, I thank him for giving full respects to my probably naïve, personal choices on public health issues. I thank for all his supports all the time.

During the journey, I met my colleagues of great kinds. Maciek showed me how the most classical purest scientist looks like to pursue the facts of nature. Matyas paved the way for initiating my projects and shared with me the crucial techniques. Ivan, a cool guy with all fantastic ideas on the abstract things, taught me to flexibly use/design tools and test ideas. Madhu, Lesia, and Mina with great sympathy accompanied me and witnessed all my emotions. Huibin, my closest friend through the Ph.D., brought ease and calm to me. Huihuang, the first student in my career, gave me great experience in playing another role. And of course, with the Chinese gang - Yuzhou, Peng, Xiang, Linlin, Xixi, etc, we made lots of fun during great hikes and food. And Shutang was even my matchmaker.

Beside science, I made another milestone in my life; that is my marriage. I found my husband Penghui, a mathematician who worked in IST. I thank him for coming to my life as a beautiful, passionate, high IQ man doing the type of math that I have never heard of. I also appreciate that we have different interests and strengths, so that we bring each other new perspectives and insights. I am grateful for his love, respect, support, and his existence.

Most importantly, I give my greatest thank to my parents Ping and Zhiwen. They gave me the opportunity and freedom to explore abroad for eight years. For the time, their only kid became most stubborn and un-easy going in different aspects, while they have never stopped missing and caring. I thank them for everything, for being the permanent harbor for my peace.

The Ph.D. is a mixture of science, life, frustration, and self-reestablishment. I thank all the people who appeared during the time. And for the future, I will keep reminding myself not to stop from thinking.

Lastly, I acknowledge two fellowships I received during the Ph.D.: The European Union's Horizon 2020 research and innovation programme under the Marie Skłodowska-Curie Grant Agreement No. 665385 and The DOC Fellowship of the Austrian Academy of Sciences.

## About the Author

Lanxin Li completed a BSc in Natural Sciences at Wuhan University (China) and an MSc in Molecular Biology at Heidelberg University (Germany), before joining IST Austria in September 2016. She worked on the research project "HECATE genes regulation on shoot apical meristem" with Jan Lohmann group in Heidelberg University in 2015-2016, and contributed to the publication in the journal *Elife*. During her PhD studies, the main research interests include rapid cell growth regulation by phytohormone auxin and peptide RALF. The main studies, as the first author, have been published in *Bio-protocol*, accepted in *Nature* and under second revision in *Trends in Plant Sciences*. The other work has contributed to the publications in *Science Advances, Plant Physiology, International Journal of Molecular Sciences, Cells* and *Plant Science.* Besides, Lanxin has presented her research results in the *EPCC* meeting in Karlsruhe in 2017, and showed posters in *ACPD* conference in Prague in 2018 and *IPGSA* conference in Paris in 2019.

## List of Publications Appearing in Thesis

- Published

**Lanxin Li**, S. F. Gabriel Krens, Matyáš Fendrych*, and Jiří Friml. Real-time Analysis of Auxin Response, Cell Wall pH and Elongation in Arabidopsis thaliana Hypocotyls. *Bio-protocol*. 2018; 8(1): e2685.

Maciek Adamowski, **Lanxin Li**, and Jiří Friml*. Reorientation of Cortical Microtubule Arrays in the Hypocotyl of Arabidopsis thaliana Is Induced by the Cell Growth Process and Independent of Auxin Signaling. *Int. J. Mol. Sci.* 2019, 20(13), 3337.

Yuzhou Zhang, Lesia Rodriguez, **Lanxin Li**, Xixi Zhang and Jiří Friml*. Functional innovations of PIN auxin transporters mark crucial evolutionary transitions during rise of flowering plants. *Science Advances* 2020, eabc8895.

Huihuang Chen, Linyi Lai, **Lanxin Li**, Liping Liu, Bello Hassan Jakada, Youmei Huang, Qing He, Mengnan Chai, Xiaoping Niu, and Yuan Qin*. AcoMYB4, an Ananas comosus L. MYB Transcription Factor, Functions in Osmotic Stress through Negative Regulation of ABA Signaling. *Int. J. Mol. Sci.* 2020, 21(16), 5727.

Zuzana Gelová. Michelle Gallei, Markéta Pernisová, Géraldine Brunoud, Xixi Zhang, Matouš Glanc, **Lanxin Li**, Jaroslav Michalko, Zlata Pavlovičová, Inge Verstraeten, Huibin Han, Jakub Hajný, Robert Hauschild, Milada Čovanová, Marta Zwiewka, Lukas Hoermayer, Matyáš Fendrych, Tongda Xu, Teva Vernouxb, Jiří Friml*. Developmental roles of Auxin Binding Protein 1 in Arabidopsis thaliana. *Plant Science*. 2020, 110750.

Madhumitha Narasimhan, Michelle Gallei, Shutang Tan, Alexander Johnson, Inge Verstraeten, **Lanxin Li**, Lesia Rodriguez, Huibin Han, Ellie Himschoot, Ren Wang, Steffen Vanneste, Judit Sanchez-Simarro, Fernando Aniento, Maciek Adamowski, Jiří Friml*. Systematic analysis of specific and nonspecific auxin effects on endocytosis and trafficking. *Plant Physiology.* 2021, *186*(2), pp.1122-1142.

Natalia Nikonorova, Evan Murphy, Cassio Flavio Fonseca de Lima, Shanshuo Zhu, Brigitte van de Cotte, Lam Dai Vu, Daria Balcerowicz, **Lanxin Li**, Xiangpei Kong, Gieljan De Rop, Tom Beeckman, Jiri Friml, Kris Vissenberg, Peter C. Morris, Zhaojun Ding, Ive De Smet *
The Arabidopsis root tip (phospho)proteomes at growth-promoting versus growth-repressing conditions reveal novel root growth regulators. *Cells.* 2021, 1204559.

- Accepted

Chapter Three
**Lanxin Li**[†], Inge Verstraeten[†], Mark Roosjen, Koji Takahashi, Lesia Rodriguez, Jack Merrin, Jian Chen, Lana Shabala, Wouter Smet, Hong Ren, Steffen Vanneste, Sergey Shabala, Bert De Rybel, Dolf Weijers, Toshinori Kinoshita, William M. Gray and Jiří Friml*. Cell surface and intracellular auxin signalling for $H^+$-fluxes in root growth. *Nature.*

- Under Revision

Chapter One
**Lanxin Li**, Michelle Gallei and Jiří Friml*. Bending to auxin: Fast acid growth for tropisms. *Trends in Plant Sciences.*

- Unpublished

Chapter 2: Cortical microtubule reorientation responses to general growth regulation
**Lanxin Li** and Jiří Friml*.

Chapter 4: Interaction of TIR1/AFB and TMK auxin signaling pathways
Lesia Rodriguez[†], **Lanxin Li**[†], Maciek Adamowski, Nataliia Gnyliukh, Lana Shabala, Huibin Han, Inge Verstraeten, Lukas Fiedler, Sergey Shabala and Jiří Friml*.

Chapter 5: RALF1 triggers biphasic root growth inhibition involving auxin signaling
**Lanxin Li**, Huihuang Chen, Saqer S. Alotaibi, Aleš Pěnčík, Maciek Adamowski, Ondřej Novák, Matyáš Fendrych, Jiří Friml*. RALF1 triggers biphasic root growth inhibition involving auxin signaling

Chapter 6: The role of Aux/IAA during auxin-induced rapid root growth inhibition
**Lanxin Li**, Behrokh Shojaie and Jiří Friml*.

# Table of Contents

# List of Figures

## Chapter 4



## Chapter 5

# List of Symbols/Abbreviations

| | |
|---|---|
| 2,4-D | 2,4-Dichlorophenoxyacetic acid |
| 2-NAA | 2-Naphthaleneacetic acid |
| BL | Brassinolide |
| CHX | Cycloheximide |
| CORD | Cordycepin |
| EGCG | Epigallocatechin gallate |
| FC | Fusicoccin |
| IAA | Indole-3-acetic acid |
| KYN | L-Kynurenine |
| MS | Murashige-Skoog |
| NAA | 1-Naphthaleneacetic acid |
| NPA | N-1-naphthylphthalamic acid |
| PEO-IAA | 2-(1H-Indol-3-yl)-4-oxo-4-phenyl |
| TIBA | 2,3,5-triiodobenzoic acid |
| YUCASIN | 5-(4-chlorophenyl)-4H-1,2,4-triazole |

# Chapter 1

## General Introduction

## Bending to auxin: Fast acid growth for tropisms

Lanxin Li, Michelle Gallei and Jiří Friml*

Institute of Science and Technology Austria, 3400 Klosterneuburg, Austria
*Correspondence: jiri.friml@ist.ac.at (J. Friml)

## *1.1 Abstract*

The phytohormone auxin is the major growth regulator governing tropic responses including gravitropism. Auxin build-up at the lower side of stimulated shoots promotes cell expansion, whereas in roots it inhibits growth, leading to upward shoot bending and downward root bending, respectively. Yet it remains an enigma how the same signal can trigger such opposite cellular responses. In this opinion, we discuss several recent unexpected insights into the mechanisms underlying auxin regulation of growth, challenging several existing models. We focus on the divergent mechanisms of apoplastic pH regulation in shoots and roots revisiting the classical Acid Growth Theory and discuss coordinated involvement of multiple auxin signaling pathways. From this emerges a more comprehensive and integrated picture how auxin regulates growth.

## *1.2 Directional growth as key mechanism for plant adaptive development*

Plant cells do not migrate during tissue patterning and the whole body plan is based on the orientation of cell division and expansion. Thus, the regulation of cell expansion is essential for the plant development and its adaptation to the environment [1]. Tropisms are spectacular examples, e.g. following gravistimulation, the phytohormone auxin is transported to the lower side of the stimulated organ, where the cell growth rate is promoted (in shoots) or inhibited (in roots). The resulting differential growth rate between the lower and upper side of cells leads to upward or downward bending respectively [2]. This is a prime example for the contribution of targeted cell expansion to general plant development and adaptive behavior. Despite the importance of auxin in cell signaling, how it regulates cell expansion oppositely in shoots and roots remained largely unknown until recently. Several contemporary studies focusing on the mechanism of auxin-induced rapid root growth inhibition and shoot growth promotion, as well as novel auxin signaling pathways provide cutting-edge insights into this topic.

## *1.3 Main entry points for the regulation of cell expansion*

To understand how the growth of plant cells is regulated, one must consider their special features. Distinct from animal cells, plant cells have a high turgor pressure ranging between 0.6 and 1 MPa [3] and are encased by a structural layer of the cell wall. Plant cell growth is the consequence of the balance between the driving force (turgor pressure) and the limiting force (cell wall). The turgor pressure increases through the mechanism of cells taking up water based

on the osmotic flow following the membrane potential, which is built up by the difference in the ion concentrations across the plasma membrane (PM). This is possibly contributed by the vacuole which accumulates water and osmotic compounds [4]. The robust cell wall prevents pressurized cells to expand. The cell wall rigidity depends not only on the composition and structural rearrangements, which are regulated by cortical microtubules (CMTs), but also on cell wall-based proteins and enzymes, whose activities are regulated by the apoplastic pH [5-7]. Hence, ion fluxes, apoplastic pH, CMTs, and vacuoles are all potentially contributing to the regulation of cell growth.

## *1.4 Auxin: one signal with manifold performances*

Auxin is the main endogenous signal regulating cell growth across the plant with shoots and roots having distinct sensitivities. Exogenous auxin promotes the elongation of arabidopsis (*Arabidopsis thaliana*) hypocotyl segments even at 10 μM [8], whereas it already inhibits root growth at 5 nM [9]. Similarly, following gravistimulation, auxin accumulation accelerates cell expansion in shoots, whereas inhibiting it in roots [10, 11]. The speed of growth responses in the two organs is also different. Following gravistimulation, arabidopsis hypocotyl starts bending after 1-2 hours and it takes ca. 4-6 hours to reach the half-bending angle [12]. By comparison, the root starts bending faster after gravistimulation (already after 10 minutes) and it takes ca. 40-60 minutes to reach the half-bending angle [13, 14]. Similarly, exogenous auxin application promotes the growth of etiolated hypocotyl segments in about 20 minutes [15] whereas inhibits it in intact roots in less than 30 seconds [9, 16], despite that the organs transcription responds to auxin in a similar time scale of ca. 20 minutes reported by DR5::LUC [9, 15]. These differences in concentration and timing suggest that the mechanism of auxin-triggered cell growth regulation differs between shoots and roots.

To understand how auxin regulates cell growth in different organs, we focus on: (i) auxin-triggered cellular responses and (ii) upstream auxin signaling. During auxin-induced root growth regulation, auxin triggers a series of cellular responses, such as CMT reorientation, vacuole constriction, $Ca^{2+}$ transient, apoplast alkalinization, membrane depolarization and $K^+$ efflux. We critically examine the involvement of those cellular responses and upstream signaling in growth regulation.

## *1.5 Cortical microtubule reorientation: a consequence not the cause*

CMTs are microtubule arrays located close to the PM. In elongating cells, they co-localize with and are required for guiding the cellulose synthase complex, which produces cellulose fibrils building the main structure of the cell wall [17, 18]. The orientation of CMTs thus determines the anisotropy of the cell wall, to either restrict or allow cell expansion in a certain direction. Therefore, CMTs contribute to growth regulation and may be, potentially, part of the mechanism by which auxin regulates growth.

In response to auxin, CMTs reorient from longitudinal to transversal in respect to the growth axis in etiolated arabidopsis hypocotyls and oppositely in roots. In both organs, the CMT orientation correlates with the growth regulation. Nonetheless, the causal relationship has remained a matter of debate over the years [19, 20]. Recent pharmacological and genetic studies in arabidopsis hypocotyls consistently argued that CMT reorientation is not a crucial part of the auxin-triggered mechanism for growth regulation [8]. For example, auxin can promote growth normally, even when CMTs are depolymerized, confirming that intact CMTs are not essential. On the other hand, auxin treatment in hyperosmotic conditions that prevent growth, does not lead to CMT reorientation. This shows that in shoots CMT reorientation responds to the growth promotion but not to auxin itself [8]. Similarly in roots, kinetic analysis of CMTs after auxin treatment demonstrated that a significant CMT reorientation occurred later than growth inhibition [16]. Furthermore, the inhibition of auxin-triggered CMT reorientation by the MT stabilizer taxol does not influence the growth inhibition by auxin [16]. Collectively, in both shoots and roots, CMT reorientation is the indirect consequence rather than cause of the auxin-induced growth change (Figure 1).

## *1.6 Vacuolar fragmentation: too late for the show*

Vacuoles are unique plant organelles. Their development is a dynamic combination of fusion and fragmentation of liquid pouches, the size of which can take up to 90% of a mature plant cell [21]. Due to its potential contribution to the osmotic properties of cells, vacuoles have been linked to the regulation of cell growth [4, 22].

During auxin-triggered root cell growth inhibition, a concomitant constriction of vacuoles has been observed [4]. Similar to CMT reorientation, the question remains whether the vacuolar constriction is the cause or the consequence of growth inhibition. The kinetics of vacuole morphology and cell length in roots after auxin treatment revealed that vacuole

changes take place within 15-25 minutes, thus seemingly preceding cell length changes, which were visible in the late meristematic zone by the applied method only after about 45-55 minutes. All genetic and pharmacological manipulations however of auxin signaling and cellular processes were analyzed only after 20 hours of the respective treatment [4, 22] not allowing for definite statements about time dynamics. Also, there was no obvious change in the auxin-induced vacuole morphology in the elongating cells [16], which have the highest capacity of growth regulation by auxin [23, 24]. This puts the process of vacuolar morphology changes well outside the time scale of auxin-triggered root growth inhibition, which occurs faster than 30 seconds [9] arguing against its direct involvement in the immediate mechanism for auxin-induced root cell growth inhibition (Figure 1).

## *1.7 Early auxin birds: $Ca2^+$ and $H^+$-fluxes across the PM*

Unlike CMT reorientation and vacuole constriction, ion fluxes across the PM change practically immediately after auxin application. The most significant ones are $Ca^{2+}$ and $H^+$ influxes (Figure 1). Specifically, a cytosolic $Ca^{2+}$ transient and a rhizospheric pH increase occurred within 7-14 seconds and 15 seconds, respectively after auxin treatment [25]. Consistently, the apoplast pH was increased upon auxin in 30 seconds [16]. During gravitropism, both cytosolic $Ca^{2+}$ levels and the rhizospheric pH changed in both upper (decreased $Ca^{2+}$ and pH) and lower (increased $Ca^{2+}$ and pH) flank 2-6 minutes after gravistimulation [25]. Therefore, the $Ca^{2+}$ transient and external pH changes are very early responses to auxin and closely correlate with auxin-induced rapid root growth inhibition [16] (Figure 1).

The possible causal relationship between the auxin-induced $Ca^{2+}$ transient, extracellular alkalinization, and root growth inhibition has been addressed pharmacologically and genetically. The $Ca^{2+}$ channel inhibitor $LaCl_3$ interferes with auxin-induced rhizosphere alkalinization [25]. Similarly, mutation of the $Ca^{2+}$ permeable cation channel Cyclic NUCLEOTIDE-GATED CHANNEL 14 (CNGC14) leads to a delay of pH and growth response of ca. 6 minutes after auxin [16, 26]. Besides, depletion of $Ca^{2+}$ in the medium results in a diminished $Ca^{2+}$ transient as well as a delay of $H^+$ and growth responses of ca. 4-6 minutes [16]. Therefore, CNGC14-mediated $Ca^{2+}$ transient contributes to auxin-induced apoplast alkalinization and growth inhibition.

In contrast to influx of $Ca^{2+}$ and $H^+$, $K^+$ is transported out of root cells after auxin [16]. The efflux of $K^+$ leads to less water uptake [27], in line with less cell expansion. Besides, the

total net ion fluxes across the PM after auxin result in a rapid membrane depolarization [28, 29], contributing to the growth inhibition.

## *1.8 In the driver's seat: apoplastic pH changes and the Acid Growth Theory*

Auxin leads to rapid apoplastic pH changes simultaneously with the growth regulation in both shoots and roots. Not only the time scale, but also the trend of the change in the apoplastic pH and growth regulation coincide. In shoots, auxin leads to acidification and growth promotion [15, 30]; while in roots, it results in alkalinization and growth inhibition [16, 25, 31]. The long-standing Acid Growth Theory suggests that the apoplastic pH directly regulates the cell growth. In particular, acidification of the apoplast activates pH-dependent expansins that loosen the otherwise rigid cell wall allowing for cell expansion. Concomitantly, the $H^+$ efflux builds up a higher membrane potential that drives the secondary ion influx, leading to an increase in turgor pressure and water uptake [27]. In this theory, $H^+$ flux across the PM coordinates both the cell wall rigidity and turgor pressure to regulate cell growth [27].

The molecular mechanism of the Acid Growth Theory has been well established in the arabidopsis hypocotyl. Auxin transcriptionally upregulates the expression level of SMALL AUXIN Up-RNA 19 (SAUR19), which binds to and inhibits the TYPE 2C PROTEIN PHOSPHATASES (PP2C) which de-phosphorylates and inhibits the activity of the PM $H^+$-ATPases [30, 32]. By inhibiting the PM $H^+$-ATPases inhibitor, this auxin-induced activation of the PM $H^+$-ATPases leads to apoplast acidification and thus promotes shoot growth [15, 33]. In addition, emerging evidences showed that the PM $H^+$-ATPases can be directly phosphorylated and activated by the cell surface kinase TRANSMEMBRANE KINASE 1 (TMK1) in both shoots and roots [16, 34]. This in shoots, adds a potential missing mechanism for initial phosphorylation of PM $H^+$-ATPases prepared for further activation [34].

In roots, the situation is more complex. Auxin leads to apoplast alkalinization and growth inhibition also following the main premise of the Acid Growth Theory that lower pH promotes and higher pH inhibits growth. However, the PM $H^+$-ATPases are activated by TMK1 after auxin during root growth inhibition [16, 35]. This counteracts the observed more dominant apoplast alkalinization, forming two antagonistic regulations fine-tuning the root growth.

The mechanism underlying apoplast alkalinization remains unclear. Besides alkalinization of the apoplast, auxin triggers simultaneously acidification in the cytosol next to the PM and increases net proton influx, suggesting that auxin promotes $H^+$ influx to alkalinize the apoplast and depolarize the PM for rapid root growth inhibition [16, 28]. The question

remains, how this is achieved. One possibility is that this inward $H^+$ flow is directly symported by the active auxin importer AUX1/LAX, with 2 $H^+$ per IAA molecule [29]. However, a conserved estimation does not favor it, the amount of auxin-induced $H^+$ influx measured in primary roots or root hairs is a magnitude more than the maximum amount of $H^+$ symported by the overexpressed AUX1 in *Xenopus laevis* oocytes [16]. Additionally, bypassing auxin import by directly injecting auxin into root hair cytosol revealed a consistent membrane depolarization resembling the external application, though with a transient hyperpolarization for 1 minute [29]. This suggests that auxin-induced membrane depolarization or $H^+$ influx is mainly not contributed by auxin import itself.

Other possibilities include that auxin regulates an ion transporter or channel that symports $H^+$, or actively opens a $H^+$ channel, or creates a $H^+$ leak in the membrane. Considered that this process seems to be linked to $Ca^{2+}$ [36], the possible $H^+$ symporter might be a $Ca^{2+}$ transporter or channel. Nonetheless, the $Ca^{2+}$ transient and pH change displayed different dynamic signatures, especially regarding their maintenance following auxin treatment or gravistimulation [25] not supporting the hypothesis that $Ca^{2+}$ and $H^+$ are symported. Therefore, it is likely that auxin actively opens a unknown $H^+$ channel that may be $Ca^{2+}$-dependent.

In summary, following the classical Acid Growth Theory, the auxin-induced apoplastic pH changes are the major cellular mechanism of the growth regulation in both shoots and roots. In shoots, auxin acidifies the apoplast via transcriptional activation [15, 30] and post-translationally maintaining the activation of PM $H^+$-ATPases [34]. In roots, though this post-translational activation of PM $H^+$-ATPases also applies, a more dominant process is immediate, auxin-triggered apoplast alkalinization, possibly occurring through non-transcriptional activation of a $H^+$ channel for a rapid $H^+$ influx [16].

## *1.9 Not so canonical: TIR1/AFB-mediated non-transcriptional responses*

The canonical, nuclear auxin signaling pathway is well characterized and has been for decades thought, exclusively as the mechanism mediating auxin effect on gene transcription. It begins with the auxin perception facilitating the binding between the co-receptors, SCF-TIR1/AFB ubiquitin ligases and the Aux/IAA transcriptional repressors. This leads to the ubiquitination of the Aux/IAAs and their further degradation via the 26S proteasome. Consequently, the repression of AUXIN RESPONSE FACTOR (ARFs) is released and they are free to act on auxin response genes [37-39] **(**Figure 2**)**.

The exception has been discovered in roots, where auxin alkalinizes the apoplast and inhibits growth faster than 30 seconds. This response time is far too fast for the transcriptional regulation to be involved and, in addition, the rapid auxin effects are observed also when transcription is inhibited [9, 16], altogether suggesting a non-transcriptional signaling mechanism.

Nonetheless, several observations clearly show that this mechanism is still dependent on TIR1/AFB receptors. For example, the *tir1-1afb2-1afb3-1* mutants display less sensitivity to auxin-triggered apoplast alkalinization and root growth inhibition [9, 16]. Furthermore, using an engineered ccvTIR1 and cvxIAA pair system, which allows for specific and selective activation of TIR1/AFB signaling [35], the cvxIAA-mediated ccvTIR1 activation is sufficient to trigger apoplast alkalinization, cytosolic $Ca^{2+}$ transient and root growth inhibition [9, 16]. These observations lead to the conclusion that TIR1/AFB signaling has a non-transcriptional branch mediating auxin effect on rapid responses including CNGC14-mediated $Ca^{2+}$ transient, apoplast alkalinization and rapid root growth inhibition [40] **(**Figure 2**)**.

Recent observations provide initial insights into this novel branch of the TIR1/AFB pathway. First, the subcellular localization of all six TIR1/AFB proteins in arabidopsis was carefully examined. In roots, AFB1 is most abundant in the cytosol while TIR1 is mainly found in the nucleus [41]. It has been proposed that the cytosolic fraction of TIR1/AFBs may contribute to the fast non-transcriptional regulation for the rapid growth response while the nuclear fraction is more responsible for the slower, transcriptional regulation **(**Figure 2**)**. Accordingly, the *afb1-3* mutant is less auxin-sensitive than WT and *tir1-10* in terms of root growth inhibition and membrane potential decrease or apoplast alkalinization [16, 28]; while *tir1-10* is more auxin-resistant to root growth inhibition than *afb1-3* in a longer term (>6h) [16].

Thus, an unknown branch of auxin signaling pathway starting with cytosolic TIR1/AFB receptors mediates rapid apoplast alkalinization, membrane depolarization and growth inhibition in roots. It remains unclear, at which point the branching occurs and whether the known downstream components such as Aux/IAAs and ARFs are involved. The ultimate question is, however, the mechanism, by which this pathway promotes influx of $H^+$ into the cell leading to collapse of the $H^+$ gradient across the PM, apoplast alkalinization and membrane depolarization. It remains a challenge for future investigations to establish what this molecular mechanism of apopolast alkalinization may be and how it is activated by the fast TIR1/AFB signaling.

## *1.10 TMKs: Receptors or receptor-likes?*

Four leucine-rich receptor-like kinases, which form the TMK family have been proposed as components of a largely elusive auxin signaling on the cell surface. TMKs act in general cell expansion regulation and downstream of auxin [42, 43]. At the concave side of the apical hook, TMK1 in response to auxin has its C-terminal kinase domain cleaved and translocated to the nucleus, where it phosphorylates and stabilizes non-canonical Aux/IAAs, resulting in gene transcription regulation [44] (Figure 2). This provides a mechanism, by which TMK1 and TIR1/AFB-Aux/IAA signaling mechanisms converge on transcriptional regulation.

On the other hand, TMKs contribute also to non-transcriptional regulation of cell growth. TMKs are required for the auxin-induced rapid activation (within 30 seconds) of RHO-RELATED PROTEIN FROM PLANTS 2 (ROP2) and ROP6 GTPases and promotes the nanoclustering of ROP6 during pavement cell expansion [45-47]. A similar mechanism may act during root gravitropism, where TMK1 is important for ROP6 activation, which regulates PIN-FORMED 2 (PIN2) localization to affect root gravitropic response [48, 49] (Figure 2).

A recent, emerging mechanism, by which the TMK pathway regulates apoplastic pH and cell growth is via PM $H^+$-ATPases. As mentioned before, TMK1 activation of PM $H^+$-ATPases[16, 34] in shoots maintains the initial phosphorylation of PM $H^+$-ATPases prepared for TIR1/AFB-mediated transcriptional regulation for a slow apoplast acidification [34]. On the other hand, in roots, TMK1-AHA2 acts antagonistically with the rapid, non-transcriptional branch of the TIR1/AFB pathway, fine-tuning the root growth regulation [16] (Figure 2).

Another TMK family member, TMK4, was identified to have a distinctive role in regulating auxin biosynthesis. In response to auxin, TMK4 phosphorylates the TRYPTOPHAN AMINOTRANSFERASE OF ARABIDOPSIS (TAA1), a key enzyme in the auxin biosynthesis pathway, leading to a suppression of auxin biosynthesis [50]. Therefore, downstream of the auxin pathway, TMK4 acts as negative feedback in the regulation of root meristem size and root hair development.

Taken together, TMKs regulate the general and the auxin-regulated cell expansion by multiple ways (Figure 2), however, the details of the downstream mechanisms are largely unknown. For example, whether auxin-triggered cleavage of TMKs' C terminus occurs and regulates other processes besides the apical hook, or how the downstream ROP activation participates in auxin-induced growth regulation, stays to be investigated.

The main open question concerns how auxin activates the TMK pathway. One possibility would be that auxin binds directly to TMKs and activates them but there are no

observations supporting this scenario. Another possibility is that the activation occurs through AUXIN BINDING PROTEIN 1 (ABP1), which has been proposed to interact with TMK1 [45]. ABP1 has been considered since decades as a possible receptor of auxin, based on the ability of the maize ABP1 to bind to auxin [51, 52]. Any function of ABP1 however was put into doubt due to lack of obvious phenotypic defects in the verified knock-out mutants [53]. A systematic analysis confirmed only minor defects in the *abp1* loss-of-function mutants, whereas gain-of-function alleles showed a broad spectrum of growth and developmental aberrations [54]. This discrepancy might be caused by functional gene redundancy[51, 55]. Nonetheless, until these potentially redundant genes will be identified and/or involvement of both ABP1 and TMK in some process(es) will be genetically verified, the role of ABP1 as part of TMK-mediated auxin signaling remains hypothetical (Figure 2).

## *1.11 Concluding Remarks*

Auxin regulates cell expansion and triggers various short and long-term cellular responses. Some are direct parts of the mechanism for auxin-induced growth regulation, others the indirect consequences of the growth regulation *per se*. Auxin-induced CMT reorientation and vacuole fragmentation belong to the latter case. Still, they regulate the capacity of cell growth and contribute to the control of the eventual cell size. In contrast, the auxin-induced $Ca^{2+}$ transient is an instant response, which may be linked to auxin-triggered $H^+$ flux and apoplastic pH change. The auxin-induced apoplastic pH change regulates cell growth following the Acid Growth Theory with acidification promoting and alkalinization inhibiting growth. However, the mechanisms how auxin regulates apoplastic pH varies between shoots and roots.

In shoots, auxin acidifies the apoplast through PM $H^+$-ATPase activation, the process regulated by both the nuclear TIR1/AFB transcriptional pathway and direct phosphorylation and activation by the cell surface-based TMK1 receptor-like kinase. In contrast, in roots, auxin alkalinizes the apoplast via rapid activation of $H^+$ influx, the process, which is mediated through an unknown, non-transcriptional branch of the cytosolic TIR1/AFB auxin pathway. While the nuclear fraction of TIR1/AFB mediate the sustained and long term effect of root growth inhibition. On the other hand, the cell surface-based TMK1 directly binds and activates PM $H^+$-ATPase also in roots; there functioning antagonistically to the apoplast alkalinization, fine-tuning the root growth regulation. A future challenge will be to unravel

the mechanism of rapid $H^+$ influx and better characterize all various auxin signaling mechanisms (see Outstanding Questions).

**Outstanding Questions:**

- What is the molecular mechanism of auxin-induced $H^+$ influx?
- How does the non-transcriptional AFBs/TIR1 signaling branch look like? Does it involve AUX/IAAs, ubiquitination and degradation?
- How can or do cytosolic and nuclear fractions of TIR1/AFBs mediate distinct functions?
- How does the TMK pathway perceive auxin?
- Which auxin signaling mechanism mediates the ultrafast phosphorylation response?

**Acknowledgments**

The authors thank Alexandra Mally for editing the text. This work was supported by the Austrian Science Fund (FWF) I 3630-B25 to Jiří Friml and the DOC Fellowship of the Austrian Academy of Sciences to Lanxin Li. All figures were created with BioRender.com.

**Author Contributions**

Lanxin Li and Jiří Friml wrote the manuscript. Michelle Gallei helped with corrections.

**Conflicts of Interest**

The authors declare no conflict of interest.

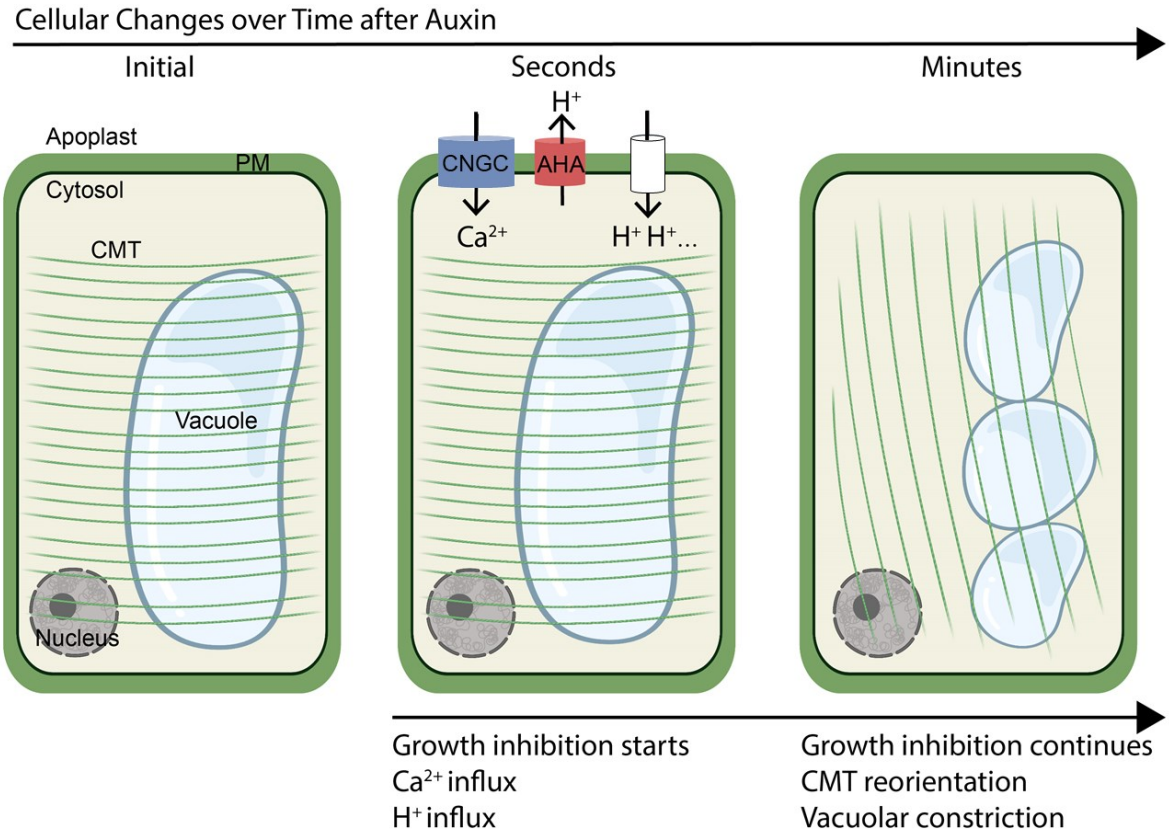


**Figure 1.** The time scale of auxin-triggered fast cellular responses in arabidopsis roots. In response to increased auxin levels, root cells show a rapid $H^+$ influx. This is contributed by CNGC14-mediated $Ca^{2+}$ transient, but not by PM $H^+$-ATPases. The resulting apoplastic alkalinization causes root growth inhibition within seconds. Responding to the growth inhibition, the cortical microtubules (CMTs, green lines) are then reoriented from transversal to longitudinal/oblique. The vacuoles are constricted at later time points; not consistent with their direct involvement in rapid auxin-induced growth inhibition. Abbreviations: PM, plasma membrane; CNGC, Cyclic NUCLEOTIDE-GATED CHANNEL; AHA, PM $H^+$-ATPase.

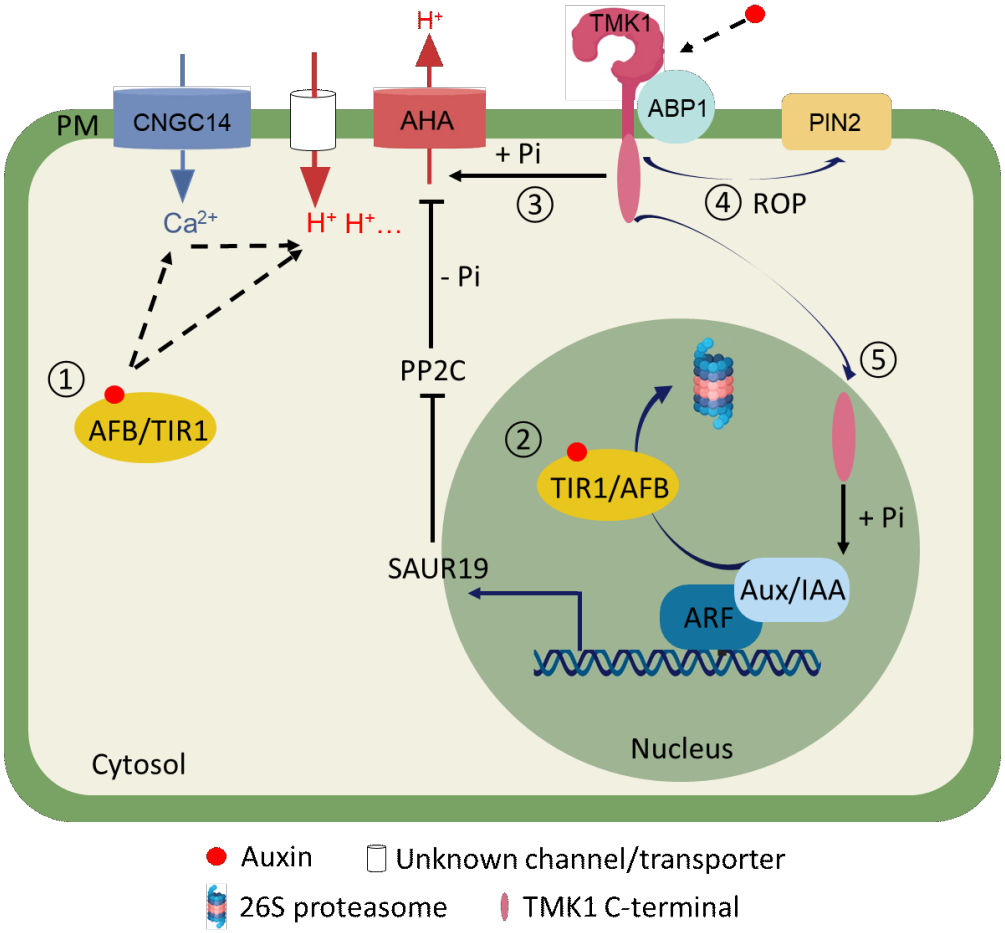


**Figure 2**. Auxin signaling pathways in arabidopsis. ① Non-transcriptional branch of the TIR1/AFB pathway in roots. Intracellular auxin perceived by the cytosolic fraction of TIR1/AFBs triggers a rapid CNGC14-mediated $Ca^{2+}$ influx and an unknown channel or transporter-mediated $H^+$ influx across the PM. The $H^+$ influx, contributed by the $Ca^{2+}$ transient, leads to apoplast alkalinization and thus rapid root growth inhibition. ② The canonical, transcriptional TIR1/AFB pathway. Intracellular auxin perceived by the nuclear fraction of TIR1/AFB and Aux/IAAs leads to ubiquitination and 26S proteasome-mediated degradation of Aux/IAAs. Consequently, the inhibition of Aux/IAAs on the ARF-regulated downstream gene transcription is released including SAUR19 which inhibits PP2C that dephosphorylates and deactivates AHA. Thereby, AHA becomes activated. ③ The PM-localized TMK1, directly phosphorylates and activates AHA in both shoots and roots. ④ The PM-localized TMK1 which presumably perceives external auxin signaling through ABP1, activates ROPs for pavement cell expansion and regulates PIN2 during root gravitropic response. ⑤ The PM-localized TMK1, in response to auxin, has its C-terminal kinase domain cleaved and translocated to the nucleus for phosphorylating and stabilizing non-canonical Aux/IAAs, regulating gene transcription in the apical hook. Abbreviations: PM,

plasma membrane; CNGC14, Cyclic NUCLEOTIDE-GATED CHANNEL 14; AHA, PM $H^+$-ATPase; TMK1, TRANSMEMBRANE KINASE 1; ABP1, AUXIN BINDING PROTEIN 1; ROP, RHO-RELATED PROTEIN FROM PLANTS; PIN2, PIN-FORMED 2; TIR1/AFB, TRANSPORT INHIBITOR RESPONSE1/AUXIN-SIGNALING F-BOX protein; ARF, AUXIN RESPONSE FACTOR; SAUR19, SMALL AUXIN Up-RNA 19; PP2C, type 2C protein phosphatases.

## *1.12 References*


1 Su, S.-H.*, et al.* (2017) Molecular mechanisms of root gravitropism. *Curr. Biol.* 27, R964-R972

2 Nakamura, M.*, et al.* (2019) Bridging the gap between amyloplasts and directional auxin transport in plant gravitropism. *Curr. Opin. Plant Biol.* 52, 54-60

3 Schopfer, P. (2006) Biomechanics of plant growth. *Am. J. Bot.* 93, 1415-1425

4 Löfke, C.*, et al.* (2015) Auxin regulates SNARE-dependent vacuolar morphology restricting cell size. *Elife* 4, e05868

5 Atanasova, L.*, et al.* (2018) Evolution and functional characterization of pectate lyase PEL12, a member of a highly expanded Clonostachys rosea polysaccharide lyase 1 family. *BMC microbiol.* 18, 1-19

6 Hocq, L.*, et al.* (2017) Connecting homogalacturonan-type pectin remodeling to acid growth. *Trends Plant Sci.* 22, 20-29

7 Samalova, M.*, et al.* (2020) Expansin-controlled cell wall stiffness regulates root growth in Arabidopsis. *bioRxiv* doi: https://doi.org/10.1101/2020.06.25.170969

8 Adamowski, M.*, et al.* (2019) Reorientation of cortical microtubule arrays in the hypocotyl of Arabidopsis thaliana is induced by the cell growth process and independent of auxin signaling. *Int. J. Mol. Sci.* 20, 3337

9 Fendrych, M.*, et al.* (2018) Rapid and reversible root growth inhibition by TIR1 auxin signalling. *Nat. Plants* 4, 453

10 Rakusová, H.*, et al.* (2016) Termination of shoot gravitropic responses by auxin feedback on PIN3 polarity. *Curr. Biol.* 26, 3026-3032

11 Pařízková, B.*, et al.* (2017) What has been seen cannot be unseen—detecting auxin in vivo. *Int. J. Mol. Sci.* 18, 2736

12 Rakusová, H.*, et al.* (2011) Polarization of PIN3-dependent auxin transport for hypocotyl gravitropic response in Arabidopsis thaliana. *Plant J.* 67, 817-826

13 Taniguchi, M.*, et al.* (2017) The Arabidopsis LAZY1 family plays a key role in gravity signaling within statocytes and in branch angle control of roots and shoots. *Plant Cell* 29, 1984-1999

14 Bailly, A.*, et al.* (2008) Modulation of P-glycoproteins by auxin transport inhibitors is mediated by interaction with immunophilins. *J. Biol. Chem.* 283, 21817-21826

15 Fendrych, M.*, et al.* (2016) TIR1/AFB-Aux/IAA auxin perception mediates rapid cell wall acidification and growth of Arabidopsis hypocotyls. *Elife* 5, e19048

16 Li, L.*, et al.* (2021) Cell surface and intracellular auxin signalling for $H^+$-fluxes in root growth. *Research Square* DOI: 10.21203/rs.3.rs-266395/v3

17 Paredez, A.R., *et al.* (2006) Visualization of cellulose synthase demonstrates functional association with microtubules. *Science* 312, 1491-1495
18 Li, S., *et al.* (2012) Cellulose synthase interactive protein 1 (CSI1) links microtubules and cellulose synthase complexes. *Proc. Natl. Acad. Sci. U.S.A.* 109, 185-190
19 Chen, X., *et al.* (2014) Inhibition of cell expansion by rapid ABP1-mediated auxin effect on microtubules. *Nature* 516, 90
20 Le, J., *et al.* (2005) Cell elongation and microtubule behavior in the Arabidopsis hypocotyl: responses to ethylene and auxin. *J. Plant Growth Regul.* 24, 166-178
21 Tan, X., *et al.* (2019) A review of plant vacuoles: formation, located proteins, and functions. *Plants* 8, 327
22 Kaiser, S. and Scheuring, D. (2020) To Lead or to Follow: Contribution of the Plant Vacuole to Cell Growth. *Front. Plant Sci.* 11, 553
23 Verbelen, J.-P., *et al.* (2006) The root apex of Arabidopsis thaliana consists of four distinct zones of growth activities: meristematic zone, transition zone, fast elongation zone and growth terminating zone. *Plant Signal. Behav.* 1, 296-304
24 Baskin, T.I., *et al.* (2020) Positioning the root elongation zone is saltatory and receives input from the shoot. *iScience* 23, 101309
25 Monshausen, G.B., *et al.* (2011) Dynamics of auxin-dependent $Ca^{2+}$ and pH signaling in root growth revealed by integrating high-resolution imaging with automated computer vision-based analysis. *Plant J.* 65, 309-318
26 Shih, H.-W., *et al.* (2015) The cyclic nucleotide-gated channel CNGC14 regulates root gravitropism in Arabidopsis thaliana. *Curr. Biol.* 25, 3119-3125
27 Arsuffi, G. and Braybrook, S.A. (2018) Acid growth: an ongoing trip. *J. Exp. Bot.* 137-146
28 Serre, N.B., *et al.* (2021) AFB1 controls rapid auxin signalling through membrane depolarization in Arabidopsis thaliana root. *Nat. Plants*, 1-10
29 Dindas, J., *et al.* (2018) AUX1-mediated root hair auxin influx governs $SCF^{TIR1/AFB}$-type $Ca^{2+}$ signaling. *Nat. Commun.* 9, 1-10
30 Spartz, A.K., *et al.* (2014) SAUR inhibition of PP2C-D phosphatases activates plasma membrane H+-ATPases to promote cell expansion in Arabidopsis. *Plant Cell* 26, 2129-2142
31 Barbez, E., *et al.* (2017) Auxin steers root cell expansion via apoplastic pH regulation in Arabidopsis thaliana. *Proc. Natl. Acad. Sci. U.S.A.* 114, E4884-E4893
32 Ren, H., *et al.* (2018) A subset of plasma membrane-localized PP2C. D phosphatases negatively regulate SAUR-mediated cell expansion in Arabidopsis. *PLoS Genet.* 14, e1007455
33 Du, M., *et al.* (2020) Rapid auxin-mediated cell expansion. *Annu. Rev. Plant Biol.* 71, 379-402
34 Yang, Z., *et al.* (2021) TMK-based cell surface auxin signaling activates cell wall acidification in Arabidopsis. *Research Square* DOI:10.21203/rs.3.rs-203621/v1
35 Uchida, N., *et al.* (2018) Chemical hijacking of auxin signaling with an engineered auxin–TIR1 pair. *Nat. Chem. Biol.* 14, 299
36 Behera, S., *et al.* (2018) Cellular $Ca^{2+}$ signals generate defined pH signatures in plants. *Plant Cell* 30, 2704-2719
37 Lavy, M. and Estelle, M. (2016) Mechanisms of auxin signaling. *Development* 143, 3226-3229

38 Leyser, O. (2018) Auxin signaling. *Plant Physiol.* 176, 465-479
39 Powers, S.K. and Strader, L.C. (2020) Regulation of auxin transcriptional responses. *Dev. Dyn.* 249, 483-495
40 Gallei, M.*, et al.* (2020) Auxin signalling in growth: Schrödinger's cat out of the bag. *Curr. Opin. Plant Biol.* 53, 43-49
41 Prigge, M.J.*, et al.* (2020) Genetic analysis of the Arabidopsis TIR1/AFB auxin receptors reveals both overlapping and specialized functions. *Elife* 9, e54740
42 Dai, N.*, et al.* (2013) The TMK subfamily of receptor-like kinases in Arabidopsis display an essential role in growth and a reduced sensitivity to auxin. *PloS One* 8, e60990
43 Gaillochet, C.*, et al.* (2020) HY5 and phytochrome activity modulate shoot-to-root coordination during thermomorphogenesis in Arabidopsis. *Development* 147
44 Cao, M.*, et al.* (2019) TMK1-mediated auxin signalling regulates differential growth of the apical hook. *Nature* 568, 240-243
45 Xu, T.*, et al.* (2014) Cell surface ABP1-TMK auxin-sensing complex activates ROP GTPase signaling. *Science* 343, 1025-1028
46 Xu, T.*, et al.* (2010) Cell surface-and rho GTPase-based auxin signaling controls cellular interdigitation in Arabidopsis. *Cell* 143, 99-110
47 Pan, X.*, et al.* (2020) Auxin-induced signaling protein nanoclustering contributes to cell polarity formation. *Nat. Commun.* 11, 1-14
48 Lin, D.*, et al.* (2012) A ROP GTPase-dependent auxin signaling pathway regulates the subcellular distribution of PIN2 in Arabidopsis roots. *Curr. Biol.* 22, 1319-1325
49 Marques-Bueno, M.M.*, et al.* (2021) Auxin-Regulated Reversible Inhibition of TMK1 Signaling by MAKR2 Modulates the Dynamics of Root Gravitropism. *Curr. Biol.* 31, 228-237. e210
50 Wang, Q.*, et al.* (2020) A phosphorylation-based switch controls TAA1-mediated auxin biosynthesis in plants. *Nat. Commun.* 11, 1-10
51 Woo, E.J.*, et al.* (2002) Crystal structure of auxin-binding protein 1 in complex with auxin. *EMBO J.* 21, 2877-2885
52 Leblanc, N.*, et al.* (1999) A novel immunological approach establishes that the auxin-binding protein, Nt-abp1, is an element involved in auxin signaling at the plasma membrane. *J. Biol. Chem.* 274, 28314-28320
53 Gao, Y.*, et al.* (2015) Auxin binding protein 1 (ABP1) is not required for either auxin signaling or Arabidopsis development. *Proc. Natl. Acad. Sci. U.S.A.* 112, 2275-2280
54 Gelová, Z.*, et al.* (2021) Developmental roles of auxin binding protein 1 in Arabidopsis Thaliana. *Plant Sci.* 303, 110750
55 Dunwell, J.M.*, et al.* (2008) Germin and germin-like proteins: evolution, structure, and function. *Crit. Rev. Plant Sci.* 27, 342-375

# Chapter 2

# Cortical microtubule reorientation responses to general growth regulation

Lanxin Li and Jiri Friml*

Unpublished

## *2.1 Introduction*

In this chapter, we aim to examine that cortical microtubule (CMT) orientation responds to general growth regulation as a support for Chapter 1.4 that CMTs respond to growth itself. Using different growth substances including phytohormone strigolactone, osmosis-regulating mannitol, and cell wall-regulating pectin methylesterase inhibitor epigallocatechin gallate (EGCG), we showed that CMT orientation correlates with the root growth regulation following different stimuli.

## *2.2 Method*

We performed root growth assay using a vertical scanner controlled by the AutoIt script, which allows automatic scanning. We scanned seedlings every 0.5 or 1 hour for 5 or 6 hours in a semi-normal growing conditions. Besides, we imaged CMTs with Zeiss LSM-800 confocal microscope using *MAP4-GFP* marker line and analyzed CMTs orientation using a Python-based application called Bioline [1].

## *2.3 Hormone strigolactone inhibited root growth and reoriented CMTs*

To test if strigolactone regulates root growth, we tracked root growth over time treated with different concentrations of GR24 and observed slight inhibition effects (Figure 1a). To check if strigolactone affects auxin-induced root growth inhibition, we treated roots with different concentrations of GR24 and 100 nM IAA. The co-treatment led to an additional effect of both on root growth (Figure 1b), suggesting that GR24 and auxin affect root growth independently. On the other hand, we analyzed CMTs in root elongating cells after 70 minutes of treatments as above. 50 μM GR24 application and 100 nM IAA led to ca. 10% and 50% increase in the vertical orientation, respectively. The co-treatment showed additional effect in CMT reorientation as well (Figure 1c-d). These results demonstrate that CMT reorientation responds to growth regulation by strigolactone.

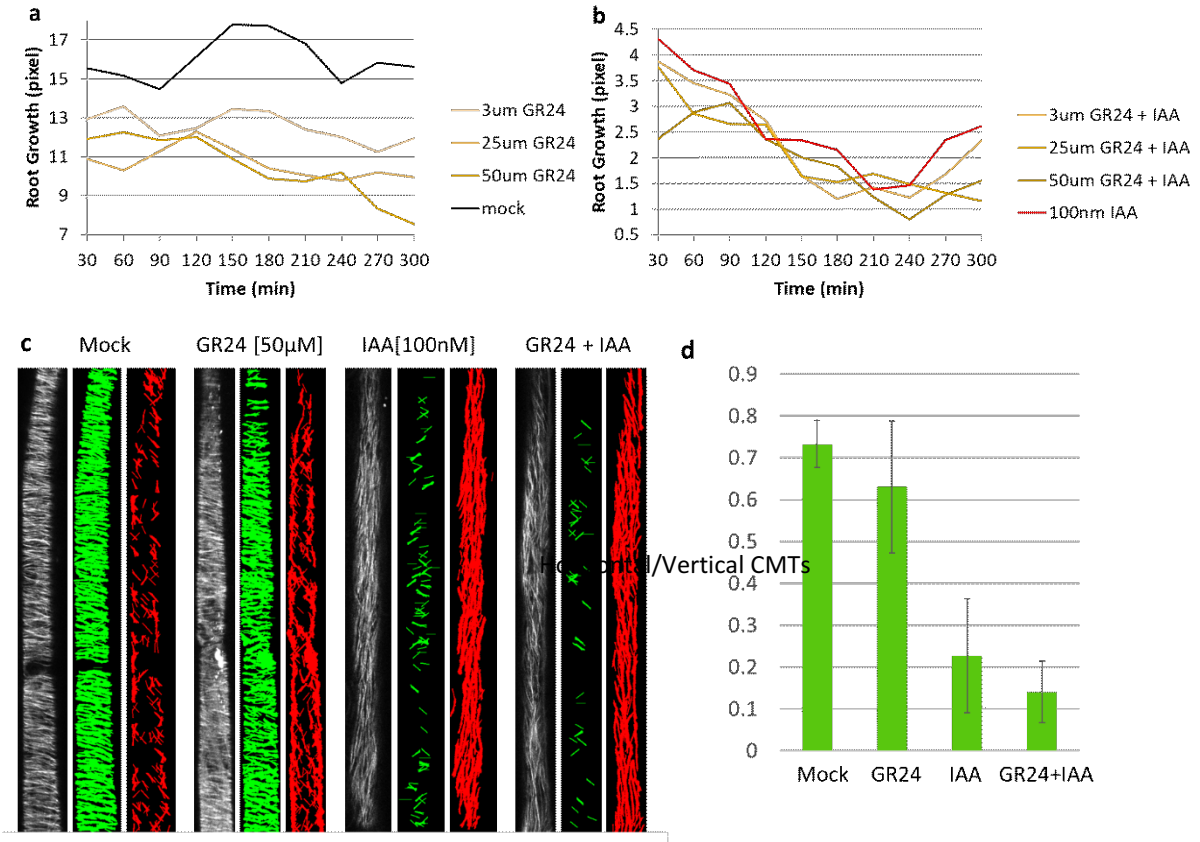


**Figure 1.** Strigolactone inhibited root growth and reoriented CMTs independently of auxin

**a-b**, Root growth tracked over time after GR24 of different concentrations (**a**) and co-treatment of GR24 and 100 nM IAA (**b**).

**c-d**, CMTs orientation in root elongating cells after 70 minutes incubation of indicated treatments. **c**, Max-projection of the Z-stack images were analyzed using Bioline script [1]. The horizontal CMTs were marked as green and vertical ones in red. **d**, quantification of CMTs intensity in horizontal orientation divided by that in vertical orientation using Bioline script.

## *2.4 Decrease of cell inner pressure by mannitol inhibited root growth and reoriented CMTs*

Besides phytohormones, we perturbed root growth by decreasing cell inner pressure (turgor) using a high osmoticum, mannitol. We observed that 150 and 300 mM mannitol for 1 hour caused a strong root growth inhibition (Figure 2a). Accordingly, CMTs were reoriented from horizontal to vertical (Figure 2b). Note that mannitol-induced CMT reorientation is different from auxin-induced ones. CMTs in later case are rather homogenously vertical in a cell (Figure 1c), while in the former case CMTs are clustered in the center of the cells with the surrounding CMTs being still horizontal (Figure 2b). The pattern of mannitol-induced CMT reorientation

is unique. We think that the vertical CMTs clustering in the center is possibly caused by the contraction of physically-linked malformed PM, while the surrounding horizontal CMTs may be due to a dynamic recovery following a sudden osmotic change. Overall, perturbation of root growth by decreasing turgor using mannitol leads to CMT reorientation, supporting that CMT reorientation responds to cell growth itself.

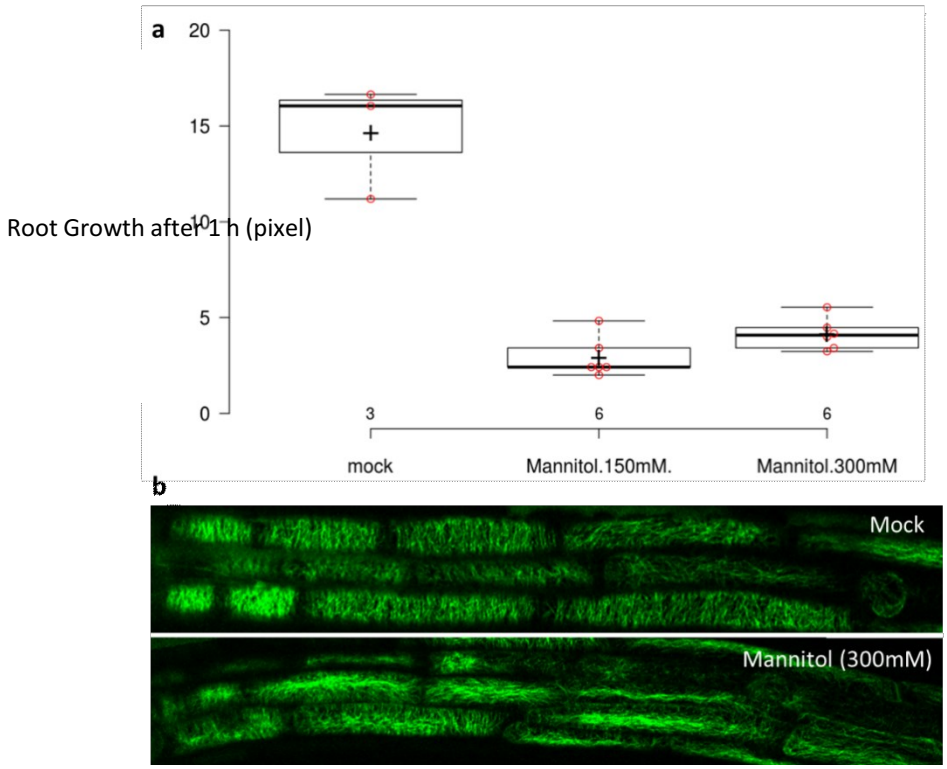


**Figure 2.** Mannitol inhibits root growth and reorients CMTs

**a**, Root growth amount after 1 hour treatment of mannitol at 150 and 300 mM.

**b**, CMTs imaged in root epidermal cells ranging from transition and elongation zone after 70 minutes incubation of 300 mM mannitol. Max projection of Z-stack images were shown.

## *2.5 Modulation on cell wall properties by pectin methylesterase inhibitor*

### *EGCG inhibited root growth and reoriented CMTs*

As another way to manipulate root growth, we tried to perturb cell wall elasticity by applying pectin methylesterase inhibitor EGCG. We found that EGCG inhibited root growth, though less than auxin did (Figure 3a). Besides, EGCG treatment for 240 minutes caused a significant increase in the portion of longitudinal CMTs (Figure 3b-c). These again support a correlation between CMT reorientation and growth response after modulation on cell wall properties.

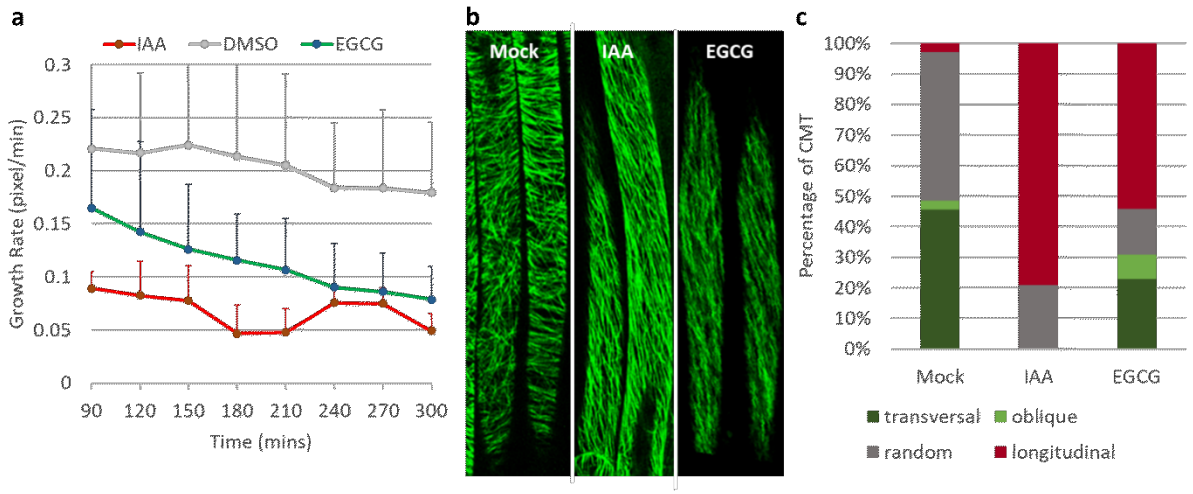


**Figure 3.** EGCG inhibited root growth and reoriented CMTs

**a**, Root growth tracked over time after treatments of 100 nM IAA or 50 μM EGCG. Both EGCG and IAA inhibited root growth.

**b-c**, CMTs imaged in root epidermal elongating cells expressing MAP4-GFP after 240 minutes incubation of 100 nM IAA or 50 μM EGCG (**b-c**). The max projection of Z-stack images were shown (**b**). The percentage of the number of cells containing the transversal, oblique, random and longitudinal CMTs after indicated treatments using Bioline script [1] (**c**).

## *2.6 Conclusions*

CMT reorientation have been observed after various stimuli including light [2], mechanical cues [3, 4], and the phytohormone brassinosteroids [5]. Often it is correlated with growth regulation. Here, we tried to manipulate root growth by a hormone strigolactone, mannitol which decreases turgor pressure, pectin methylesterase inhibitor EGCG which regulates cell wall elasticity. We found that all those substances regulated root growth and led to CMT reorientation. These support further our discussion in Chapter 1.4 that CMTs respond to growth itself.

## *2.7 References*

1. Adamowski, M., Li, L. & Friml, J. Reorientation of cortical microtubule arrays in the hypocotyl of Arabidopsis thaliana is induced by the cell growth process and independent of auxin signaling. *Int. J. Mol. Sci.* **20**, 3337 (2019).

2. Sambade, A., Pratap, A., Buschmann, H., Morris, R. J. & Lloyd, C. The influence of light on microtubule dynamics and alignment in the Arabidopsis hypocotyl. *Plant Cell* **24**, 192-201 (2012).

3. Hamant, O. *et al.* Developmental patterning by mechanical signals in Arabidopsis. *Science* **322**, 1650-1655 (2008).
4. Sampathkumar, A. *et al.* Subcellular and supracellular mechanical stress prescribes cytoskeleton behavior in Arabidopsis cotyledon pavement cells. *Elife* **3**, e01967 (2014).
5. Catterou, M. *et al.* Brassinosteroids, microtubules and cell elongation in Arabidopsis thaliana. II. Effects of brassinosteroids on microtubules and cell elongation in the bul1 mutant. *Planta* **212**, 673-683 (2001).

# Chapter 3

## Cell surface and intracellular auxin signalling for $H^+$-fluxes in root growth

**Authors:** Lanxin Li[†1], Inge Verstraeten[†1], Mark Roosjen[2], Koji Takahashi[3,4], Lesia Rodriguez[1], Jack Merrin[1], Jian Chen[5,6], Lana Shabala[7], Wouter Smet[5,6], Hong Ren[8], Steffen Vanneste[5,9,10], Sergey Shabala[7,11], Bert De Rybel[5,6], Dolf Weijers[2], Toshinori Kinoshita[3,4], William M. Gray[8] and Jiří Friml[*1]

**Affiliations:**

[1] Institute of Science and Technology (IST) Austria – 3400 Klosterneuburg (Austria).

[2] Department of Agrotechnology and Food Sciences, Laboratory of Biochemistry, Wageningen University – 6708 WE Wageningen (the Netherlands).

[3] Institute of Transformative Bio-Molecules, Nagoya University, Division of Biological Science – 464-8602 Chikusa Nagoya (Japan).

[4] Graduate School of Science, Nagoya University – 464-8602 Chikusa Nagoya (Japan).

[5] Ghent University, Department of Plant Biotechnology and Bioinformatics – 9052 Gent (Belgium).

[6] VIB Center for Plant Systems Biology – 9052 Gent (Belgium).

[7] Tasmanian Institute of Agriculture, College of Science and Engineering, University of Tasmania – Hobart (Australia).

[8] Department of Plant & Microbial Biology, University of Minnesota – MN-55108, St. Paul (United States).

[9] Lab of Plant Growth Analysis, Ghent University Global Campus – Incheon 21985 (Republic of Korea)

[10] Department of Plants and Crops – HortiCell, Ghent University – 9000 Gent (Belgium).

[11] International Research Centre for Environmental Membrane Biology, Foshan University – 528000 Foshan (China)

*Correspondence to: jiri.friml@ist.ac.at

† These authors contributed equally to this work

## 3.1 Abstract

Growth regulation tailors plant development to its environment. A showcase is response to gravity, where shoots bend up and roots down[1]. This paradox is based on opposite effects of the phytohormone auxin, which promotes cell expansion in shoots, while inhibiting it in roots via a yet unknown cellular mechanism[2]. Here, by combining microfluidics, live imaging, genetic engineering and phospho-proteomics in *Arabidopsis thaliana*, we advance our understanding how auxin inhibits root growth. We show that auxin activates two distinct, antagonistically acting signalling pathways that converge on the rapid regulation of the apoplastic pH, a causative growth determinant. Cell surface-based TRANSMEMBRANE KINASE1 (TMK1) interacts with and mediates phosphorylation and activation of plasma membrane $H^+$-ATPases for apoplast acidification, while intracellular canonical auxin signalling promotes net cellular $H^+$-influx, causing apoplast alkalinisation. The simultaneous activation of these two counteracting mechanisms poises the root for a rapid, fine-tuned growth modulation while navigating complex soil environment.

## 3.2 Introduction

Auxin, a major growth regulator in plants, acts oppositely in shoots and roots. In shoots, canonical/intracellular auxin TRANSPORT INHIBITOR RESPONSE1 (TIR1)/AUXIN-SIGNALING F-BOX (AFB) receptors by downstream transcriptional regulation activate $H^+$-pumps to acidify the apoplast a promote cell elongation[3,4], in accordance with the Acid Growth Theory, which postulates that low apoplastic pH promotes growth[5]. In roots of many species including *Arabidopsis*, auxin inhibits growth. These contrasting responses are the basis for positive versus negative bending of roots and shoots in response to gravity and light[1]. The inhibitory auxin effect in roots also involves TIR1/AFB receptors but its rapid timing points towards an unknown non-transcriptional signalling branch[6]. Besides, a cell surface-based pathway involving TMK1 regulates development[7], including differential growth in the apical hook[8], while its role in auxin-regulated root growth remains unclear. Hence, the auxin signalling mechanism and the downstream processes for regulating root growth remain elusive.

In this study, we revealed antagonistic action of intracellular TIR1/AFB and cell surface TMK1 auxin signalling converging on regulation of apoplastic pH, which we confirm as the key cellular mechanism allowing immediate and sensitive root growth regulation.

### *3.3 Growth inhibition correlates with $H^+$-influx*

Auxin rapidly inhibits root growth through a non-transcriptional branch of TIR1/AFB signalling[6]. Although several cellular processes, including cortical microtubule (CMT) reorientation[9,10], vacuolar fragmentation[11] and apoplastic pH changes[12-14] have been implicated, the causal mechanism remains unidentified.

We critically re-evaluated the kinetics of these processes using the vRootchip[6] (Extended Data Fig. 1a) in combination with vertical confocal microscopy[15]. Growth inhibition by 10nM natural auxin indole-3-acetic acid (IAA) was observed within 30s[6]. In contrast, less than 5% CMTs in elongating epidermal cells reoriented after 1min even at 100nM IAA and pharmacological inhibition of this reorientation had no effect on auxin-induced growth inhibition (Extended Data Fig. 1b-f). Similarly, we could not detect changes in vacuolar morphology in elongating cells even after 30min of 100nM IAA treatment (Extended Data Fig. 1g). These results argue against direct involvement of CMT reorientation and vacuole constriction in the rapid auxin-triggered growth inhibition.

To evaluate the kinetics of apoplastic pH, we applied a membrane-impermeable ratiometric pH indicator: 8-hydroxypyrene-1,3,6-trisulfonic acid (HPTS) and imaged apoplastic pH, while simultaneously tracking root tip growth. We detected an apoplastic pH gradient[12] in the root, decreasing from transition to elongation zone but regardless of their position, all cells showed a rapid (30s) apoplastic pH increase (Fig. 1a, b and Extended Data Fig. 2a). This provides higher temporal and spatial resolution to previous observations of auxin-induced apoplast alkalinisation[12] and reveals that auxin-triggered alkalinisation and root growth inhibition occur simultaneously (Fig. 1b). The pH increase was robust and extended to the external medium (Extended Data Fig. 2b). Using the *PM-Cyto* reporter for monitoring intracellular pH[16], we also detected simultaneous (30s) decrease in the PM-adjacent cytosolic pH after 5nM IAA treatment (Fig. 1c). Concomitant apoplastic increase and intracellular pH decrease implies $H^+$-influx into the cells. This was confirmed using non-invasive microelectrodes monitoring direct net $H^+$-exchange across the plasma membrane (PM) of elongating root epidermis cells after IAA treatment (Extended Data Fig. 2c), consistent with similar observations in root hair cells[17].

Overall, auxin triggers rapid apoplast alkalinisation by increasing the net cellular $H^+$-influx. Spatial and temporal correlation with root growth inhibition suggests apoplast alkalinisation as the underlying cellular mechanism.

### *3.4 Apoplastic pH regulates root growth*

To investigate the causal relationship between apoplast alkalinisation and root growth inhibition, we manipulated the apoplastic pH by changing the medium pH (Extended Data Fig. 2d, e) and monitoring the impact on root growth. This extended previous observations of prolonged (2.5h) external extreme pH manipulation[12]. Replacement of the basal medium at pH 5.8 by more alkaline (pH 6.15) medium caused instant reduction of root growth; the growth rate restored rapidly after washout with the original pH 5.8 medium (Fig. 1d, e). Gradual alkalinisation of the medium resulted in gradual root growth inhibition (Extended Data Fig. 2f). Replacing basal medium by more acidic (pH 5.1) medium increased root growth instantly and washout restored original growth (Fig. 1f, g).

Thus, exogenous manipulation of apoplastic pH has immediate and reversible effects on root growth, with alkaline pH inhibiting and acidic pH promoting growth. This strongly supports that auxin-induced apoplast alkalinisation is the key downstream cellular mechanism for rapid root growth inhibition.

### *3.5 Auxin triggers PM $H^+$-ATPases activation*

The auxin effect on apoplast alkalinisation occurs too fast to involve transcriptional regulation as also confirmed by pharmacological interference with translation (cycloheximide) or transcription (cordycepin) (Extended Data Figure 3a, b). To gain insights into the underlying mechanism, we mined recent datasets from Mass Spectroscopy (MS)-aided phospho-proteomics in WT root tips treated for 2min with 100nM IAA[18]. Among the differentially phosphorylated targets were two PM $H^+$-ATPases: AHA1 and AHA2. Multiple putative auxin-regulated phosphorylation sites were identified in the auto-inhibitory C-terminal region, leading to both activation and deactivation of $H^+$-pump activity[19] (Fig. 2a and Supplemental Table 1).

To test whether auxin changes the activity of PM $H^+$-ATPases in roots, we performed an ATP hydrolysis assay measuring the hydrolytic release of inorganic phosphate from ATP, representing the activity of PM $H^+$-ATPases. After 1h treatment with 100nM IAA, we detected increased ATP hydrolysis activity in root protein extracts (Fig. 2b). This suggests that auxin activates $H^+$-pumps, which should, however, lead to apoplast acidification instead of the observed alkalinisation (see Fig. 1b).

We next reanalysed the phospho-proteomics data specifically for the phosphorylation

of $Thr^{947}$ in AHA2, a well-known activation site[19]. $Thr^{947}$ was significantly more phosphorylated after IAA treatment (Fig. 2c). To confirm this, we used an antibody against the AHA2 catalytic domain and the anti-pT947-AHA2 antibody revealing that 10nM IAA induced phosphorylation of $Thr^{947}$ in 10min (Extended Data Fig. 3c). Thus, auxin induces AHA2 phosphorylation leading to its activation.

Our results show that auxin rapidly induces AHA phosphorylation leading to $H^+$-pump activation in roots. This is similar to shoots[20,21], however, is opposite to the observed auxin-induced $H^+$-influx (see Fig. 1), suggesting that in roots $H^+$-pump activation may act antagonistically to auxin-triggered apoplast alkalinisation.

## *3.6 $H^+$-ATPases counteract apoplast alkalinisation*

To better understand the role of $H^+$-pump activation during auxin-triggered apoplast alkalinisation, we used the fungal toxin Fusicoccin (FC), which stabilizes the pump in the activated form[19] without affecting transcriptional auxin signalling (Extended Data Fig. 3d). FC caused rapid apoplast acidification and promoted root growth[12] (Extended Data Fig. 3e, f), opposite to auxin. When FC and IAA were applied simultaneously or sequentially, we observed an intermediate response proportional to the auxin/FC ratio (Fig. 2d and Extended Data 3e-k). These suggest that FC-triggered $H^+$-ATPase activation and IAA-triggered apoplast alkalinisation act antagonistically.

To test this genetically, we analysed auxin response of loss- and gain-of-function *aha* mutants. Single *aha1* and *aha2* mutants showed no growth defects (Extended Data Fig. 3l), while the double mutant is embryo-lethal[19]. To overcome the redundancy, we used a synthetic trans-acting siRNA targeting *AHA1/2/7/11* (*AtTAS1c-AHA*), expressed from the *PIN2* promoter[22]. *AHAs* were downregulated in two independent transgenic lines (Extended Data Fig. 3m) and both were hypersensitive to auxin for apoplast alkalinisation (Fig. 2e) and root growth inhibition (Extended Data Fig. 3n). In contrast, constitutive activation of AHA1 in the *ost2-3D* mutant resulted in decreased auxin sensitivity of apoplastic pH (Fig. 2e) and root growth (Extended Data Fig. 3n).

These observation show that $H^+$-ATPase activation antagonizes auxin-induced apoplast alkalinisation in roots.

## *3.7 TMK1 interacts with $H^+$-ATPases*

To address how auxin signalling regulates apoplastic pH, we performed co-immunoprecipitation (co-IP) followed by MS-assisted identification of proteins associated with either the TIR1/AFB1 receptor or PM-localized TMK1 auxin signalling component[7] (Extended Data Fig. 4a). For TIR1/AFB1 this approach did not reveal any relevant components, while for TMK1, AHAs were among the top enriched associated peptides (Extended Data Fig. 4b-d and Supplemental Table 2, 3).

We verified the interaction between AHAs and TMK1 by co-IP from *pTMK1::TMK1-FLAG* (Fig. 3a) and *pAHA2::AHA2-GFP* (Extended Data Fig. 4e) roots. From TMK1-FLAG pulldowns, we detected associated AHA2 and reciprocally from the AHA2-GFP pulldowns, we detected TMK1. Additional *in vivo* verification was provided by bimolecular fluorescent complementation (BiFC) in tobacco leaves co-transformed with TMK1 and AHA2 (Fig. 3b and Extended Data Fig. 4f,g).

These observations show that TMK1, the component of cell surface auxin signalling, interacts with PM $H^+$-ATPase.

## *3.8 TMK1 mediates auxin effect on $H^+$-ATPases*

To test the role of TMK1 in $H^+$-ATPase phosphorylation, we performed phospho-proteomic analysis in *tmk1-1* roots compared to WT and detected strong hypo-phosphorylation of AHAs (Fig. 3c and Supplemental Table 1) suggesting TMK1 involvement in $H^+$-ATPases phosphorylation.

To verify this, we cloned *p35S::TMK1-HA* and two kinase-dead versions with mutations in the ATP binding site: $TMK1^{K616E}$ or $TMK1^{K616R}$. Transient overexpression of the wild type ($TMK1^{WT}$), but not the kinase-dead constructs resulted in rapid wilting of tobacco leaves (Extended Data Fig. 5a), an effect consistent with PM $H^+$-ATPase activation[23]. We further generated *Arabidopsis* dexamethasone (DEX)-inducible gain-of-function lines. Compared to $TMK1^{WT}$, root extracts of $TMK1^{K616R}$ did not show IAA-induced phosphorylation of $AHA^{Thr947}$ (Extended Data Fig. 5b). Importantly, *in vitro* [$\gamma$-$^{32}$P]-ATP kinase assays confirmed that $TMK1^{WT}$, but not kinase-dead $TMK1^{K616E}$ directly phosphorylates the AHA2 C-terminal domain (Fig. 3d and Extended Data Fig. 5c).

Next, we analysed different *tmk* loss-of-function mutants. We detected less auxin-induced AHA2 phosphorylation in *tmk1-1* single, *tmk1,3* and the stunted *tmk1,4* double mutant

roots (Fig. 3e and Extended Data Fig. 5d, e). Besides, the ATP hydrolysis assay showed that auxin-stimulated $H^+$-ATPase activity diminished in the *tmk1-1*, *tmk4-1* and *tmk1,4* roots (Fig. 3f).

Collectively, this demonstrates that active TMK1 mediates auxin-triggered phosphorylation and activation of $H^+$-ATPases in roots.

### *3.9 TIR1 and TMK1 converge on pH regulation*

Our results show that TMK1 directly phosphorylates and activates PM $H^+$-ATPases leading to apoplast acidification (see Fig. 2 and 3). This is opposite to the observed auxin-induced apoplast alkalinisation leading to growth inhibition (see Fig. 1) prompting us to address the underlying signalling mechanism.

*aux1-100* mutants in the auxin influx transporter AUXIN RESISTANT1 (AUX1) that are impaired in uptake of IAA[24] were less sensitive to auxin, both for growth inhibition[6] (Extended Data Fig. 6b, d) and apoplast alkalinisation (Extended Data Fig. 6a, c) suggesting requirement of intracellular auxin perception.

Given that intracellular TIR1/AFB receptors mediate auxin-triggered rapid growth inhibition[6], we evaluated apoplastic pH in parallel to growth in the *tir1 afb2 afb3* (*tir triple*) mutant. *tir triple* roots were resistant to IAA in both apoplast alkalinisation and growth inhibition (Fig. 4a and Extended Data Fig. 6e). AFB1 with its predominant cytosolic localization was proposed to be the major auxin receptor mediating auxin effect on growth and membrane depolarization[25,26]. We found that both TIR1 and AFB1 contribute to this regulation with *tir1-10* more auxin-resistant in the long term, while *afb1-3* showed pronounced resistance for rapid auxin effects (Extended Data Fig. 6h-k). We also applied the PEO-IAA anti-auxin to block downstream TIR1/AFB signalling[27]. Simultaneous addition of 10µM PEO-IAA and 5nM IAA prevented apoplast alkalinisation and growth inhibition (Extended Data Fig. 6f, g). We also took advantage of the cvxIAA-ccvTIR1 system, in which the engineered concave (ccv) TIR1 receptor cannot interact with natural IAA, but only with a synthetic convex (cvx) IAA, allowing specific activation of TIR1/AFB signalling[28]. Application of 50nM cvxIAA resulted in apoplastic alkalinisation in *ccvTIR1* plants (Fig. 4b), confirming that specific activation of TIR1 is sufficient to trigger apoplast alkalinisation. These approaches demonstrate involvement of intracellular TIR1/AFB receptors in auxin-induced apoplast alkalinisation.

This effect is counteracted by the cell surface TMK1-mediated $H^+$-ATPase activation for apoplast acidification and growth promotion. Indeed, in the steady state, TMK1 is

redundantly required for root growth as demonstrated by shorter roots in *tmk* mutants[7] (Extended Data Fig. 6l). In response to low concentrations of auxin, *tmk1*-related mutants were hypersensitive (Fig. 4c), while overexpressing TMK1 (*pUBQ10::TMK1-3HA*) led to a slight auxin resistance (Extended Data Fig. 6m). This resembles the corresponding loss- and gain-of-function *aha* mutants (see Fig. 2) providing additional support for the antagonistic, growth-promoting role of TMK-mediated AHA activity.

We also created a *tmk1 tir1* double mutant and analysed the auxin effect on apoplastic pH and root growth. As expected, *tmk1 tir1* mutants showed intermediate auxin sensitivity compared to the single mutants both for growth and apoplastic pH (Fig. 4d, e and Extended Data Fig. 6n, o).

Collectively, we propose that auxin activates two antagonistic signalling pathways: (i) cell surface TMK1-mediated $H^+$ export acidifying apoplast and (ii) more dominant, intracellular TIR1/AFB-dependent apoplast alkalinisation leading to rapid growth inhibition (Fig. 4f).

## *3.10 Conclusions*

Our findings provide novel insights into a long-standing question how plant root growth is regulated. In particular, we address the old mystery of opposite growth regulation in shoots and roots by the phytohormone auxin and we also clarify the downstream cellular mechanism of auxin-triggered root growth inhibition.

Auxin regulates root growth very rapidly, utilizing a non-transcriptional branch of a signalling pathway downstream of intracellular TIR1/AFB receptors[6]. The same branch mediates apoplast alkalinisation, which we confirm as the causative cellular mechanism for root growth regulation, thus extending the classical Acid Growth Theory also for root growth inhibition.

Remarkably, auxin-induced apoplast alkalinisation in roots does not occur through regulation of PM $H^+$-ATPases as observed in shoots, where the TIR1/AFB transcriptional auxin signalling leads to PM $H^+$-ATPase activation and apoplast acidification[4,20]. Instead, in roots, PM $H^+$-ATPases are phosphorylated and activated by the cell surface TMK1-based auxin signalling, which leads to apoplast acidification. This mechanism, acts antagonistically to the more dominant TIR1/AFB-mediated alkalinisation.

A key open question concerns the downstream mechanism, by which TIR1/AFB signalling mediates apoplast alkalinisation. A plausible scenario would be a rapid increase in

$H^+$ permeability across the PM, which is intertwined with changes in PM potential[25] (Extended Data Fig. 7a-c). Such auxin-triggered $H^+$-influx cannot be easily explained by $IAA^-/2H^+$ symport via the AUX1 influx carrier as proposed[17] (Extended Data Fig. 7d) and does not seem to require the PM-localized receptor-like kinase FERONIA, a mediator of the rapid apoplast alkalization in response to Rapid ALkalization Factor 1 (RALF1)[29] as evidenced by normal auxin-induced rapid root growth inhibition in the mutant (Extended Data Fig. 8). On the other hand, it may involve previously reported[14] auxin-triggered cytosolic $Ca^{2+}$ transients (Extended Data Fig. 9). Another persistent mystery is the auxin perception mechanism for the TMK1 pathway. Does this occur via direct activation of TMK1 by auxin or through another yet to be established auxin receptor?

With cell surface-based TMK1 activating $H^+$-pumps and intracellular TIR1/AFB signalling causing net cellular $H^+$-influx, two auxin-triggered mechanisms converge on regulation of extracellular pH, which directly determines root growth. This seemingly counterproductive simultaneous 'gas and brake' action presumably poises the root tip for rapid and flexible directional growth changes during the challenging task to navigate through complex soil environments.

## *3.11 Figures and Legends*

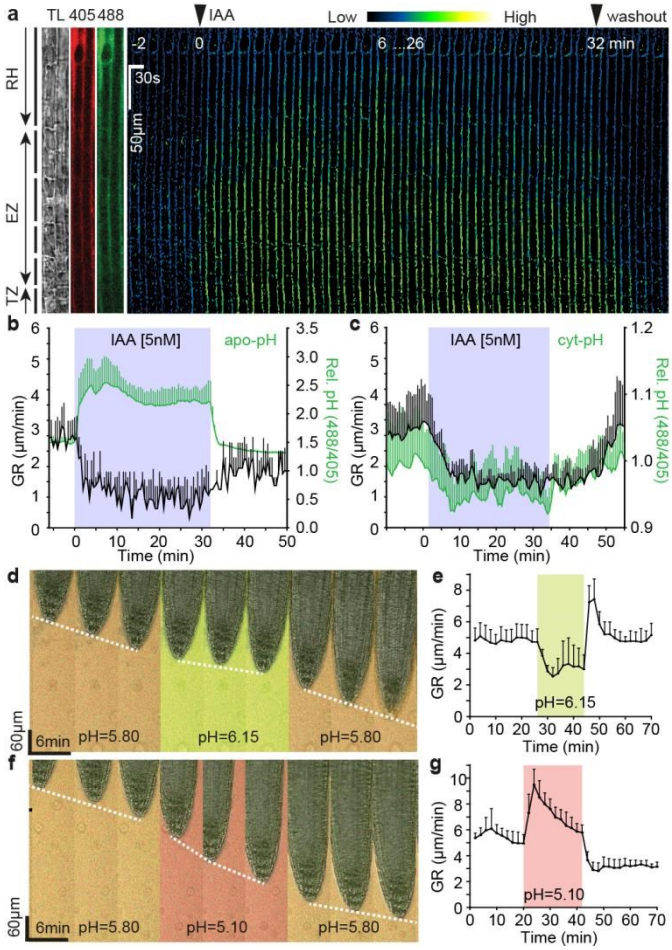


**Figure 1. Auxin rapidly inhibits root growth by apoplast alkalinisation.**

**a**, Time-lapse of apoplastic pH in 5nM IAA treated root tip epidermal cells followed by washout in vRootchip. Ratiometric image (488nm/405nm) of HPST staining to monitor pH in Root hair (RH), elongation (EZ) and transition zone (TZ). TL is transmitted light. **b,** Quantification of apoplastic pH and growth rate (GR) in the EZ following 5nM IAA and washout as in (**a**). Mean of 4 roots+SD. **c**, Quantification of cytosolic pH (using *PM-Cyto* reporter) and GR in the EZ upon 5nM IAA in vRootchip. Mean of 3 roots+SD. **d-g**, Root growth response to alkaline (pH 6.15) (**d**) or acidic medium (pH 5.10) (**f**). The white dotted line tracks the root tip over time. Quantifications of GR in **d** ($n$=8 roots) (**e**) and **f** ($n$=7 roots) (**g**). Shaded areas represent the duration of treatments. Mean+SD.

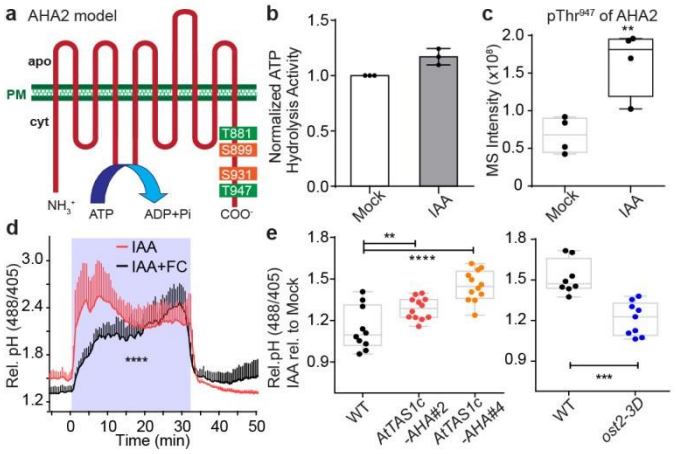


**Figure 2. Auxin-triggered H$^+$-ATPase activation counteracts auxin-triggered apoplast alkalinisation.**

**a**, AHA2 phospho-sites identified in the phospho-proteomic analysis of roots after 2min of 100nM IAA. Green reflects activation and orange inhibition of H$^+$-translocation. **b**, Quantification of ATP hydrolysis in roots treated 1h with 100nM IAA normalized to mock. Bars indicate mean of 3 biological replicates+SD. Unpaired t-test, *p=0.0138. **c,** Thr$^{947}$-phosphorylation of AHA2 in roots after 2min 100nM IAA treatment. n= 4 biological replicates. Box plot depicts minimum to maximum, mean±SD. Unpaired t-test, **p=0.0077. **d**, Activation of H$^+$-ATPases by 10µM FC affected 10nM IAA-induced alkalinisation. The shaded area represents the duration of the treatment. Mean of 4 roots+SD. ****p≤0.0001 from 0–32min, Two-way ANOVA. **e**, Apoplast alkalinisation in *AtTAS1c-AHA*#2 and #4 ($n$>9 roots) and *ost2-3D* gain-of-function roots ($n$>5 roots) after 30min 5nM IAA normalized to Mock. Box plots depict minimum to maximum, mean±SD. **p≤0.01, ***p≤0.001, ****p≤0.0001, One-way ANOVA.

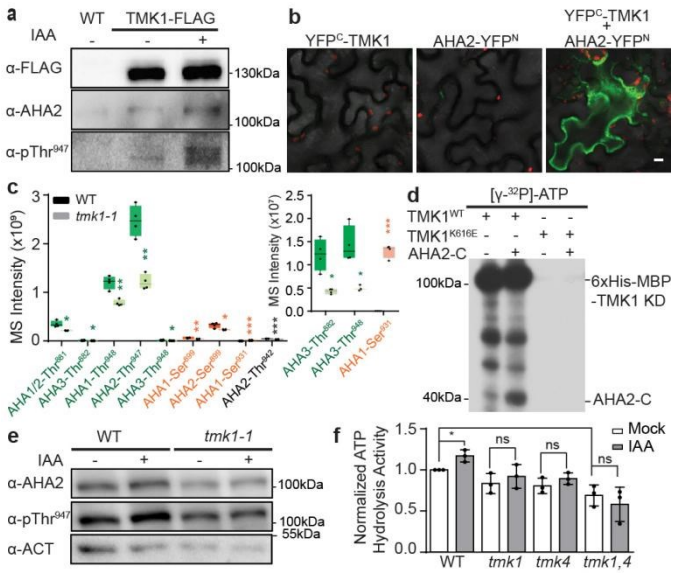


**Figure 3. TMK1 directly mediates auxin-induced H$^+$-ATPase activation.**

**a**, Co-immunoprecipitation (co-IP) of *pTMK1::TMK1-FLAG* roots after 30min 100nM IAA, followed by Western blot detection of AHA2 and pThr$^{947}$-AHA2. **b,** Bimolecular Fluorescent Complementation (BiFC) in *Nicotiana benthamiana* leaves transiently transformed either with *YFP$^C$-TMK1*, *AHA2-YFP$^N$* or both. Scale bar=10µm. **c**, Phospho-sites of AHAs in *tmk1-1* and WT. Green indicates known activation, orange inhibitory, and grey unknown function. The smaller insert shows sites with lower detected values. n=4 biological replicates, Box plot depicts minimum to maximum, mean±SD. Student t-test, *p≤0.05,**p≤0.01,***p≤0.001. **d,** *In vitro* kinase assay with [γ-$^{32}$P]-ATP, C-terminal AHA2 (AHA2-C) and the kinase domain of TMK1$^{WT}$ or kinase dead TMK1$^{K616E}$. AHA2-C is phosphorylated by TMK1$^{WT}$ and not by TMK1$^{K616E}$. Autophosphorylation of TMK1$^{WT}$ is also detected. **e,** Western blot analysis of AHA2 Thr$^{947}$ phosphorylation in WT and *tmk1-1* roots treated 1h with 100nM IAA. **f,** Auxin-induced ATP hydrolysis activity is impaired in *tmk* mutants (1h 100nM IAA). Levels were normalized to mock-treated WT. Mean of 3 biological replicates+SD. *p≤0.05, ns p>0.05, One-way ANOVA.

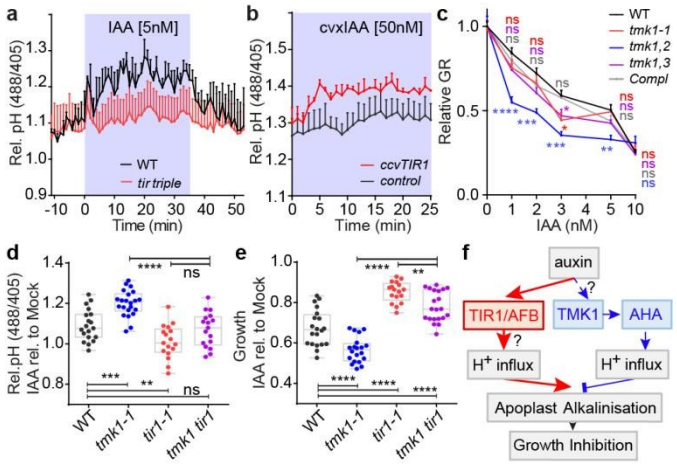


**Figure 4. Antagonistic TIR1/AFB and TMK1 signalling converge on apoplastic pH for growth regulation.**

**a**, Apoplastic pH response in *tir triple* mutant (red) compared to WT roots (black) in vRootchip. Mean of 3, 2 roots+SEM. **b,** Apoplastic pH analysis in *ccvTIR1* (red) compared to *control* (black) in response to cvxIAA in vRootchip. Mean of 2, 3 roots+SEM. Shaded area represents duration of treatment. **c**, Dose-response of root growth inhibition of *tmk1*-related mutants and *pTMK1::TMK1-FLAG* in *tmk1-1* (*Compl*). Relative growth is the ratio of auxin to mock GR in the same genotype. *n*>15 roots. *p≤0.05, **p≤0.01, ***p≤0.001, ****p≤0.0001, Welch ANOVA. **d-e**, Apoplastic pH (**d**) and root growth (**e**) measurement in *tmk1-1*, *tir1-1* and *tmk1 tir1* mutants in response to 5nM IAA for 50min (**d**) and 6h (**e**). *n*>16 roots. Box plot depicts minimum to maximum, mean±SD. ns p>0.05, **p≤0.01, ***p≤0.001, ****p≤0.0001, one-way ANOVA. **f**, Model for auxin-induced root growth regulation. An intracellular, non-transcriptional branch of TIR1/AFB signalling pathway (red) mediates rapid $H^+$-influx for apoplast alkalinisation and growth inhibition. Cell surface TMK1 activates $H^+$-pumps (AHAs) (blue) to acidify apoplast and promote growth.

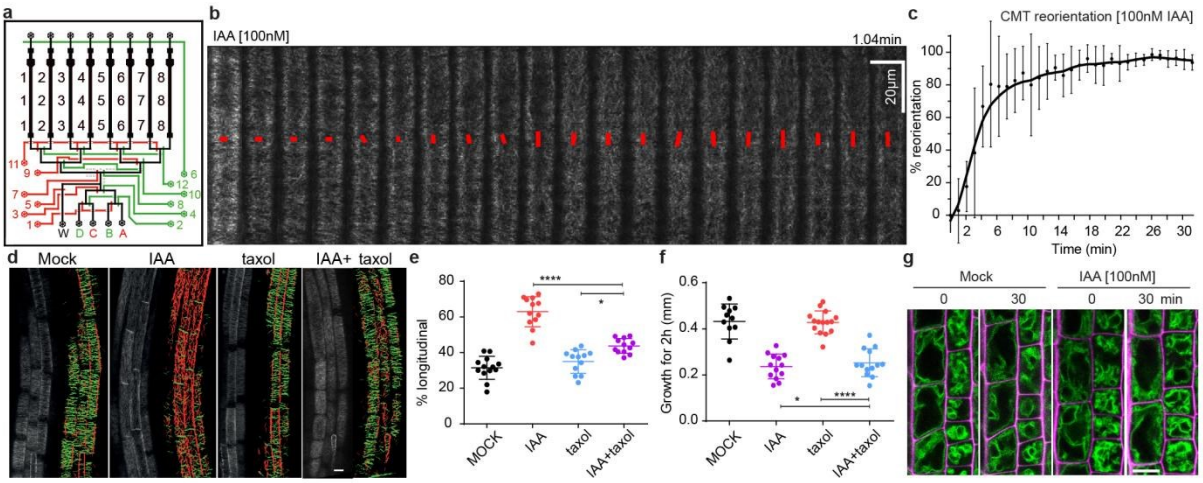


**Extended Data Figure 1. Investigation of CMT and vacuolar morphology in auxin-induced rapid root growth inhibition.**

**a**, Scheme of the modified vRootchip adding valve 6 and with adjusted valve routes. **b-c**, Dynamic cortical microtubule (CMT) transversal to longitudinal reorientation in response to 100nM IAA treatment. CMT were imaged at 6.25s intervals in elongating root epidermal cells in the *pEB1b::EB1b-GFP* marker line in vRootchip. Max Z-projection of 10 subsequent time frames was analysed using the FibrilTool. Average orientation of CMT is represented by the slope of the red line and the length of the line represents its anisotropy (**b**). (**c**) Quantification of CMT reorientation as in **b**. CMT reorientation at every time point is calculated as the difference in angle of that time point minus the initial time point angle divided by the difference in the angles of the initial time point and end time point (42min). Mean of 5 elongating cells±SD (**c**). **d-f**, Analysis of CMT reorientation in elongating root epidermal cells (**d, e**) and root growth (**f**) of *35S::MAP4-GFP* in response to 10nM IAA, 10µM taxol and IAA+taxol co-treatment. CMT orientation was analysed with the Bioline script. Green-colored CMTs mark transversal oriented CMT (angle between -45° and +45°), while red-colored CMTs indicate longitudinal orientation (angle between +45° and 135°). Scale bar=15µm (**d**). Percentage of longitudinal CMT. *n*>11 roots, One-way ANOVA (**e**). Growth on respective treatments after 2h. *n*>10 roots. Box plots depicts minimum to maximum, mean±SD. One-way ANOVA without modifications for multiple comparison (**f**). *p≤0.05, ****p≤0.0001. **g,** Vacuolar morphology tracked using *pSYP22::SYP22-YFP* (green signal) in elongating cells before and after 30min of 100nM IAA. Scale bar=15µm. Magenta signal represents propidium-iodide stained cell walls.

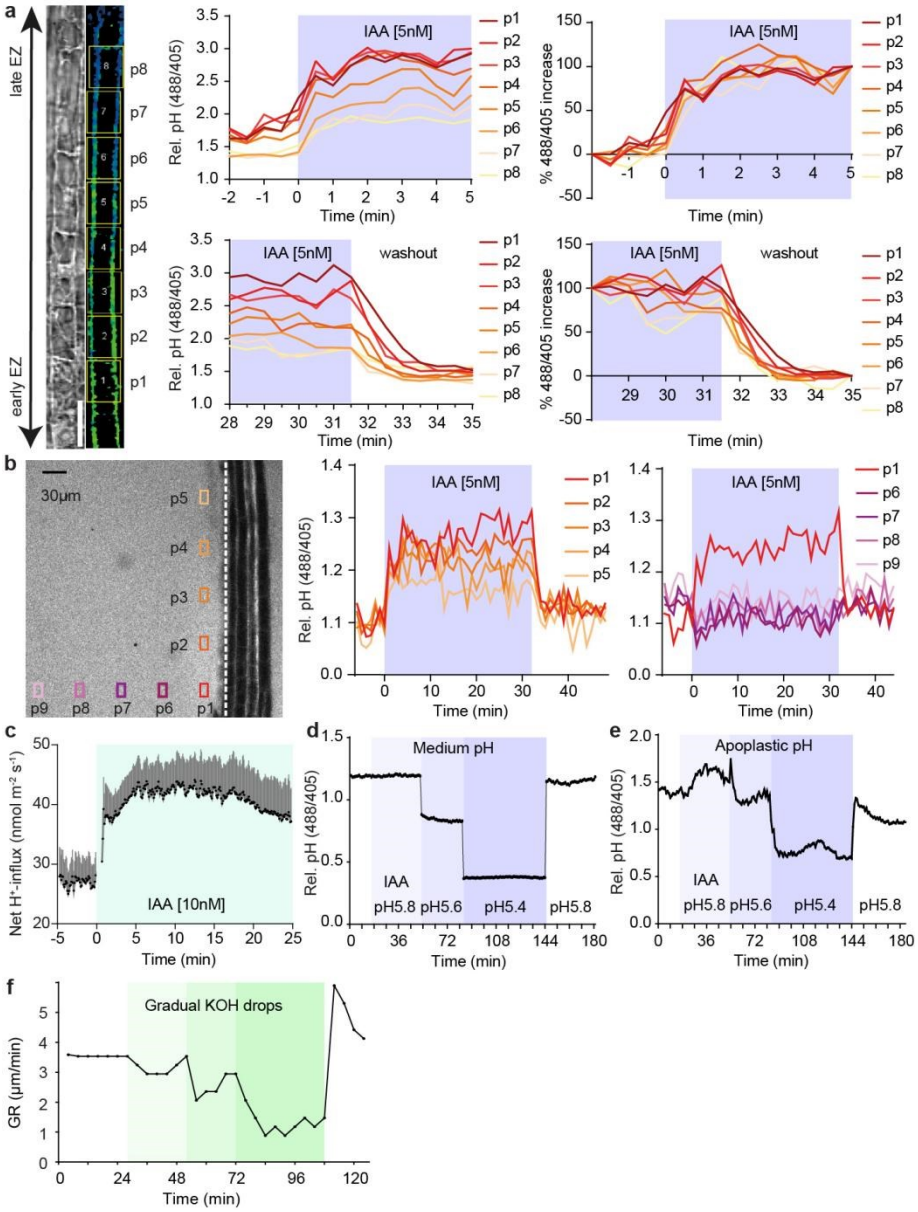


**Extended Data Figure 2. Apoplastic pH in auxin-induced rapid root growth inhibition.**

**a,** Apoplastic pH dynamics measured across the whole EZ (p1-p8) in vRootchip. The TL and blue-yellow scale image are from the same sample shown in **Fig. 1a**. Scale bar=30µm. The upper charts depict apoplastic pH in the indicated cells in response to 5nM IAA, and the lower charts represent the pH in response to washout. The right two charts show the speed at which each cell reaches its maximum pH change calculated as the difference between pH at a given time point and pre-stimulus pH, divided by the final pH change. **b,** Dynamics of root surface pH and medium pH in vRootchip. The left graph shows the elongation zone of the root. ROIs p1-p5 were chosen vertically along the root, 30µm away from the root surface indicated by the vertical white dotted line, while ROIs p6-p9 were distanced horizontally away from the root. The pH at the surface of the root (p1-p5) increased after IAA and recovered within 30s after

washout. In contrast, the pH away from the root surface did not change significantly (p6-p9). **c**, $H^+$-net influx measured by a non-invasive microelectrode before and after 10nM IAA treatment in the elongating zone of WT roots. Mean of 9 roots+SEM. **d-e**, Changes in medium pH (**d**) and apoplastic pH (**e**) after different medium pH exchanges in vRootchip. Sequentially used media: basal medium at pH 5.8, auxin-containing medium at pH 5.8, more acidic medium of pH 5.6, followed by pH 5.4 and again basal medium at pH 5.8. **f,** Quantification of root growth in response to gradual addition of KOH in the medium in the vRootchip. The greener the shade, the more KOH was added and followed by washout with initial pH 5.8 medium.

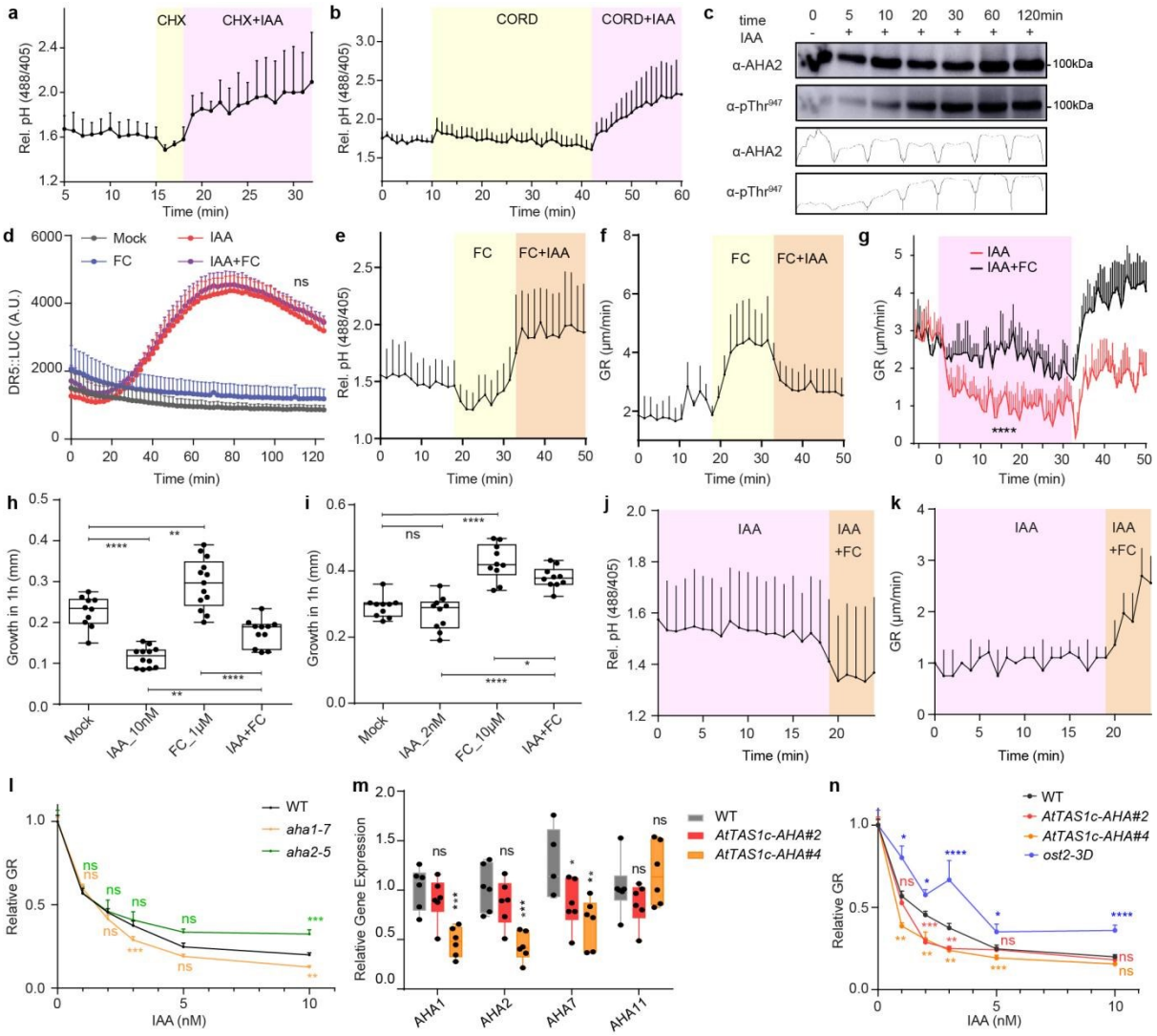


**Extended Data Figure 3. H$^+$-ATPase activation counteracts auxin-mediated apoplast alkalinisation and growth inhibition**

**a-b,** Apoplastic pH of WT elongating root cells pre-treated (yellow) with 1µM cycloheximide (CHX) for 3min (**a**), or 50µM cordycepin (CORD) for 32min (**b**) followed by addition of 5nM IAA (pink). Mean of 3 (**a**) or 4 (**b**) roots+SD. **c**, 10nM IAA induced Thr$^{947}$ phosphorylation in roots using AHA2 and pThr947 specific antibodies. Band intensities of the different lanes were quantified by the Gel Analysis function in ImageJ. **d**, Measurement of *DR5::LUC* luminescence intensity in the root tip after 10µM FC, 10nM IAA and IAA+FC co-treatment. $n$>3 roots. IAA and IAA+FC are significantly different from the mock ($p \leq 0.0001$). No significant difference between IAA and IAA+FC (ns, $p>0.05$). Two-way ANOVA. **e-k**, FC and IAA counteract each other. In vRootchip, addition of IAA still increased apoplastic pH (**e**) and inhibited root growth (**f**) in presence of FC, while addition of FC decreased apoplastic pH (**j**) and promoted root growth (**k**) in presence of IAA. Upon simultaneous addition of 10µM FC

and 10nM IAA, both apoplastic pH (**Fig 2d**) and root growth (**g**) were less affected than by IAA alone. Shaded area represents the duration of the treatments. Mean of 4 roots+SD. ****p≤0.0001 between IAA and IAA+FC from 0–31min (**g**), Two-way ANOVA. (**h-i**) Steady-state 1h root growth after FC, IAA and co-treatment was obtained by scanner. 1µM FC and 10nM IAA were used in (**h**) while 10µM FC and 2nM IAA were used in (**i**). *n*>9 roots. Box plot depicts minimum to maximum, mean±SD. ns p>0.05, *p≤0.05, **p≤0.01, ****p≤0.0001, One-way ANOVA (**h**, **i**). **l**, Dose-response of auxin-induced root growth inhibition of *aha* single mutants. *n*>22 roots. Relative GR is ratio between auxin-affected growth and mock for the same genotype. ns p>0.05, **p≤0.01, ***p≤0.001, Welch ANOVA. **m**, Quantitative Real-time PCR on the *AHA1,2,7,11* expression in root tips of *AtTAS1c-AHA#2* and *#4*. The expression level was normalized to *EF1α* as housekeeping gene. Mean of 6 biological replicates in 3 technical replicates+SD. Box plot depicts minimum to maximum, mean±SD. ns p>0.05, *p≤0.05, **p≤0.01, ***p≤0.001, One-way ANOVA. **n,** Dose-response of auxin-induced root growth inhibition of *AtTAS1c-AHA* lines and *ost2-3D* mutants reveals hypersensitivity and resistance respectively to IAA in comparison to WT (*n*>15 roots). Relative GR is calculated as mentioned in (**l**). ns p>0.05, *p≤0.05, **p≤0.01, ***p≤0.001, ****p≤0.0001, Welch ANOVA.

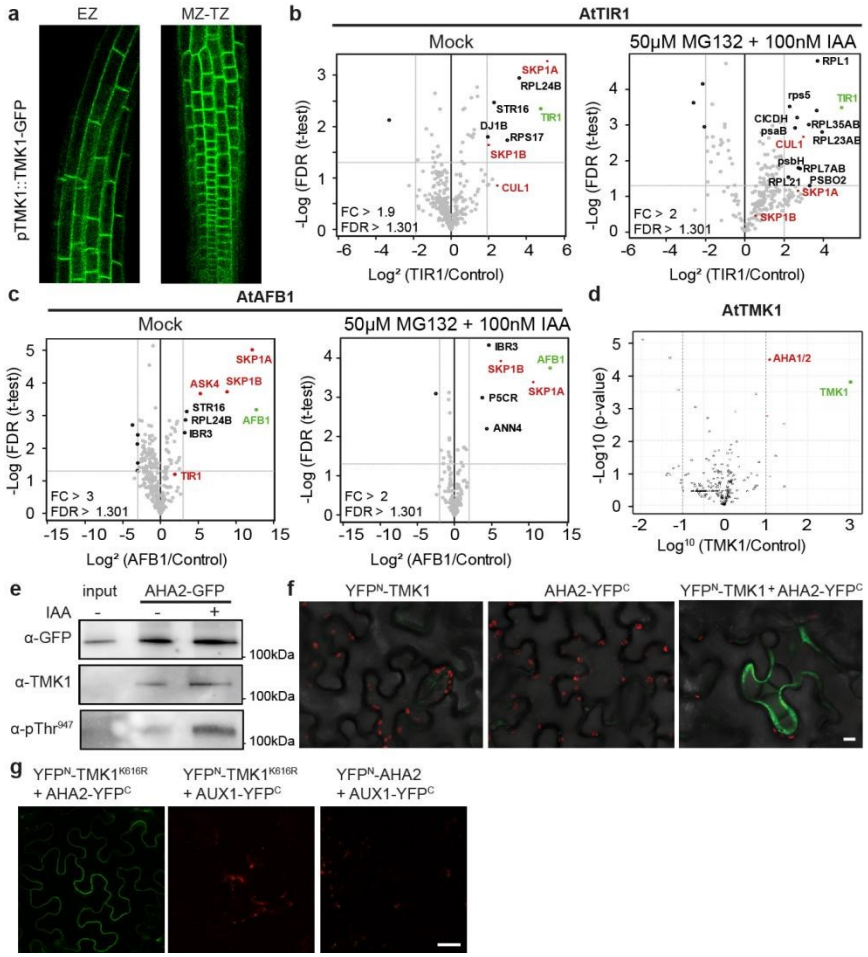


**Extended Data Figure 4. TMK1 interacts with PM H$^+$-ATPase.**

**a,** TMK1 expression pattern in the elongation zone (EZ), meristematic and transition zone (MZ-TZ) in the primary root shown by *pTMK1::TMK1-GFP*. Scale bar=60 µm. **b-c**, IP-MS/MS on *pTIR1::TIR1-VENUS* in *tir1-1* (**b**) and *pAFB1::AFB1-VENUS* in *afb1-3* (**c**) under mock condition compared to 1h 50µM MG132 pre-treatment and 2min 100nM IAA treatment. Proteins surpassing the threshold FDR of 0.05 are marked. Green depicts the respective bait protein and red depicts known members of the SCF E3 ubiquitin ligase complex. Pulldowns were performed in triplicate, LFQ analysis. **d**, IP-MS/MS on *pTMK1::TMK1-GFP*. Peptides corresponding to AHA1/2 are shown in red. p-values are calculated based on three biological replicates using two-sided t-tests. **e**, Co-IP of *pAHA2::AHA2-GFP* roots, followed by Western blot detection of TMK1 and Thr$^{947}$-phosphorylated AHA2 after 100nM IAA for 30min. Auxin did not affect interaction, but induced AHA2-phosphorylation. Input of *pAHA2::AHA2-GFP* roots was the control. **f,** Bimolecular Fluorescent Complementation (BiFC) in *Nicotiana benthamiana* leaves transiently transformed with the reciprocal controls for **Fig. 3b**: *YFP$^N$-TMK1*, *AHA2-YFP$^C$* or both. Scale bar=10µm.

**g,** Demonstration of specific interaction between *YFP$^{N}$-TMK1$^{K616R}$* and *AHA2-YFP$^{C}$* as no complementation was observed in the leaves expressing *YFP$^{N}$-TMK1$^{K616R}$* and *AUX1-YFP$^{C}$* or leaves expressing *YFP$^{N}$-AHA2* and *AUX1-YFP$^{C}$*. Scale bar=100μm.

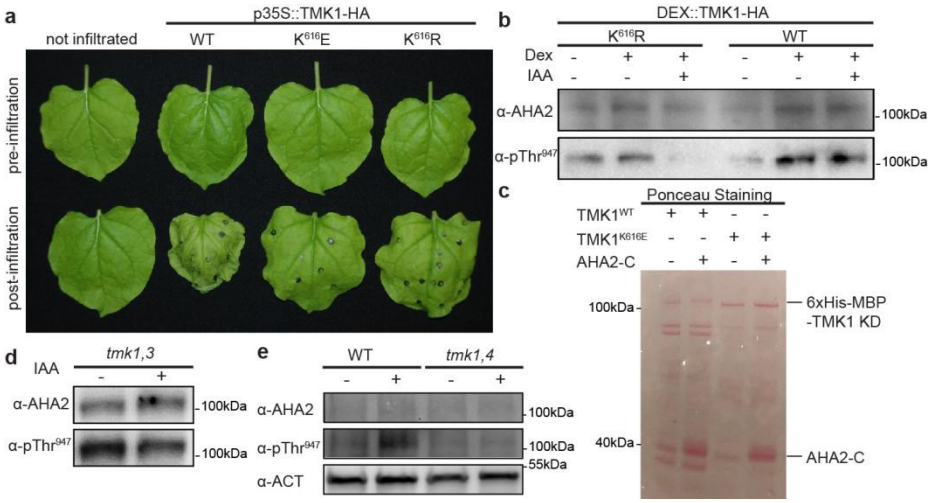


**Extended Data Figure 5. TMK1 directly phosphorylates PM H$^+$-ATPases.**

**a**, Wilting *N. benthamiana* leaves that transiently express *TMK1$^{WT}$* and ATP-site mutated forms *TMK1$^{K616E\ or\ K616R}$*. **b**, Western blot analysis of the AHA2 levels and the Thr$^{947}$ phosphorylation in roots of *DEX::TMK1$^{WT\ or\ K616R}$-HA* treated +/- DEX (30µM for 24h) and +/- IAA (100nM for 1h). **c,** Ponceau-stained SDS-PAGE gel as loading control for *in vitro* kinase assay with [γ-$^{32}$P]-ATP, substrate C-terminal AHA2 (AHA2-C) and the intracellular kinase domain of TMK1$^{WT}$ or kinase dead TMK1$^{K616E}$. **d-e**, Western blot detection of AHA2 levels and Thr$^{947}$ phosphorylation in *tmk1,3* roots (**d**) or *tmk1,4* roots (**e**) treated with 100nM IAA for 1h. WT control for (**d**) is shown in **Fig. 3e**.

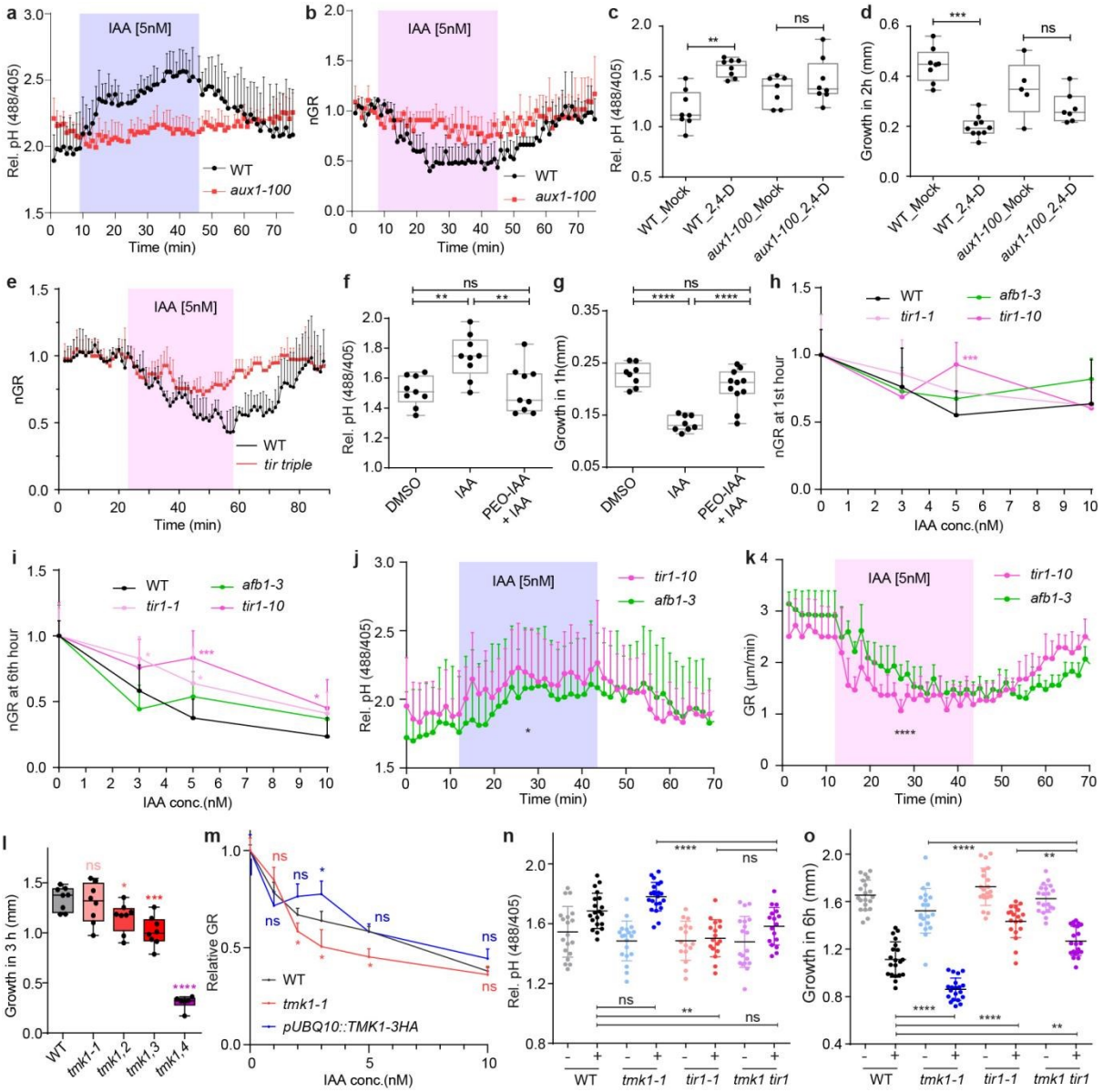


**Extended Data Figure 6. Cytosolic TIR1/AFB mediates rapid apoplast alkalinisation and root growth inhibition.**

**a-b**, Apoplastic alkalinisation (**a**) and root growth inhibition (**b**) in response to IAA measured in *aux1-100* mutant compared to WT roots in vRootchip. Mean of 3 roots+SD. ****p ⩽ 0.0001, Two-way ANOVA. **c-d**, Apoplastic alkalinisation (**c**) and root growth inhibition (**d**) in response to 2,4-D in *aux1-100* mutant compared to WT roots. Steady state pH measured 30min after 100nM 2,4-D treatment. Mean of >6 roots+SD, One-way ANOVA (**c**). (**d**) Growth obtained in 2h was captured by scanner. Mean of >4 roots+SD, One-way ANOVA. ns p>0.05, **p≤0.01, ***p≤0.001. **e**, Root growth of *tir triple* mutants compared to WT in response to 5nM IAA in the vRootchip. Mean of 3, 2 roots+SD. ****p≤0.0001, two-way ANOVA. **f-g**, Apoplastic pH (**f**) and root growth (**g**) after 10μM PEO-IAA and 5nM IAA. The steady state

pH was measured 30min after treatments, while the root growth obtained in 1h was recorded by scanning. Mean of >7 roots+SD. ns p>0.05, **p≤0.01, ****p≤0.0001, One-way ANOVA. **h-i**, Dose-response of auxin-induced root growth inhibition of *tir1-1, tir1-10* and *afb1-3* mutants reveals slight resistance to 5nM IAA in comparison to WT (*n*>6 roots). Relative GR is calculated as the ratio of GR at 1h (**h**) or 6h (**i**) after IAA treatments relative to mock-treated GR of the same genotype. Mean+SD. *p≤0.05, ***p≤0.001, One-way ANOVA. **j-k**, Apoplastic pH (**j**) and root growth (**k**) analysis comparing *tir1-10* null mutant and *afb1-3* mutants in response to IAA in vRootchip. Shaded area represents the duration of the treatment. Mean of 4 roots for each treatment+SD. p≤0.0001 (**j**) and p≤0.05 (**k**), Two-way ANOVA. **l**, Steady-state root growth over 6h in *tmk1*-related mutants. n=6 roots for *tmk1,4*; n>26 for others. Mean+SD. Box plot depicts minimum to maximum, mean±SD. ****p≤0.0001, One-way ANOVA. **m**, Dose-response of auxin-induced root growth inhibition of *pUBQ10::TMK1-3HA* compared to WT and *tmk1-1*. Relative GR is the ratio between auxin-affected growth to the mock growth in the same genotype. Mean of >7 roots+SD. ns p>0.05, *p≤0.05, Welch ANOVA. **n-o,** Raw data for **Figure 4d, e**, respectively. *n*>16 roots. Box plot depicts minimum to maximum, mean±SD. ns p>0.05, **p≤0.01, ****p≤0.0001, One-way ANOVA.

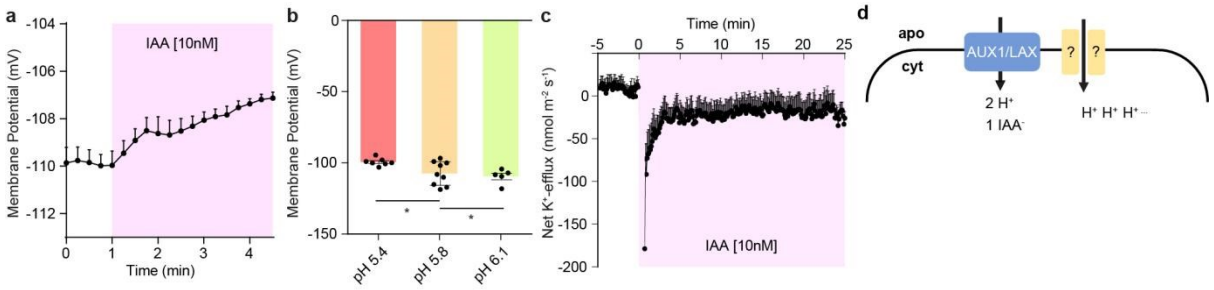


**Extended Data Figure 7. PM potential and AUX1 involvement in auxin-induced apoplast alkalinisation**

Since auxin causes simultaneously membrane depolarization[25] and apoplast alkalinisation, both of which are interdependent and required for growth, we addressed which of them mediates the auxin effect on root inhibition. By manipulating the external pH, we found that pH and growth were correlated (**Fig. 1d-g**) while membrane potential (MP) was uncoupled (**a, b**). Additionally, we observed that $K^+$-efflux (**c**) compensates auxin-induced $H^+$- and $Ca^{2+}$-influx (**Extended Data Fig. 2c, Extended Data Fig. 8a**), suggesting that auxin-induced MP change is the result of complex ion fluxes, while $H^+$-influx and resulting apoplastic pH change for growth regulation is just a subset of those.

**a-b,** Membrane potential recorded by invasive micro-electrode in root elongating cells with IAA treatment (magenta). 4 roots+SEM (**a**). Membrane potential measured in root elongating cells after 40min incubation in different pH medium. n>5 roots±SEM. *p≤0.05, One-way ANOVA (**b**). Alkaline medium, which alkalinised the apoplast and inhibited root growth (**Fig. 1d, e**) mimicking the auxin effect, did not result in membrane depolarization. Acidic medium, which acidified the apoplast and promoted root growth (**Fig. 1f, g**) depolarized membrane. MP is thus uncoupled from growth and apoplastic pH. **c,** PM net $K^+$-efflux measured by a non-invasive microelectrode before and after 10nM IAA treatment in the elongating zone of WT roots. 16 roots+SEM. **d,** Scheme showing AUX1/LAX-mediated $IAA^-/2H^+$ symport and mechanistically elusive $H^+$ influx. $IAA^-/2H^+$ symport by AUX1 auxin influx carrier was proposed[17] a possible mechanism of auxin-induced $H^+$ influx and apoplast alkalinisation. Comparison of $H^+$ influx rates in root hair cells[17], or elongating root epidermal cells (**Extended Data Fig. 2c**) and conservative estimates of AUX1-mediated $^3$H-IAA transport in Xenopus oocytes[24,64] argue against this. Below we show that calculations based on data of Xenopus oocytes, primary root and root hairs suggest that AUX1-mediated $H^+$ symport is not sufficient to account for the auxin-induced $H^+$-fluxes:

(1) $^3$H-IAA transport in the AUX1 overexpressing Xenopus oocytes after 100nM $^3$H-IAA[24]:

ca. $2.6x10^{-14}molmin^{-1}$

- Min. diameter of the Xenopus oocyte at stage V/VI[64] is ca. 1.0mm so the surface area is minimally $3.142x10^{-6}m^2$

- Max. speed of IAA uptake across the membrane is calculated as:

$2.6 \times 10^{-14}mol/(60s \times 3.142x10^{-6}m^2) = 1.38x10^{-10}molm^{-2}s^{-1}$

- Based on 2 $H^+$ per $IAA^-$, the max. speed of AUX1-symported $H^+$ is $2.76x10^{-10}$ $molm^{-2}s^{-1}$.

(2) $H^+$ uptake after 10nM IAA (ten times less than in Xenopus) in *Arabidopsis* root elongating cells: $1.7x10^{-8}molm^{-2}s^{-1}$ (**Extended Data Figure 2c**). This is still 62 times more than the conservatively estimated Max. speed in (**1**)

(3) $H^+$ uptake NAA in *Arabidopsis* root hairs[17] is ca. $1.0x10^{-7}molm^{-2}s^{-1}$. This is 362 times more than the conservatively estimated Max. speed in (**1**)

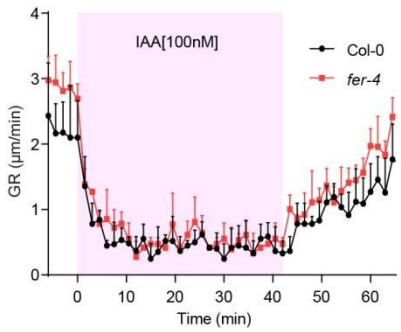


**Extended Data Figure 8. *FER* does not mediate auxin-induced rapid growth inhibition**

Root growth of *fer-4* compared to Col-0 in response to application and washout of 100nM IAA in vRootchip. Shaded area indicates IAA treatment. Mean of 5 roots for Col-0 and 3 for *fer-4*+SD. ns, p>0.05, Two-way ANOVA.

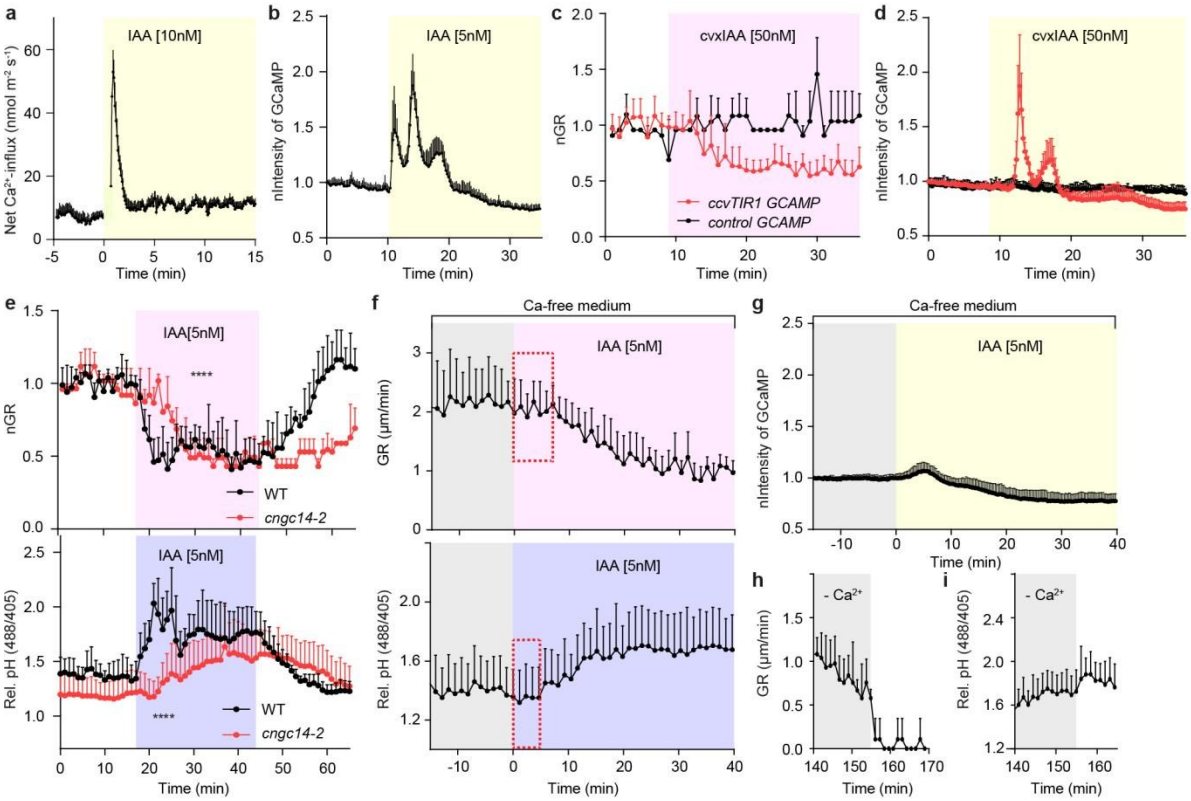


**Extended Data Figure 9. TIR1-mediated $Ca^{2+}$-signalling contributes to auxin-induced apoplast alkalinisation**

Another rapid output of TIR1/AFB perception mechanism are cytosolic $Ca^{2+}$-transients in root hairs[17]. Therefore, we evaluated $Ca^{2+}$-transients in apoplast alkalinisation and root growth inhibition. Using vRootchip, *GCaMP3* $Ca^{2+}$-marker[33], non-invasive microelectrodes and cvxIAA-ccvTIR1 system[28], we confirmed that auxin via TIR1/AFB triggered rapid $Ca^{2+}$-influx correlates with root growth inhibition (**a-d**). We noted a distinct $Ca^{2+}$-response measured by the microelectrode (**a-b**) and *GCaMP3* (**c**). Namely, $Ca^{2+}$-channels are activated at the plasma membrane resulting in net influx, while the *GCaMP3* reported more complex responses possibly involving intracellular $Ca^{2+}$-storage and release. Moreover, the use of cvxIAA-ccvTIR1 (**d**) provided additional proof that TIR1-mediated auxin perception activates $Ca^{2+}$-signalling. Further, we verified that mutants in the $Ca^{2+}$-permeable cation channel *Cyclic NUCLEOTIDE-GATED CHANNEL 14* (*CNGC14*) have delayed auxin-induced apoplast alkalinisation and root growth inhibition (**e**) similarly as reported[14] Furthermore, depletion of external $Ca^{2+}$ resulted in attenuated auxin-induced $Ca^{2+}$-spike, delayed apoplast alkalinisation and growth inhibition (**b, f, g**). $Ca^{2+}$-addition resulted in rapid growth inhibition (**h, i**). These observations collectively suggest that TIR1/AFB-mediated $Ca^{2+}$-signalling is part of the mechanism for auxin-induced rapid apoplast alkalinisation and growth inhibition.

**a,** PM net $Ca^{2+}$-influx measured by a non-invasive microelectrode before and after 10nM IAA treatment in the elongating zone of WT roots. 9 roots+SEM. **b,** Normalised fluorescence intensity of *GCaMP3*, cytosolic $Ca^{2+}$-marker, in elongating cells responding to 5nM IAA treatment in vRootchip. The intensity was normalized to the initial intensity of the same root. Mean of 7 roots+SD. Note the three peaks in cytosol compared to the single major peak outside of cells (**a**). **c-d**, Root growth (**c**) and fluorescence intensity in elongating cells (**d**) in *GCaMP3* crossed into *ccvTIR1* compared to *control*. Growth rate and intensity are normalized to the pre-stimulus value. Mean of 7 for *ccvTIR1* and 2 for *control*+SD. ****p≤0.0001, Two-way ANOVA. **e**, Root growth (upper graph) and apoplastic pH (lower graph) analysis in *cngc14-2* and WT in response to IAA in vRootchip. Mean of 5 roots for WT and 3 for *cngc14-2*+SD. ****p≤0.0001, Two-way ANOVA. **f-g**, Root growth (upper graph in **f**) and apoplastic pH (lower graph in **f**) in WT, as well as cytosolic $Ca^{2+}$ analysis in *GCaMP3* reporter marker line in vRootchip (**g**) with 140min pre-treatment of $Ca^{2+}$-free medium (grey) followed by 5nM IAA addition (magenta for growth, blue for pH in **f** and yellow for $Ca^{2+}$ in **g**). Auxin induced significant less $Ca^{2+}$-response in Ca-free medium, compared to normal medium in (**b**). The red dotted square marked the non-responsive delay after auxin. Mean of 5 (**f**) and 6 (**g**) roots+SD. **h-i**, Root growth (**h**) and apoplastic pH (**i**) analysis in WT upon $Ca^{2+}$ addition after 140min $Ca^{2+}$-free medium in the presence of 5nM IAA in vRootchip. Mean of 5 roots+SD.

**Acknowledgements**

We thank Nataliia Gnyliukh and Lukas Hörmayer for technical assistance and Nadine Paris for sharing *PM-Cyto* seeds. We gratefully acknowledge Life Science, Machine Shop and Bioimaging Facilities of IST Austria. This project has received funding from the European Research Council Advanced Grant (ETAP-742985) and the Austrian Science Fund (FWF) I 3630-B25 to J.F., the National Institutes of Health (GM067203) to W.M.G., the Netherlands Organization for Scientific Research (NWO; VIDI-864.13.001.), the Research Foundation-Flanders (FWO; Odysseus II G0D0515N) and a European Research Council Starting Grant (TORPEDO-714055) to W.S. and B.D.R., the VICI grant (865.14.001) from the Netherlands Organization for Scientific Research to M.R and D.W., the Australian Research Council and China National Distinguished Expert Project (WQ20174400441) to S.S., the MEXT/JSPS KAKENHI to K.T. (20K06685) and T.K. (20H05687 and 20H05910), the European Union's Horizon 2020 research and innovation programme under the Marie Skłodowska-Curie Grant Agreement No. 665385 and the DOC Fellowship of the Austrian Academy of Sciences to L.L.,

the China Scholarship Council to J.C.

**Author contributions**

L.L., I.V. and J.F. conceived and designed the experiments. L.L. and I.V. carried out most of the experiments and analysis. M.R. and D.W. performed the phospho-proteomics analysis and TIR1/AFB1 IP-MS/MS. I.V., W.S. and B.D.R. performed TMK1 IP-MS/MS experiments and statistical analysis. MS/MS analysis was performed by the VIB Proteomics Core. L.S. and S.S. performed MIFE experiments. K.T. and T.K. did the ATP hydrolysis assays. J.C. and S.V. created and shared the *AtTAS1c-AHA* lines. L.R. and L.L. created transgenic lines and crosses. H.R. and W.M.G. conducted [$\gamma$-$^{32}$P]-ATP kinase assay, leaf wilting phenotype analysis, shared plasmids, seeds materials and contributed to discussion of the results. J.M. and L.L. modified the microfluidic chip. L.L., I.V. and J.F. wrote the manuscript.

**Competing interests**

The authors declare no competing interests.

**Correspondence**

Additional information is available from the corresponding author upon request.

**Data availability statement**

The data and full blots are available within the paper and the Supplementary Information. All source data used for graphs are available.

**Code availability statement**

All codes used in the manuscript are provided in Supplementary Information.

## *3.12 References*

1 Estelle, M. Plant tropisms: the ins and outs of auxin. *Curr. Biol.* **6**, 1589-1591 (1996).

2 Gallei, M., Luschnig, C. & Friml, J. Auxin signalling in growth: Schrödinger's cat out of the bag. *Curr. Opin. Plant biol.* **53**, 43-49 (2020).

3 Spartz, A. K. *et al.* SAUR inhibition of PP2C-D phosphatases activates plasma membrane $H^+$-ATPases to promote cell expansion in Arabidopsis. *Plant Cell* **26**, 2129-2142 (2014).

4 Fendrych, M., Leung, J. & Friml, J. TIR1/AFB-Aux/IAA auxin perception mediates rapid cell wall acidification and growth of Arabidopsis hypocotyls. *Elife* **5**, e19048 (2016).

5 Du, M., Spalding, E. P. & Gray, W. M. Rapid auxin-mediated cell expansion. *Annu. Rev.Plant Biol.* **71**, 379-402 (2020).

6 Fendrych, M. *et al.* Rapid and reversible root growth inhibition by TIR1 auxin signalling. *Nat. Plants* **4**, 453 (2018).

7 Dai, N., Wang, W., Patterson, S. E. & Bleecker, A. B. The TMK subfamily of receptor-like kinases in Arabidopsis display an essential role in growth and a reduced sensitivity to auxin. *PloS One* **8**, e60990 (2013).

8 Cao, M. *et al.* TMK1-mediated auxin signalling regulates differential growth of the apical hook. *Nature* **568**, 240-243 (2019).

9 Chen, X. *et al.* Inhibition of cell expansion by rapid ABP1-mediated auxin effect on microtubules. *Nature* **516**, 90 (2014).

10 Adamowski, M., Li, L. & Friml, J. Reorientation of cortical microtubule arrays in the hypocotyl of Arabidopsis thaliana is induced by the cell growth process and independent of auxin signaling. *Int. J. Mol. Sci.* **20**, 3337 (2019).

11 Scheuring, D. *et al.* Actin-dependent vacuolar occupancy of the cell determines auxin-induced growth repression. *PNAS* **113**, 452-457 (2016).

12 Barbez, E., Dünser, K., Gaidora, A., Lendl, T. & Busch, W. Auxin steers root cell expansion via apoplastic pH regulation in Arabidopsis thaliana. *PNAS* **114**, E4884-E4893 (2017).

13 Monshausen, G. B., Miller, N. D., Murphy, A. S. & Gilroy, S. Dynamics of auxin-dependent $Ca^{2+}$ and pH signaling in root growth revealed by integrating high-resolution imaging with automated computer vision-based analysis. *Plant J.* **65**, 309-318 (2011).

14 Shih, H.-W., DePew, C. L., Miller, N. D. & Monshausen, G. B. The cyclic nucleotide-gated channel CNGC14 regulates root gravitropism in Arabidopsis thaliana. *Curr. Biol.* **25**, 3119-3125 (2015).

15 Von Wangenheim, D. *et al.* Live tracking of moving samples in confocal microscopy for vertically grown roots. *Elife* **6**, e26792 (2017).

16 Martinière, A. *et al.* Uncovering pH at both sides of the root plasma membrane interface using noninvasive imaging. *PNAS* **115**, 6488-6493 (2018).

17 Dindas, J. *et al.* AUX1-mediated root hair auxin influx governs $SCF^{TIR1/AFB}$-type $Ca^{2+}$ signaling. *Nat. Commun.* **9**, 1-10 (2018).

18 Han, H. *et al.* Rapid auxin-mediated phosphorylation of Myosin regulates trafficking and polarity in Arabidopsis. *bioRxiv* doi: https://doi.org/10.1101/2021.04.13.439603. (2021).

19 Haruta, M., Gray, W. M. & Sussman, M. R. Regulation of the plasma membrane proton pump ($H^+$-ATPase) by phosphorylation. *Curr. Opin. Plant Biol.* **28**, 68-75 (2015).

20 Takahashi, K., Hayashi, K.-i. & Kinoshita, T. Auxin activates the plasma membrane $H^+$-ATPase by phosphorylation during hypocotyl elongation in Arabidopsis. *Plant Phys.* **159**, 632-641 (2012).

21 Yang, Z. *et al.* TMK-based cell surface auxin signaling activates cell wall acidification in Arabidopsis. Research Square doi: 10.21203/rs.3.rs-203621/v1 (2021).

22 Zhang, Y., Xiao, G., Wang, X., Zhang, X. & Friml, J. Evolution of fast root gravitropism in seed plants. *Nat. Commun.* **10**, 1-10 (2019).

23 Kinoshita, T. & Shimazaki, K.-i. Analysis of the phosphorylation level in guard-cell plasma membrane $H^+$-ATPase in response to fusicoccin. *Plant Cell Physiol.* **42**, 424-432 (2001).

24 Yang, Y., Hammes, U. Z., Taylor, C. G., Schachtman, D. P. & Nielsen, E. High-affinity auxin transport by the AUX1 influx carrier protein. *Curr. Biol.* **16**, 1123-1127 (2006).

25 Serre, N. B. *et al.* AFB1 controls rapid auxin signalling through membrane depolarization in *Arabidopsis thaliana* root. *Nat. Plants,* 1-10 (2021).

26 Prigge, M. J. *et al.* Genetic analysis of the Arabidopsis TIR1/AFB auxin receptors reveals both overlapping and specialized functions. *Elife* **9**, e54740 (2020).

27 Hayashi, K.-i. *et al.* Rational design of an auxin antagonist of the $SCF^{TIR1}$ auxin receptor complex. *ACS Chem. Biol.* **7**, 590-598 (2012).

28 Uchida, N. *et al.* Chemical hijacking of auxin signaling with an engineered auxin–TIR1 pair. *Nat. Chem. Biol.* **14**, 299 (2018).

29 Haruta, M., Sabat, G., Stecker, K., Minkoff, B. B. & Sussman, M. R. A peptide hormone and its receptor protein kinase regulate plant cell expansion. *Science* **343**, 408-411 (2014).

## *3.13 Methods*

**Plant materials and growth conditions**

All *Arabidopsis thaliana* mutants and transgenic lines used are in Columbia-0 (WT) background. The *pEB1b::EB1b-GFP*[30], *p35S::MAP4-GFP*[31], *pSYP22::SYP22-YFP*[32], *DR5::LUC*[33], *PM-Cyto*[16], *GCaMP3*[34] marker lines were described previously. The *tir1-10*[35], *afb1-3*[26], *tir1-1 afb2-1 afb3-1* mutant[36], *pTIR1::ccvTIR1* in *tir1-1 afb2-3*[28], *pTIR1::TIR1* in *tir1-1 afb2-3* (we called it *control* for *ccvTIR1*)[28] and *aux1-100*[37], *cngc14-2*[14] and *fer-4*[29] were donated by the authors. The *pTIR1::TIR1-VENUS* in *tir1-1*[38], *pAFB1::AFB1-VENUS* in *afb1-3*[39] are shared by Stefan Kepinski. The *aha* mutants are the following: *aha2-5* (SALK_022010)[40], *aha1-7* (SALK_065288)[40], *ost2-3D*[41] shared by Atsushi Takemiya. Two independent lines *AtTAS1c-AHA#2* and *#4* were generated by Jian Chen and Steffen Vanneste as follows: the syn-tasiRNA target sequence was inserted into *pENTR-AtTAS1c-B/c*[42] using hybridized primers TAS-AHA pair (**Supplemental Table 4**) and was recombined into *pH7m24GW*[43] together with *pDONR P4-P1R*[44] carrying the *pPIN2* promoter[22], to generate *pPIN2:AtTAS1c-AHA*. The *pAHA2::AHA2-GFP*[45] seeds were donated by Anja T. Fuglsang. The *tmk* mutants are the following: *tmk3-2* (SALK_107741) ordered from NASC; Tongda Xu[8,46] kindly contributed *tmk1-1* (SALK_016360), *tmk2-1* (SAIL_1242_H07), *tmk4-1* (GABI_348E01), the complemented *pTMK1::gTMK1-FLAG* in *tmk1-1* and *tmk1-1 tmk4-1* (*tmk1,4*) double mutant seeds. The *tmk1-1 tmk2-1* (*tmk1,2*) and *tmk1-1 tmk3-2* (*tmk1,3*) were generated by crosses using alleles above. The transgenic plant lines carrying *DEX::TMK1-HA*

and *DEX-TMK1$^{K616R}$-HA* were generated by Hong Ren and William M. Gray. The *DEX::TMK1$^{WT}$ (or TMK1$^{K616R/E}$)-HA* constructs were done by cloning the cDNA of *TMK1$^{WT}$* (or *TMK1$^{K616R/E}$*) without stop codon (**Supplemental Table 4**) into *pENTR/D-TOPO*, and subsequently recombining into the *pBAV154*[47] binary vector used Gateway system. The *pUBQ10::gTMK1-3HA* and *pTMK1::gTMK1-eGFP* lines were generated by amplifying *TMK1* full length gDNA without stop codon from WT genomic DNA using the primers indicated in **Supplemental Table 4**. *TMK1* gDNA was inserted into *pDONR221,* subsequently recombined into *pB7m34GW* together with *pDONR P4-P1R* carrying the *UBQ10* or *TMK1* promoter and *pDONR P2R-P3 3xHA* or *pDONR P2R-P3 eGFP,* respectively. The constructs were transformed into the *Agrobacterium tumefaciens* strain pGV3101 by electroporation and further into WT plants by floral dip.

Seeds were surface-sterilized by chlorine gas, sown on half-strength Murashige and Skoog (½MS) medium supplemented with 1% (w/v) sucrose and 0.8% (w/v) phyto agar (pH 5.9), stratified in the dark at 4°C for 2d and then grown vertically at 21°C with a long-day photoperiod (16h light/8h dark). Light sources used were Philips GreenPower LED production modules [in deep red (660nm)/far red (720nm)/blue (455nm) combination, Philips], with a photon density of 140.4µmolm$^{-2}$s$^{-1}$±3%.

Treatment with inhibitors of gene translation, cycloheximide[6], or transcription, cordycepin[48] were done in the concentration and duration verified previously.

**Microfluidics**

The microfluidic vRootchip was used mostly to analyze root tip growth and apoplastic pH in real-time. The manufacturing of the chip, sample preparation procedure and data analysis of root tip growth were performed as described previously[6]. Our new design contains an additional valve in the control layer that closes the ends of the root channels (**Extended Data Fig. 1a**). In case of air bubbles appeared in the root channels, the additional valve allows pressurizing the channel and air will be absorbed into the Polydimethylsiloxane (PDMS) chip material within 2-10min. Afterwards, experiments started after adaptation of at least 2h. Besides, we introduced a graphical user interface (**Supplementary Script 1**) using the Processing software (https://processing.org/) with the ControlP5 package (http://www.sojamo.de/libraries/controlP5/) that sends serial commands to the Arduino. A sketch (**Supplementary Script 2**) runs on the Arduino to operate the electronics and receive commands. For one vRootchip, maximum 8 samples were used. When comparing two

genotypes, 3-4 seedlings were used for each genotype and mounted in alternating channels to minimize the time difference between imaging two genotypes. For each root, we imaged one ROI containing early elongating epidermal cells and the other ROI covering the root tip. As these two ROIs were captured sequentially, we imaged the apoplastic pH and the growth of the same root close to simultaneously.

In vRootchip, we used basal liquid medium ¼MS+0.1% sucrose, pH 5.8 (adjusted with KOH). The media of different pH was prepared with basal medium adjusted pH by HCl or KOH. Besides, $Ca^{2+}$-free liquid medium was prepared without $CaCl_2$.

**Scanner growth assay**

To complement the real-time imaging in vRootchip, growth analysis was performed on a vertical scanner with bigger sample sizes allowing more conditions to be evaluated. This growth measurement we called steady-state. 4d-old seedlings were transferred to 60×15mm petri dishes filled with 5ml ½MS medium with treatments as indicated. The petri dishes were placed on a vertically mounted flatbed scanner (Epson perfection V370) and seedlings were imaged through the layer of medium. Either wet black filter paper or ½MS medium containing activated charcoal was added in the lid to improve background contrast. The samples were automatically imaged every 10 or 30min using the AutoIt script described previously[49] and scans were taken at 1200dpi. The resulting image series were analyzed using StackReg stabilization and the Manual Tracking plugin in ImageJ, or using an in-house generated MATLAB-based application RootGrowth tracker[50].

**Imaging and measuring apoplastic pH with HPTS dye**

All apoplastic pH data were obtained using 8-hydroxypyrene-1,3,6-trisulphonic acid (HPTS), a ratiometric fluorescent pH dye[12]. pH measurements were done both in steady-state condition and real-time vRootchip imaging. For steady-state pH analysis, 4d-old seedlings were transferred to ½MS medium containing 1mM HPTS (Thermo Scientific 6358-69-6, dissolved in $ddH_2O$) and treatments were performed for 30 or 50min. Subsequently, seedlings on a slice of the treatment medium were mounted into a Lab-Tek Chambered Coverglass.

Real-time imaging of the apoplastic pH was done in vRootchip containing medium (¼MS+0.1% sucrose) supplemented with 1mM HPTS with or without treatment. All imaging was performed on the in-house established vertical Zeiss LSM 800 confocal microscope[15]. Fluorescent signals for protonated HPTS (excitation 405nm, emission 514nm, visualized in red) and deprotonated HPTS (excitation, 488nm, emission 514nm, visualized in green) were

detected with a 20x/0.8 air objective. Image analysis was performed on a cropped region of elongating epidermis cells using batch processing of a previously described the ImageJ macro[12]. Relative pH value is calculated as the background-subtracted intensity of the deprotonated intensity divided by that of the protonated intensity. Resulting relative pH data were plotted over time and statistically evaluated in GraphPad Prism 6. Note that we did not transform the relative pH value to absolute pH values, which would require the generation of a calibration curve for each experiment.

**Imaging and measuring cytosolic pH with *PM-cyto* reporter**

Real-time imaging of the cytosolic pH near the PM was done by using *PM-Cyto* reporter line[16] in vRootchip and a vertical Zeiss LSM 800 confocal microscope[15]. Sequential illumination at 488 and 405nm with emission 514nm for both, corresponding to the two absorption peaks of pHluorin, were taken with a 20x/0.8 air objective. For each root in vRootchip, two ROIs were tracked over time with one containing elongating epidermal cells for measuring the cytosolic pH and the other covering the root tip for measuring the root growth rate. Image analysis was performed similar to the HPTS analysis described above.

**Imaging microtubule orientation, vacuolar morphology and cytosolic $Ca^{2+}$ spike**

The *pEB1b::EB1b-GFP* maker line[30] was used to track the dynamics of CMTs orientation in vRootchip. Images were obtained every 6.25s and the analysis of the CMTs orientation was done in ImageJ by max Z-projection on every 10 frames and quantification by a for batch processing modified version of the Fibril Tool macro[51]. The *p35S::MAP4-GFP* marker line[31] was used for capturing the CMTs orientation after treatment for the indicated time period (steady state). The CMTs orientation angle was calculated using the Bioline script[10]. For both marker lines, the GFP (excitation 488nm, emission514 nm) signal was detected by Plan-Apochromat 20x/0.8 air objective in the vertical Zeiss LSM 800 confocal microscope[15].

The *pSYP22::SYP22-YFP* marker line[32] was used for imaging vacuolar morphology. We used a mounting system[52], which allows the injection of new liquid medium during imaging. Images were taken before and 30min after Mock or 100nM IAA treatment and the YFP (excitation 488 nm, emission 527 nm) intensity was detected with C-Apochromat 40x/1.20 W Korr objective in an inverted Zeiss LSM 800 confocal microscope.

The *GCaMP3* marker line[34] was crossed into *ccvTIR1* and *control* transgenic plants[28] and used for imaging cytoslic $Ca^{2+}$ level in vRootchip. Images were taken every 14.4s for 1h.

GFP (excitation 488nm, emission 514 nm) signal was detected by Plan-Apochromat 20x/0.8 air objective in the vertical Zeiss LSM 800 confocal microscope[15].

**Non-invasive microelectrode (MIFE) ion flux measurements**

Net fluxes of $H^+$, $K^+$, and $Ca^{2+}$ were measured using the non-invasive microelectrode ion flux estimation (MIFE) technique essentially as described elsewhere[53]. In brief, microelectrodes were pulled out by PE-22 puller (Narishige), dried in an oven and silanized with tributylchlorosilane (Cat 90794, Sigma-Aldrich, Australia). The prepared electrode blanks were backfilled with respective solutions for each measured ion and electrode tips front-filled with selective liquid ion exchangers (LIX) purchased from Sigma-Aldrich) to measure ions of interest ($H^+$ - Cat. 95291; $K^+$- Cat. 99311, $Ca^{2+}$- Cat. 99310). A root of intact 6d-old *Arabidopsis* WT seedlings was immobilised in a measuring chamber using Perspex holders and basic salt media (BSM) added. The composition of the BSM solution was 0.5mM KCl and 0.1mM $CaCl_2$; pH 5.8, unbuffered. Measurements were recorded from root elongating epidermal cells (~450µm from the root tip). After 40min of conditioning, the microelectrodes were positioned 20µm from the root surface and moved in a slow (6s cycle, 100µm amplitude) square-wave by a computer-driven micromanipulator (MHW-4, Narishige). Net ion fluxes were calculated by the MIFEFLUX software based on the measured difference in electrochemical gradient between these two positions using the cylindrical diffusion geometry as described elsewhere[53]. The steady fluxes were recorded for 5-10min to make sure that steady state condition was reached. Then 10nM IAA was applied to the measuring chamber, and transient $H^+$, $K^+$, and $Ca^{2+}$ kinetics were measured for further 20min. At least 9 individual plants from several batches were used. The sign convention is "influx positive".

**Membrane potential measurements**

Membrane potential (MP) values were measured from root epidermal elongating cells of intact Arabidopsis seedlings. Conventional microelectrodes (Harvard Apparatus) were filled with 1M KCL and connected to the MIFE electrometer via the Ag/AgCl half-cell. During MP measurement, the microelectrode with a tip diameter of 0.5µm was manually impaled into the epidermal cells of elongation (~450µm from root tip) using a 3D-micromanipulator (MHW-4, Narishige). MP values were recorded by the MIFE CHART software for at least two minutes after stabilization[53]. Prior to measurements, a 6d-old seedling was immobilised on a Perspex block using Parafilm strips, the block then was inserted into a vertical Perspex measuring chamber and filled with basic salt media (BSM: 0.5mM KCl and 0.1mM $CaCl_2$; unbuffered, of

required pH). After 40min conditioning in BSM, the measuring chamber was mounted on a MIFE microscope stage located in a Faraday cage for MP measurements. MP measurements were conducted in two ways: under steady state conditions (at different pH values) and as transient kinetics (in response to IAA application). In the steady state experiments, MP values were recorded from roots of 5-6 individual seedlings with a new electrode being used for each measurement to ensure that the electrode tip was not blocked. At least 4 measurements were made for each seedling. In transient kinetics experiments, MP was recorded from a root in BSM (pH 5.8) for 1-2min after the initial cell penetration and then IAA prepared in BSM was added to the chamber (final concentration 10nM) followed by 5min MP recording.

**Evaluating the TIR1-transcriptional response using *DR5::LUC***

4d-old *DR5::LUC* seedlings[33] are placed on the surface of solidified ½MS medium with 200µl of 5mM D-luciferin dissolved in a 1x PBS drop on the root tips for 30min as pre-treatment. Subsequently, the samples were transferred to solidified ½MS medium supplemented with mock, 10nM IAA, 10µM FC and IAA+FC, and immediately imaged in an in-house established dark box with a Photometric Evolve® EMCCD camera equipped with a 17mm fixed lens/0.95 and an additional 125mm lens[49]. The multiplier EMCCD gain was set to 70s and the exposure time to 35s, and images were acquired every 2min. The resulting time-lapse video was analysed in ImageJ as described previously[49].

**Identification of TMK1-interacting proteins using IP/MS-MS**

Immunoprecipitation (IP) experiments were performed in 3 biological replicates as described previously[54] using 1g of roots of 7d-old seedlings from the *pTMK1::TMK1-eGFP* transgenic line and 1g of roots from WT. Interacting proteins were isolated by incubating total protein extracts with 100µL anti-GFP coupled magnetic beads (Miltenyi Biotech). 3 replicates of *pTMK1::TMK1-eGFP* were compared to 3 WT replicates. Tandem mass spectrometry (MS) on a Q-Exactive device (Thermo Fisher) and statistical analysis using MaxQuant and Perseus software was performed as described previously[55].

**Identification of TIR1- and AFB1-interacting proteins using IP/MS-MS**

For immunoprecipitation, ground plant material of *pTIR1::TIR1-VENUS* in *tir1-1* and *pAFB1::AFB1-VENUS* in *afb1-3* transgenic lines was lysed in mild lysis buffer (50mM Tris pH 7.5, 150mM NaCl, 2mM $MgCl_2$, 0.2mM EDTA, 1xCPI, 0.5mM DTT, 0.2% NP40 and

1mg/ml DNAse) and mildly sonicated using a Bioruptor (Diagenode). After lysate clearance, supernatant was submitted to enrichment using GFP-Trap agarose beads (Chromotek) for 45min at 4°C while gently rotating. Beads were subsequently washed twice in lysis buffer, twice in detergent-free lysis buffer and trice in 50mM Ammoniumbicarbonate (ABC) (Sigma) with intermediate centrifuging for 2min at 2000g at 4°C. After the final wash, bead-precipitated proteins were alkylated using 50mM Acrylamide (Sigma). Precipitated proteins were submitted to on-bead trypsin digestion using 0.35µg trypsin (Roche) per reaction. After overnight incubation at 25°C, peptides were desalted and concentrated using C18 Stagetips.

After Stagetip processing, peptides were applied to online nanoLC-MS/MS using a 60min acetonitrile gradient from 8-50%. Spectra were recorded on a LTQ-XL mass spectrometer (Thermo Scientific) and the statistical analysis using MaxQuant and Perseus software was performed as described previously[55].

**Phospho-proteomics of auxin-treated roots**

Roots from 5d-old plants were treated and immediately harvested and flash frozen in liquid nitrogen. They then were ground to fine powder in liquid nitrogen. Powder was suspended in SDS lysis buffer (100mM Tris pH 8.0, 4%SDS and 10mM DTT) and sonicated using a cooled Biorupter (Diagenode) for 10min using high power with 30s on 30s off cycle. Lysate was cleared by centrifugation at maxiumum speed for 30min. Protein concentrations were determined using the Bradford reagent (Bio-Rad).

For FASP 30kDa cut-off amicon filter units (Merck Millipore) were used. Filters were first tested by appling 50µl urea buffer UT buffer (8M Urea and 100mM Tris pH 8.5) and centrifuging for 10min at 11000rpm at 20°C. The desired amount of protein sample was next mixed with UT buffer until a volume of 200µl, applied to filter and centrifuged for 15min. All centriguge steps were at 11000rpm at 20°C. Filter was washed with UT buffer for 15 min. Retained proteins were alkylated with 50mM acrylamide (Sigma) in UT buffer for 30min at 20°C while gently shaking followed by a triple wash step with UT buffer for 15 minutes and three washes with 50mM ABC buffer. After last wash proteins were cleaved by adding trypsin (Roche) in a 1:100 trypsin to protein ratio. Digestion was completed overnight. The following day filter was changed to a new tube and peptides were eluted by centrifuging for 15min. Further elution was completed by adding two times 50mM ABC buffer and centrifuging for 10min on 11000rpm at 20°C.

For peptide desalting and concentrating 200 µl tips were fitted with 2 plugs of C18 octadecyl 47mm Disks 2215 *(Empore™)* material and 1mg:10µg of LiChroprep® RP-

18:peptides (Merck). Tips were sequentially equilibrated with 100% methanol, 80% ACN in 0.1% formic acid and twice with 0.1% formic acid for 4min at 1500g. After equilibration peptides were loaded for 20min at 400g. Bound peptides were washed with 0.1% formic acid and eluted with 80% ACN in 0.1% formic acid for 4min at 1500g. Eluted peptides were subsequently concentrated using a vacuum concentrator for 30min at 45°C and resuspended in 50µl of 0.1% formic acid.

For phosphopeptide enrichment magnetic $Ti^{4+}$-IMAC (MagResyn) were used according to manufactures protocol. Enrichments were perfromed with 1mg of peptides in biological quadruplicate.

After Stagetip processing, peptides were applied to online nanoLC-MS/MS using a 120min acetonitrile gradient from 8-50% for phospho-proteomics. Spectra recording and statistical analysis were as previously described, with the addition of phosphorylation as a variable modification[55]. Filtering of datasets was done in Perseus in as described[56].

**Phospho-proteomics in WT and *tmk1-1* roots**

4 biological replicates of WT and *tmk1-1* roots were prepared and treated as indicated above. They were submitted to the phospho-proteomic pipeline[55,56] and differentially phosphorylated peptides belonging to $H^+$-ATPases were specifically filtered out of the big dataset (**Supplemental Table 1**).

***in vitro* kinase assay with [γ-$^{32}$P]-ATP**

6xHis-MBP-$TMK1^{WT}$ kinase domain (or kinase-dead $TMK1^{K616E}$) was purified from *E. coli*. Briefly, ca. 100ng of purified protein was added to reactions containing 5 mM HEPES, pH 7.5, 10 mM $MgCl_2$, 10mM $MnCl_2$, 1mM DTT and the assay initiated by adding 1µl of ATP solution containing 100µM (unlabeled) ATP and 33nM [γ-$^{32}$P]-ATP (3000 Ci/mmol). ca. 150ng of purified GST-AHA2 C-terminal was added as indicated. Reactions were incubated at 28°C for 40min, stopped with SDS-PAGE sample buffer, run out on SDS-PAGE and phosphorylation was visualized by autoradiography. Ponceau staining was performed as loading control.

**Protein extraction and Western blot analysis for co-IP and determination of AHA2 phosphorylation state**

To isolate PM $H^+$-ATPases and potential interactors, 5-7d-old plant roots were harvested at the indicated time points after 10 or 100nM IAA auxin treatment. 24h prior to the evaluation of

auxin effects, these seedlings were sprayed with ½AM solution containing 30µM kynurenine. The root samples were flash frozen in liquid nitrogen and ground (Retsch mill, 2x 1min at 20Hz). The root powder was then resuspended in a 1:1 (w/v) ratio in protein extraction buffer (25mM Tris-HCl, pH 7.5, 150mM NaCl, 1% Triton X-100, 1xRoche cOmplete™ Protease Inhibitor Cocktail, 1xRoche PhosSTOP™, 1mM EDTA, 1mM DTT and 0.5mM PMSF). The samples were incubated on ice for 30min, followed by a centrifuging step at 10000*g* to discard the plant debris. The cleared supernatant containing the proteins of interest was collected and the total protein content was determined using Quick Start Bradford reagent (Bio-Rad). This could further be used for co-immunoprecipitation analysis or for SDS-PAGE analysis. In order not to lose relevant proteins, protein samples were not boiled in the presence of reducing Laemmli buffer and no harsher PM extraction or membrane enrichment was attempted.

For co-immunoprecipitation, root extracts (obtained by extraction in the Lysis buffer supplied in the Miltenyi µMACs kit, supplemented with 1xRoche cOmplete™ Protease Inhibitor Cocktail, 1mM DTT and 0.5mM PMSF), were incubated with magnetic beads from the Miltenyi anti-GFP, anti-HA or anti-FLAG µMACs kits (depending on the tags of the proteins of interest) and kept rotating for 4h at 4°C. Elution was performed with room-temperature denaturing elution buffer and the proteins were analyzed by SDS-PAGE and Western blot.

Following separation of proteins by SDS-PAGE in a 10% acrylamide gel (Protean® TGX™, Bio-Rad), proteins were transferred to PVDF membranes by electroblotting (Trans-blot® Turbo™, Bio-Rad). The membranes were then incubated in blocking buffer (0.05% Tween-20, 5% milk powder or 3% BSA, 20mM Tris-HCl, pH 7.5 and 150mM NaCl) for at least 60min and incubated with antibody solution against the protein of interest. All raw images of blots are provided in **Supplementary Figure 1**.

**Antibodies**

The anti-AHA2 and anti-Thr$^{947}$ AHA2 antibody were shared by Toshinori Kinoshita and used as described previously[57] at final dilution of 1:5000 in TBST buffer+3% BSA, followed by anti-rabbit IgG secondary antibody conjugated to horseradish peroxidase (HRP) (GE Healthcare, NA934) at a dilution of 1:10000 and chemiluminescence reaction (SuperSignal West Femto, Thermo Scientific). To allow multiple antibody detections using the same PVDF membrane, mild stripping was performed using 15g/L glycine, 1g/L SDS, 10mL/L Tween-20 buffer at pH 2.2 for 2-5min.

**ATP hydrolysis in root samples**

To deplete endogenous auxin levels in the seedlings, 14d-old plants were pre-treated with 30μM kynurenine for 24h in the dark. Then, the pretreated seedlings were incubated in presence and absence of 100nM IAA for 60min under dark condition. The roots excised from the seedlings were homogenized in homogenization buffer (50mM MOPS-KOH,pH 7.0, 100mM $KNO_3$, 2mM sodium molybdate, 0.1mM NaF, 2mM EGTA, 1mM PMSF and 20μM leupeptin) and the homogenates were centrifuged at 10000*g* for 10min. The obtained supernatant was further ultra-centrifuged at 45000 rpm for 60min. The resultant precipitate (microsomal fraction) was resuspended in the homogenization buffer. ATP hydrolytic activity in the microsomal fraction was measured by the release of inorganic phosphate from ATP in a vanadate-sensitive manner following the method published[58] with the following modifications. The microsomal fraction (22.5μL, 0.2mg/mL) was mixed with the equal volume of the reaction buffer (60mM MES-Tris. pH 6.5, 6mM $MgSO_4$, 200mM $KNO_3$, 1 mM ammonium molybdate, 10μg/mL oligomycin, 2mM $NaN_3$, 0.1% Triton X-100, 1mM PMSF and 20μM leupeptin) with or without 1μL of 10mM sodium orthovanadate. The reaction was started by adding 5μL of 2mM ATP and terminated by adding 50μL of the stop solution (2.6% [w/v] SDS, 0.5% [w/v] sodium molybdate and 0.6N $H_2SO_4$) after incubating at 30ºC for 30min.

**Bimolecular Fluorescence Complementation (BiFC)**

Following the method described[3], the full-length coding sequences of AHA2 and TMK1 without stop codons were amplified by PCR (primers in **Supplemental Table 4**), cloned into *pENTR/D-TOPO* or *pDONR207* and recombined in *pSPYNE* and *pSPYCE*[59] to generate BiFC expression constructs. The resulting binary vectors were introduced in *Agrobacterium* GV3101 by electroporation and these were cultured until $OD_{600}$ 0.8. Syringe infiltration was performed in *Nicotiana benthamiana* leaves as described[60]. For the constructs of interest, final $OD_{600}$ of 0.2 was used and p19 was co-infiltrated at $OD_{600}$ 0.1 to avoid gene silencing. Infiltration buffer of pH 5.8 contained: 10mM $MgSO_4$, 10mM MES-KOH and 0.15mM acetosyringone. TMK1 overexpression, even transiently, has a strong effect on the viability of the leaves, so samples were taken daily after infiltration to determine the optimal balance between expression level and viable leaf cells. To avoid this effect, $TMK1^{K6161R}$ was expressed and still interacted with AHA2, while no interaction was observed with AUX1 (**Extended Data Fig. 4g**). For AHA2, expressed in the same system, the non-existence of interaction with AUX1 was published

before[61,62] (**Extended Data Fig. 4g**). To visualize protein interactions, sections of the leaves were imaged using a Zeiss LSM 700 confocal microscope.

**Quantitative RT-PCR**

RNA was extracted from 5d-old light-grown root tips with the RNAeasy Plant Mini Kit (Qiagen), with three biological replicates for each genotype. 2µg of RNA was used for cDNA synthesis (Qiagen). Samples were pipetted in three technical replicates using an automated JANUS Workstation (PerkinElmer) and measured by the Real-time PCR Roche LightCycler 480 using Luna® Universal qPCR mastermix (NEB, M3003S). Primers utilized for assessing gene expression are listed in **Extended Table 4**. Expression levels were normalized to Elongation factor 1-alpha (At5G60390)[63].

**Statistical analysis and reproducibility**

All graphs were generated using GraphPad Prism 6 or 8. For statistical analysis of vRootchip data, Two-way ANOVA was performed for the entire time frame of the experiment, except when a specific time interval is indicated. Welch ANOVA analysis was applied for the scanner growth assay with multiple time points, and one-way ANOVA assays were used for steady state (one incubation time point) pH and scanner growth datasets. Stars indicate significant differences on all graphs with ns for $p>0.05$, * for $p\leq0.05$, ** for $p\leq0.01$, *** for $p\leq0.001$ and **** for $p\leq0.0001$. Experiments always included sufficient biological replicates and were repeated at least twice independently with similar results. The depicted data show the results from one representative experiment.

## *3.14 Methods and Extended Data Figure references*


30 Komaki, S. *et al*. Nuclear-localized subtype of end-binding 1 protein regulates spindle organization in Arabidopsis. *J. Cell Sci* **123**, 451-459 (2010).

31 Marc, J. *et al.* A GFP–MAP4 reporter gene for visualizing cortical microtubule rearrangements in living epidermal cells. *Plant Cell* **10**, 1927-1939 (1998).

32 Robert, S. *et al.* Endosidin1 defines a compartment involved in endocytosis of the brassinosteroid receptor BRI1 and the auxin transporters PIN2 and AUX1. *PNAS* **105**, 8464-8469 (2008).

33 Moreno-Risueno, M.A. *et al*. Oscillating gene expression determines competence for periodic Arabidopsis root branching. *Science* **329**, *1306-11 (2010)*

34 Toyota, M. *et al*. Glutamate triggers long-distance, calcium-based plant defense signaling. *Science* 361, 1112-1115 (2018).

35 Parry, G. *et al*. Complex regulation of the TIR1/AFB family of auxin receptors. *PNAS* **106**, 22540-22545 (2009).

36 Dharmasiri, N. *et al.* Plant development is regulated by a family of auxin receptor F box proteins. *Dev. Cell* **9**, 109-119 (2005).

37 Swarup, R. *et al.* Structure-function analysis of the presumptive Arabidopsis auxin permease *AUX1*. *Plant Cell* **16**, 3069-3083 (2004).

38 Wang, R. *et al.* HSP90 regulates temperature-dependent seedling growth in Arabidopsis by stabilizing the auxin co-receptor F-box protein TIR1. *Nat. Commun.* **7**, 1-11 (2016).

39 Rast-Somssich, M. I. *et al.* The Arabidopsis *JAGGED LATERAL ORGANS* (*JLO*) gene sensitizes plants to auxin. *J. Exp. Bot.* **68**, 2741-2755 (2017).

40 Haruta, M. *et al.* Molecular characterization of mutant Arabidopsis plants with reduced plasma membrane proton pump activity. *J. Biol. Chem.* **285**, 17918-17929 (2010).

41 Yamauchi, S. *et al.* The plasma membrane $H^+$-ATPase AHA1 plays a major role in stomatal opening in response to blue light. *Plant Phys.* **171**, 2731-2743 (2016).

42 Carbonell, A. *et al.* New generation of artificial microRNA and synthetic trans-acting small interfering RNA vectors for efficient gene silencing in Arabidopsis. *Plant Phys.* **165**, 15-29 (2014).

43 Karimi, M., Bleys, A., Vanderhaeghen, R. & Hilson, P. Building blocks for plant gene assembly. *Plant Phys.* **145**, 1183-1191 (2007).

44 Marquès-Bueno, M. M. *et al.* A versatile multisite gateway-compatible promoter and transgenic line collection for cell type-specific functional genomics in Arabidopsis. *Plant J.* **85**, 320-333 (2016).

45 Fuglsang, A. T. *et al.* Receptor kinase-mediated control of primary active proton pumping at the plasma membrane. *Plant J.* **80**, 951-964 (2014).

46 Wang, Q. *et al.* A phosphorylation-based switch controls *TAA1*-mediated auxin biosynthesis in plants. *Nat. Commun.* **11**, 1-10 (2020).

47 Lee, J. *et al.* Type III secretion and effectors shape the survival and growth pattern of *Pseudomonas syringae* on leaf surfaces. *Plant Phys.* **158**, 1803-1818 (2012).

48 Robert, S. *et al*. ABP1 mediates auxin inhibition of clathrin-dependent endocytosis in Arabidopsis. *Cell* **143**, 111-121 (2010).

49 Li, L., Krens, S. G., Fendrych, M. & Friml, J. Real-time analysis of auxin response, cell wall pH and elongation in Arabidopsis thaliana hypocotyls. *Bio Protoc.* **8** (2018).

50 Gelová, Z. *et al*. Developmental roles of auxin binding protein 1 in Arabidopsis Thaliana. *Plant Sci.* **303**, 110750 (2021).

51 Boudaoud, A. *et al.* FibrilTool, an ImageJ plug-in to quantify fibrillar structures in raw microscopy images. *Nat. Protoc.* **9**, 457-463 (2014).

52 Narasimhan, M. et al. Systematic analysis of specific and nonspecific auxin effects on endocytosis and trafficking. *Plant Phys.* **186**, 1122-1142 (2021).

53 Shabala, S. N., Newman, I. A. & Morris, J. Oscillations in $H^+$ and $Ca^{2+}$ ion fluxes around the elongation region of corn roots and effects of external pH. *Plant Phys.* **113**, 111-118 (1997).

54 De Rybel, B. *et al.* A bHLH complex controls embryonic vascular tissue establishment and indeterminate growth in Arabidopsis. *Dev. Cell* **24**, 426-437 (2013).

55 Wendrich, J. R., Boeren, S., Möller, B. K., Weijers, D. & De Rybel, B. in *Plant Hormones*: 147-158 (Springer, 2017).

56 Nikonorova, N. *et al.* Early mannitol-triggered changes in the Arabidopsis leaf (phospho)proteome reveal growth regulators. *J. Exp. Bot.* **69**, 4591-4607 (2018).

57 Hayashi, Y. *et al.* Biochemical characterization of in vitro phosphorylation and dephosphorylation of the plasma membrane $H^+$-ATPase. *Plant Cell Physiol.* **51**, 1186-1196 (2010).

58 Inoue, S.-i., Takahashi, K., Okumura-Noda, H. & Kinoshita, T. Auxin influx carrier AUX1 confers acid resistance for Arabidopsis root elongation through the regulation of plasma membrane $H^+$-ATPase. *Plant Cell Physiol.* **57**,2194-2201 (2016).

59 Walter, M. *et al.* Visualization of protein interactions in living plant cells using bimolecular fluorescence complementation. *Plant J.* **40**, 428-438 (2004).

60 Leuzinger, K. *et al*. Efficient agroinfiltration of plants for high-level transient expression of recombinant proteins. *J. Vis. Exp.* **77**: 50521 (2013).

61 Ren, H., Park, M.Y., Spartz, A.K., Wong, J.H. & Gray, W.M. A subset of plasma membrane-localized PP2C.D phosphatases negatively regulate SAUR-mediated cell expansion in Arabidopsis. *PLoS Genet.* **14**, e1007455 (2018).

62 Wong, J.H., Spartz, A.K., Park, M.Y., Du, M. & Gray, W.M. Mutation of a conserved motif of PP2C.D phosphatases confers SAUR immunity and constitutive activity. *Plant Phys.* **181**, 353-366 (2019).

63 Czechowski, T., Stitt, M., Altmann, T., Udvardi, M. K. & Scheible, W.-R. Genome-wide identification and testing of superior reference genes for transcript normalization in Arabidopsis. *Plant Phys.* **139**, 5-17 (2005).

64 Dumont, J. N. Oogenesis in Xenopus laevis (Daudin). I. Stages of oocyte development in laboratory maintained animals. *J. Morphol* **136**, 153-179 (1972).

# Chapter 4

## Interaction of TIR1/AFB and TMK auxin signaling pathways

Lesia Rodriguez[†1], Lanxin Li[†1], Maciek Adamowski[1], Nataliia Gnyliukh[1], Lana Shabala[2,3], Huibin Han[1], Inge Verstraeten[1], Sergey Shabala[2,3], and Jiří Friml*[1].

[1]Institute of Science and Technology (IST) Austria – 3400 Klosterneuburg (Austria).
[2]Tasmanian Institute of Agriculture, College of Science and Engineering, University of Tasmania – Hobart (Australia).
[3]International Research Centre for Environmental Membrane Biology, Foshan University – 528000 Foshan (China)

*Correspondence to: jiri.friml@ist.ac.at
† These authors contributed equally to this work

Unpublished

## *4.1 Introduction*

In Chapter 3, we discovered that TIR1/AFB and TMK1 have opposite roles during auxin-induced root growth inhibition. The open questions are how they converge on the regulations, whether their relation is conserved in the shoot growth regulation, and how TMK1 mediates auxin signaling. Here, we aim to dissect the relation between TIR1/AFB1 and TMK1 pathway.

## *4.2 TIR1/AFB and TMK1 act antagonistically during auxin-regulated growth in roots and hypocotyls.*

Auxin has dual functions in growth regulation. It inhibits root growth and promotes shoot growth. To analyze the roles of TIR1/AFB and TMK during auxin-regulated growth, we performed dynamic analysis on primary root growth and segmented etiolated hypocotyl in *tir1-1, tmk1-1,* and *tir1-1tmk1-1* double mutants. As shown previously, *tir1-1* was less sensitive to auxin in both root inhibition and shoot promotion (Figure 1a-b). Oppositely, *tmk1-1* was more sensitive. The double mutants showed the intermediate responses compared to each single mutants in both organs (Figure 1a-b). These support that TIR1/AFB and TMK1 counteract in both shoots and roots, and likely that one functions epistatically to the other.

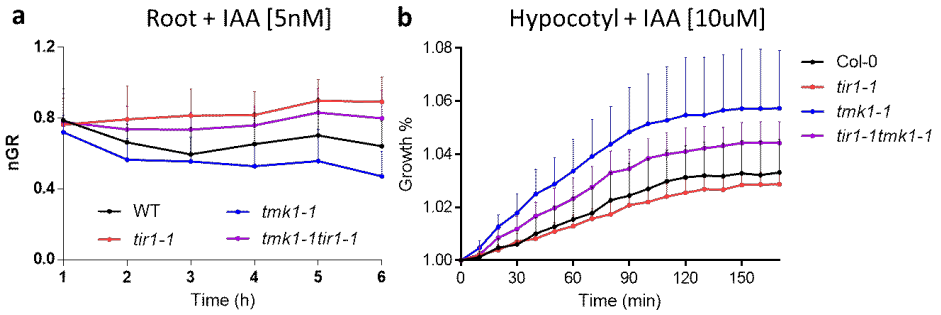


**Figure 1.** TIR1 and TMK1 act antagonistically in auxin-regulated growth in roots and hypocotyls.

**a**, Root growth rate over time after IAA treatment (5 nM) normalized to that after mock treatment.

**b**, Hypocotyl expansion after 10 μM IAA. The segmented etiolated hypocotyls had no expansion on mock treatment but were elongated after auxin treatment. The percentage of growth is calculated as the total length divided by the initial length.

## *4.3 Both TIR1/AFB and TMK1 regulate AHA2 in the steady state and in response to auxin*

The Chapter 3 depicts that TMK1 directly binds, phosphorylates and activates the PM $H^+$-ATPases to acidify apoplast, which counteracts the TIR1/AFB regulation on $H^+$ influx. To test if TIR1/AFB also regulate PM $H^+$-ATPases, we examined the role of TIR1/AFB and TMK in regulation on $H^+$-flux and AHA for both the steady state (without auxin treatment) and auxin application.

Apart from analysis of AHA in *tmk* mutants in Chapter 3, we further confirmed the regulation of TMK on AHA by using non-invasive micro-electrode. We found that *tmk1,2* has about two times higher $H^+$ influx than WT did in the steady state (Figure 2a). Besides, *tmk1* has lower level of AHA2 and phosphorylated AHA2 than WT did (Figure 2b). These confirmed that TMK1 contributes to the AHA2 level and its activity, to counteract with $H^+$ influx and thus promotes growth. This is in line with that *tmk* mutants have slower growth rate (in Chapter 3). On the other hand, when auxin level is increased, *tmk1,2* seemed to respond stronger (Figure 2a), in line with hypersensitivity to auxin in pH and growth (in Chapter 3). Thus, TMK1 regulates both the steady state and auxin-induced AHA2 activity.

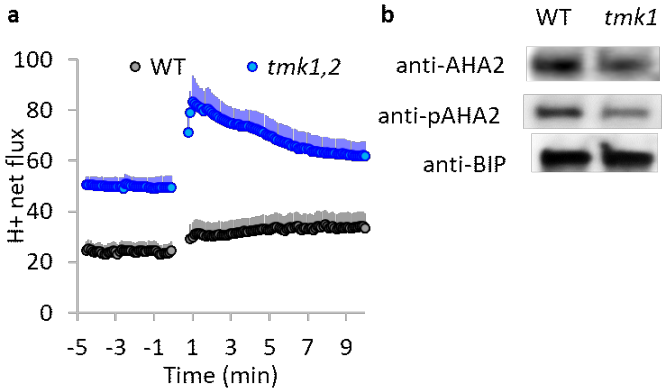


**Figure 2.** TMK1 promotes AHA2 activity contributing to $H^+$-efflux.

**a**, $H^+$ net-flux measured in the root epidermal elongating cells in WT or *tmk1,2* using non-invasive micro-electrode. Positive value represents influx. Time 0 started application of 10 nM IAA.

**b**, AHA2 and Thr948-phosphorylated AHA2 detected in WT or *tmk1-1* in western blot using 5-day-old roots. BIP, a luminal binding protein, was used as a loading control.

Next, we analyzed TIR/AFB regulation on AHA by analyzing the level and phosphorylation of AHA in *tir triple* mutants. In the steady state, *tir triple* had less

phosphorylated AHA2 (Figure 3a). After auxin treatment, it showed no auxin-induced increase in the level of AHA2 (Figure 3a). These suggesting that TIR1/AFB regulates AHA2 in both steady state and in response to auxin.

To definitely examine whether AHA2 can be regulated specifically by TIR1, we applied cvxIAA to the *ccvTIR1* line in comparison to the *control* line. A strong induction of AHA2 phosphorylation was observed, demonstrating that TIR1 is involved in auxin-induced AHA2 phosphorylation.

Collectively, we propose that both TMK1 and TIR1/AFB regulate AHA in the steady state and in response to auxin. Together with the notion that TMK1 directly binds and activates AHA2, these results suggest that TIR1/AFB could be upstream of TMK1 in the regulation of AHA2.

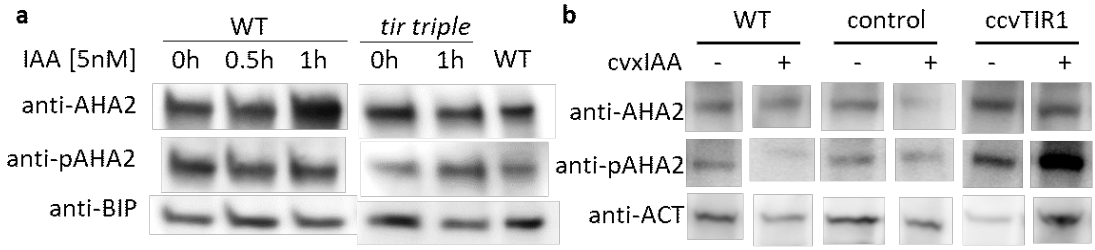


**Figure 3.** TIR1 regulates AHA2 in both steady state and in response to auxin.

**a**, AHA2 and Thr948-phosphorylated AHA2 detected in WT or *tir triple* in western blot using 5-day-old roots treated with 5 nM IAA over time. BIP, a luminal binding protein, was used as a loading control.

**b**, AHA2 and Thr948-phosphorylated AHA2 detected in WT, *control* and *ccvTIR1* lines in western blot using 5-day-old roots after 50 nM cvxIAA treatment. ACTIN was used as a loading control.

## *4.4 TIR1/AFB mediate auxin-induced TMK1 increase*

Previously, we observed that auxin treatment led to an increase in TMK1 abundance (Lesia *et al*, unpublished). To test if it is mediated by TIR1/AFB, we analyzed TMK1 protein level in *tir triple* background after auxin treatment by western blot. The *tir triple* had normal amount of TMK1 in steady state. Notably, the increased TMK1 level after auxin treatment was disappeared in *tir triple* background (Figure 4). This suggests that TIR1/AFB mediates auxin-induced TMK1 increase, and that TIR1/AFB could be upstream of TMK1.

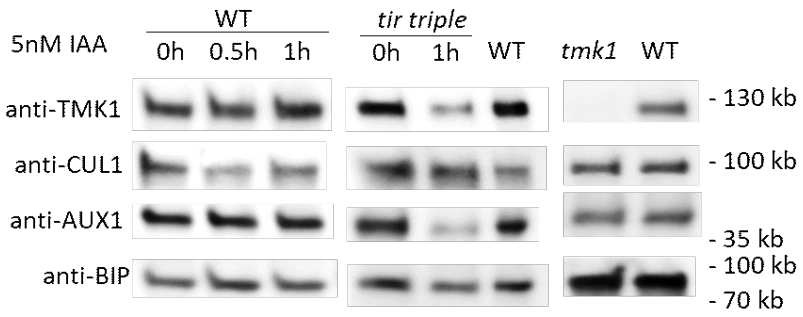


**Figure 4.** TIR1/AFB mediate auxin-induced TMK1 increase in roots.
Protein level of TMK1, CUL1, and AUX1 detected in WT and *tir triple* mutants after 5 nM IAA treatment over time. 5 day-old roots were used. BIP was used as loading control.

## *4.5 TIR1/AFB are upstream of TMK1 during auxin-induced root growth inhibition*

To examine if TIR1/AFB is upstream of TMK1 during auxin-induced root growth inhibition, we specifically induced TIR1 pathway using an engineered system ccvTIR1-cvxIAA in absence or presence of TMK1. We used CRISPR to mutate *TMK1* at the same position (Figure 5a) as in *tmk1-1* mutant in the background of ccvTIR1 (in *tir1afb2*), to generate line *tmk1c in ccvTIR1*. We analyzed the root growth response and apoplastic pH in elongating cells after cvxIAA treatment. First, cvxIAA at 250 nM did not affect the *control* line (Figure 5b-c), suggesting that its off-target effect is negligible. Notably, we found that *tmk1c in ccvTIR1* was more sensitive than *ccvTIR1* to cvxIAA treatment in both growth (Figure 5b) and pH responses (Figure 5c). These suggest that TMK1 and TIR1 are in the same pathway. Together with previous results, we propose that TIR1/AFB is upstream of TMK1 during auxin-induced root growth inhibition and apoplast alkalinization.

Considered that *ccvTIR1* line is in the *tir1afb2* background, we applied IAA and observed *tmk1c in ccvTIR1 (tir1afb2)* line being hypersensitive compared to *ccvTIR1 (tir1afb2)* in growth response (Figure 5d-e), supporting again for the counteracting effect between TMK1 and TIR1/AFB in regulation of root growth.

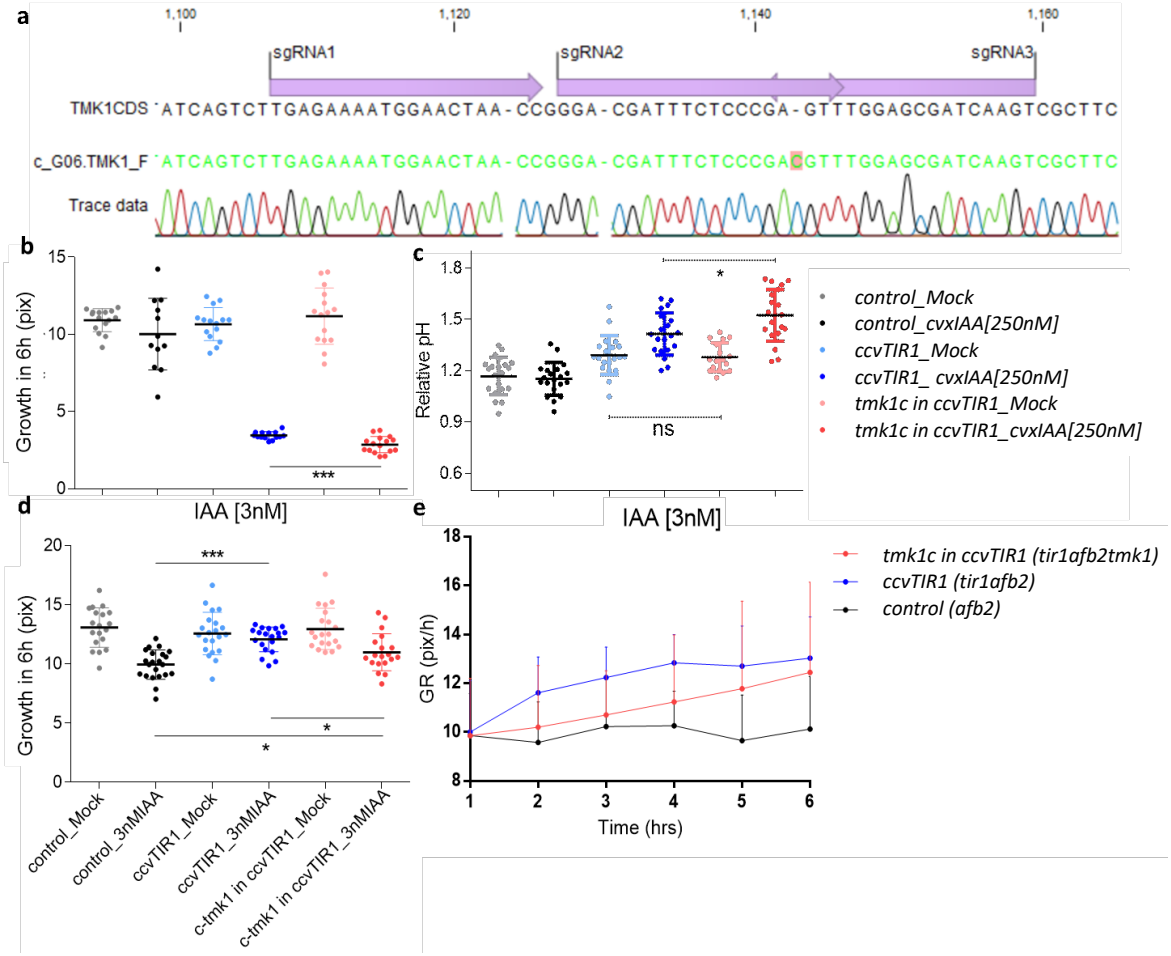


**Figure 5.** TIR1 and TMK1 are in the same pathway during auxin-induced root growth inhibition.

**a**, Scheme including TMK1 CDS sequence, CRISPR guide RNA design (arrows in purple), and a sequencing result containing one nucleotide mutation leading to a frame shift.

**b-c**, Growth (**b**) and apoplastic pH in elongating root cells (**c**) were analyzed after 250 nM cvxIAA treatment. *control* line (*pTIR1::TIR1 in tir1afb2*), *ccvTIR* line (*pTIR1::ccvTIR1 in tir1afb2*), and *tmk1c in ccvTIR1* (crispr-mutated *tmk1 in pTIR1::ccvTIR1 in tir1afb2*) were used.

**d-e**, Growth amount after 6 h (**d**) and dynamic analysis of root growth rate over 6 h (**e**) after 3 nM IAA treatment. The same plants were used in **b-c**.

## *4.6 TIR1/AFB1 interact with TMK1 using Co-IP and BIFC*

The above observations suggested that TIR1/AFB act upstream of TMK1 during auxin-induced growth regulation. To further dissect the relationship between TIR1/AFB and TMK1, we tested their potential interaction. Using the transgenic lines *pTIR1::TIR1-VENUS* and *pAFB1::AFB1-*

*VENUS,* we performed Co-Immunoprecipitation on the root samples. We found that TIR1-GFP degraded dramatically and only free GFP were detected (not shown). However, AFB1 was stable and associated TMK1 can be detected (Figure 6a), indicating that AFB1 and TMK1 interact. Besides, 5 nM IAA treatment for 2 hours increased the amount of the associated TMK1, suggesting that auxin increases the interaction between AFB1 and TMK1.

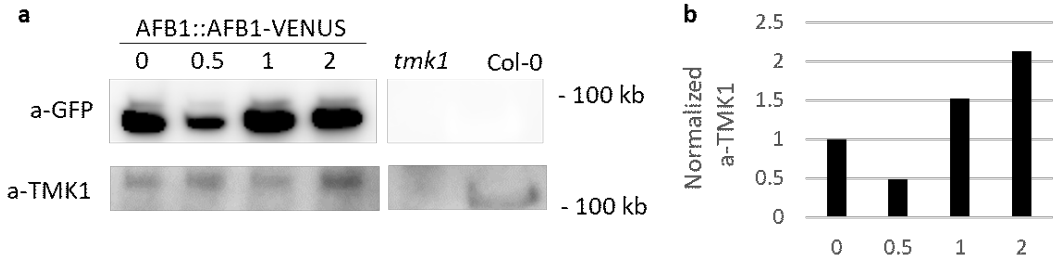


**Figure 6.** AFB1 interacts with TMK1 in CoIP.
**a-b**, CoIP *pAFB1::AFB1-VENUS* roots using GFP beads can detect TMK1 using anti-TMK1 antibody (**a**) and the quantification of band intensity in TMK1 normalized to that in GFP, representing the proportion of TMK1 associated with AFB1 (**b**). 5-day-old seedlings were treated with 5 nM IAA over time (in hours) and roots were harvested.

To verify the interaction, we performed Bimolecular Fluorescent Complementation (BiFC) through transient transformation into tobacco leaves. As a positive control, IAA17 interacted with AFB1 in the nucleus (Figure 7). Notably, AFB1 interacted with TMK1 but not with two mutated versions: TMK1 without kinase domain or mutations for a constitutive kinase activity (Figure 7). Similarly, TIR1 also interacted only with the WT TMK1 (Figure 8). Besides, the interaction were unaffected by auxin application for 1 hour; however, a possible insufficient penetration of auxin in tobacco leaves should be taken into account.

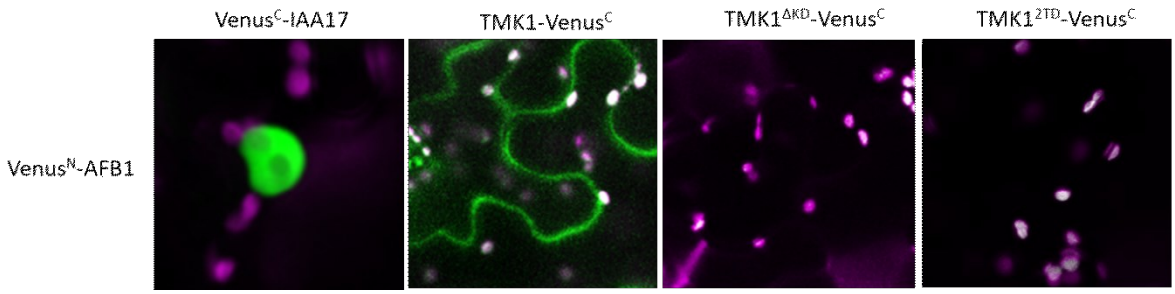


**Figure 7.** AFB1 interacts with TMK1 in BiFC.

BiFC was performed in tobacco leaves transiently expressing N-terminal VENUS fused with AFB1 and C-terminal VENUS fused with IAA17 (as positive control), TMK1, TMK1ΔKD (kinase domain deletion) and TMK12TD (constitutive kinase activity). Magenta for auto-fluorescence and green for VENUS signal.

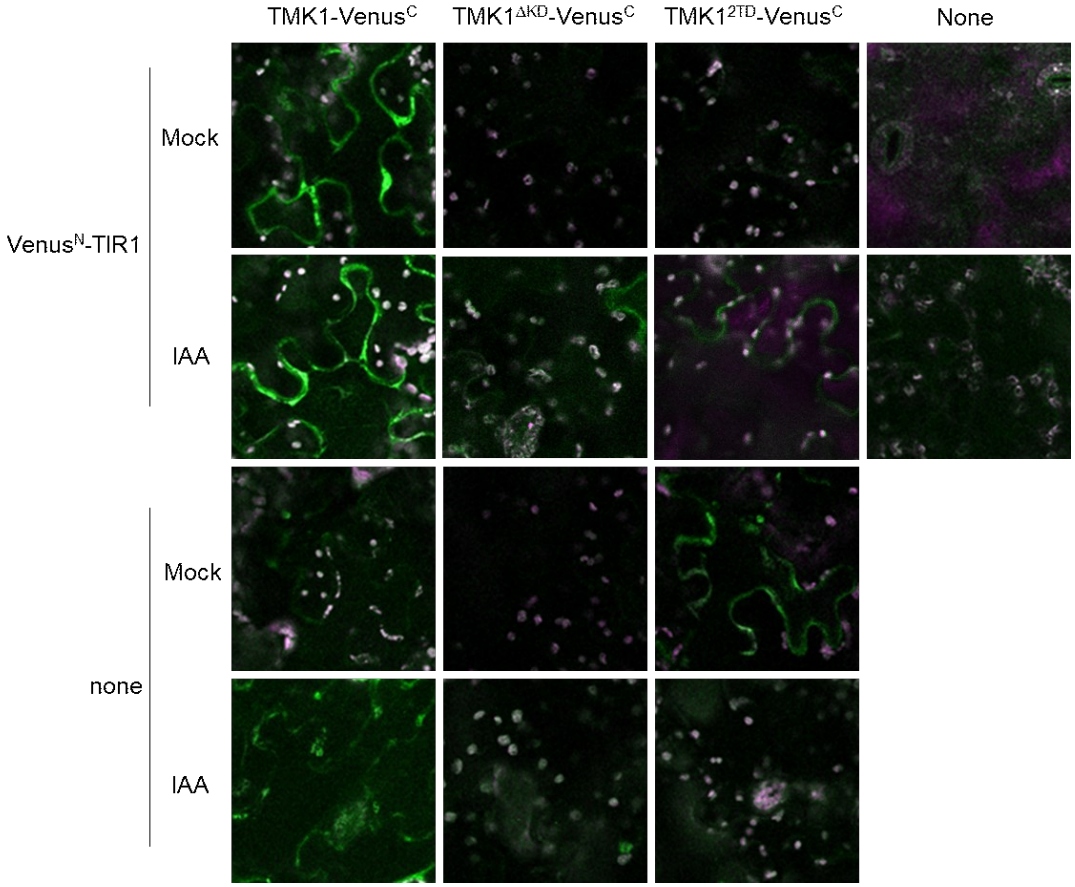


**Figure 8.** TIR1 interacts with TMK1 in BiFC.

BiFC was performed in tobacco leaves transiently expressing N-terminal VENUS fused with TIR1 and C-terminal VENUS fused with TMK1, TMK1ΔKD (kinase domain deletion) and TMK12TD (constitutive kinase activity). Magenta for auto-fluorescence and green for VENUS signal. Tobacco leave disks were cut and immerged in the liquid medium containing 10 μM IAA or mock for 1 hour before imaging.

## *4.7 TIR1/AFB1 may interact with TMK1 at the PM-cytosol interface*

TIR1/AFB1 interact with TMK1 biochemically and *in vivo.* To analyze where and how they may interact, we examine their localization. We performed fractionation western blot on *pAFB1::AFB1-VENUS* as AFB1 is relatively stable and observed that it is mostly found in cytosol and less in the nucleus (Figure 9), in line with the previous publications [1].

Additionally, we found a small portion of AFB1 in the microsomal part (Figure 9) where TMK1 mostly is localized, providing a possible location for the interaction; however, a proper control showing no contamination from other compartments will be needed.

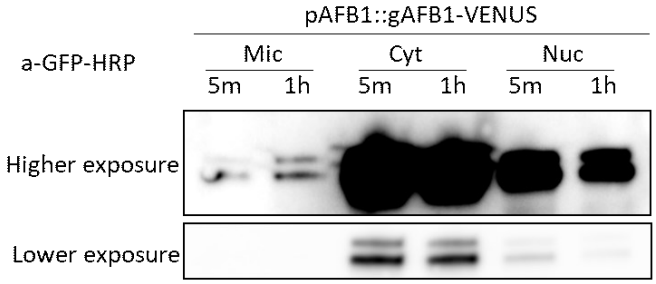


**Figure 9.** AFB1 appear in all cellular compartments.
CoIP performed on different fractionations (microsomal, cytosol and nuclear) of 4-day-old *pAFB1::gAFB1-VENUS* roots using GFP beads. Protein extracted from roots treated with 5 nM IAA for 5 minutes and 1 hour were blotted using anti-GFP-HRP antibody. Upper and lower lane showed imaging with higher and lower exposure time, respectively.

Considered that TIR1 is mostly localized in the nucleus and its proportion in other cellular compartment is rather difficult during imaging Arabidopsis TIR reporter line, we alternatively overexpressed TIR1 in protoplasts and examined the localization of both TIR1 and TMK1 after co-expressing *p35S::mCherry-TIR1* and *p35S::TMK1-GFP* in protoplasts. The positive control IAA7 and TIR1 showed an overlap in their localization. In contrast, no obvious overlap was observed between TIR1 and TMK1 variants. Despite that, we detected significant amount of TIR1 in endoplasmic reticulum (ER) or cytosolic compartments (Figure 10), hinting for that TIR1 is able to be localized near the PM for a potential interaction with PM-localized TMK1. However, a better resolution such as using electron microscope will be needed to clarify whether a small portion of TIR1 is localized near the PM.

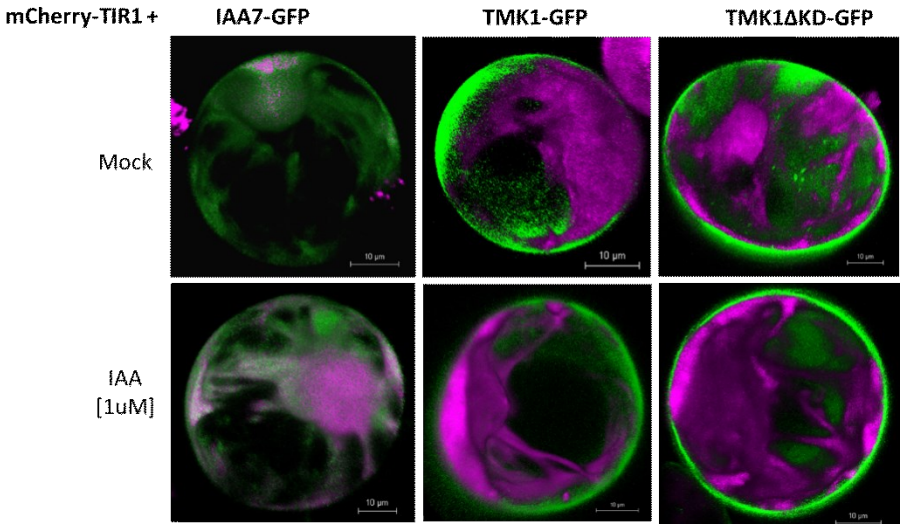


**Figure 10.** TIR1 and TMK1 co-expression in protoplasts.
3D presentation of protoplasts transiently expressing *p35S::mCherry-TIR1* and *p35S::IAA7-GFP* (as positive control) or *p35S::TMK1-GFP* or *p35S::TMK1ΔKD-GFP* (kinase domain deletion). Mock and 1 µM IAA treatment for 1 hour shown in upper and lower lane, respectively. Green represents GFP signal and magenta indicates mCherry signal.

As AFB1 can be found in the microsomal fraction (Figure 9), we further tested if AFB and TIR1 can directly bind to membrane lipids. We prepared the lipids of Phosphatidylserine (PS), the intracellular phospholipid component of the cell membrane, and of Phosphatidylcholine (PC), the extracellular phospholipid component of cell membranes as a key structural lipid, mixed with *in vitro* synthesized AFB or TIR1 using Wheat Germ Mix transcription system. After centrifuge, all TIR1, AFB1 and AFB4 can be detected together with the pelleted lipid with only little remaining in the supernatant, indicating that TIR1/AFB can strongly associate with membrane lipids, independent of auxin (Figure 11a). Alternatively, we verified it using the lipid strips containing different species of lipids. We found a high abundance of AFB1 attached to Phosphatidylinositol 3-phosphate (PI(3)P), the lipid located in ER, to Phosphatidylinositol 4-phosphate (PI(4)P), the lipid located in Golgi and PM, and to Phosphatidylinositol 5-phosphate (PI(5)P) that is localized in the nucleus. Additionally, low but detectable amount of AFB1 can be found in PS but not PC lipids (Figure 11b), in line with the previous result. Taken together, TIR1/AFB can interact with different membrane lipids including PM lipids, providing a basis for their interaction with PM-localized TMK1.

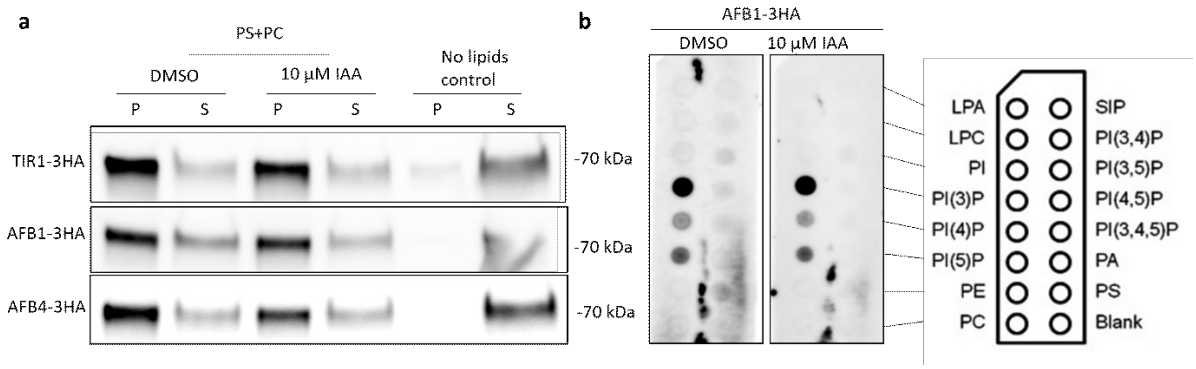


**Figure 11.** TIR1/AFB bind to lipids.

**a**, Lipid binding assay analyzing protein TIR1-3HA, AFB1-3HA and AFB4-3HA that were synthesized *in vitro* using Wheat Germ Mix transcription/translation system. The Phosphatidylserine (PS) and Phosphatidylcholine (PC) lipids were mixed with TIR1/AFB in presence of 10 μM IAA or mock (1 hour incubation), followed by centrifuge. P, proteins pelleted with lipid after centrifuge; S, supernatant after centrifuge. Synthesized protein mixed with solution without lipid as negative control. Anti-HA antibody was used.

**b**, Lipid strips embedded with various lipids incubated with synthesized (the same as in **a**) AFB1-3HA with or without 10 μM IAA for 1 hour. Anti-HA antibody was used.

## *4.8 CUL1 interacts with TMK1*

In canonical auxin pathway, TIR1/AFB, as F-box proteins, form the SCF E3 ligase together with CUL1. We showed that TIR1/AFB can interact with TMK1. Here, we tested whether CUL1, another component in SCF machinery, can bind to TMK1 or not.

We analyzed the localization of CUL1 by immunostaining using anti-CUL1 antibody and found that it was localized mostly in the nucleus in the elongating cells but also at the PM of the cells in the transition and meristematic zones (Figure 12a). Besides, TMK1 is mostly localized at the PM in all cell types (Figure 12b). Thus, their expression pattern do overlap.

Furthermore, we CoIP TMK1 using *pTMK1::TMK1-FLAG* or *pUBQ10::TMK1K616R-cMyc-mCherry* lines and detected CUL1 only in the WT version of TMK1 (Figure 12c) but not in the K616R mutated version (kinase dead) (Figure 12d). Besides, auxin application led to an increased CUL1 detection, indicating that auxin increases the interaction between CUL1 and TMK1 (Figure 11c), in line with auxin-induced interaction between AFB1 and TMK1. This result, though, cannot distinguish whether TIR1/AFB-CUL as a complex interact with TMK1 or the detection of CUL1 resulting from its endogenous association with TIR1/AFB. (These

two scenarios can be tested by in vitro pull down assay.) However, it still supports that TIR1/AFB interacts with TMK1 and auxin increases their interaction.

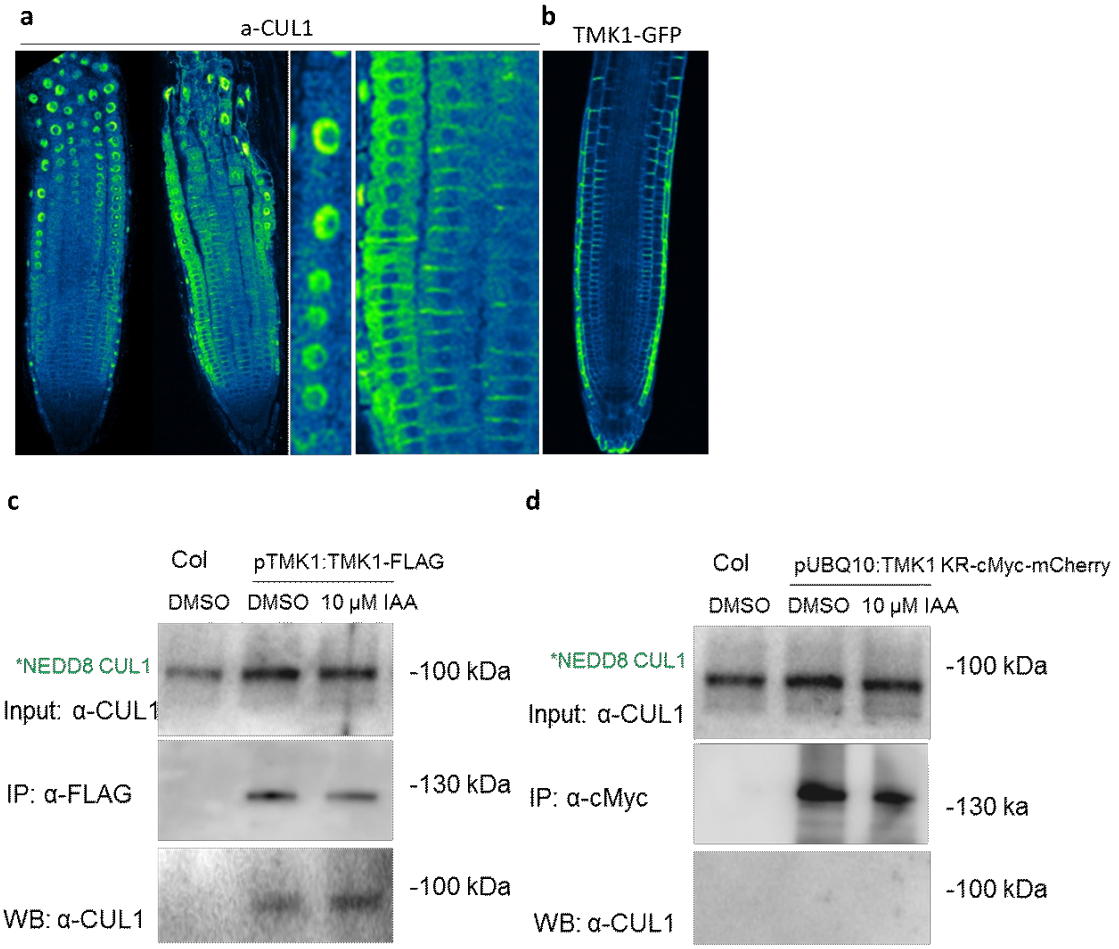


**Figure 12.** CUL1 interacts with TMK1.

**a**, Localization of CUL1 in roots detected by anti-CUL1 antibody using immunostaining. Two individual roots are shown on the left, and the close-up images are shown on the right. Pseudo color Green-Fire-Blue LUT was applied. Green for higher intensity and blue for lower intensity.

**b**, Localization of TMK1 in roots using *pTMK1::TMK1-GFP* lines. Pseudo color Green-Fire-Blue LUT was applied. Green for higher intensity and blue for lower intensity.

**c-d**, CoIP TMK1-FLAG (**c**) or TMK1KR-cMyc-mCherry (**d**) from root samples of *pTMK1::TMK1-FLAG* or *pUBQ10::TMK1KR-cMyc-mCherry*. 5-day-old seedlings were treated with 10 μM IAA and roots were harvested.

## *4.9 Another role: TMK1 contributes significantly to TIR1/AFB-mediated gravitropism*

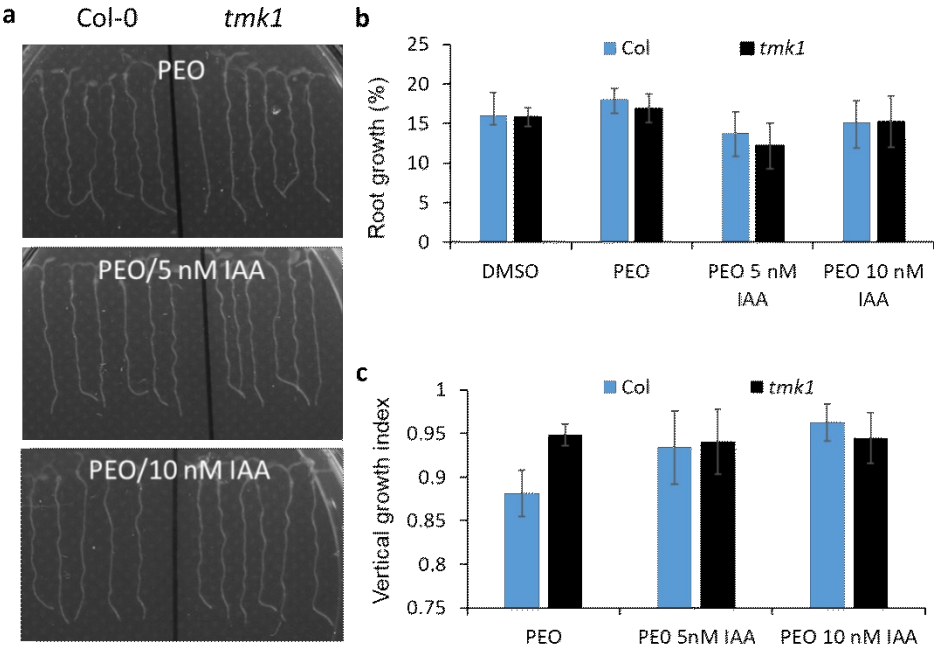


**Figure 13.** TMK1 is involved in TIR1/AFB-mediated root gravitropism.
Visualization (**a**) and quantification of root growth percentage (**b**) and vertical growth index (**c**) in *tmk1-1* seedlings after treatments of 10 μM PEO-IAA alone, PEO-IAA together with 5-10 nM IAA.

We tried to block TIR pathway using 10 μM PEO-IAA and examine the role of TMK1 during root growth regulation and gravitropism. We found that *tmk1* showed normal response to PEO-IAA for root growth (Figure 13a-b), in line with the notion in the Chapter 3 that TIR1/AFB mediate auxin-induced root growth regulation while TMK1 is a part of the feedback mechanism. On the other hand, we observed that PEO-IAA led to agravitropic response in WT roots but not in *tmk1* (Figure 13a, c). As this effect can be rescued by IAA in both mutants and WT (Figure 13a, c), we think that it is unlikely that PEO-IAA activates TMK1 pathway independently for a gravitropic response (otherwise IAA will not rescue it). Thus, these suggest that when TIR1/AFB function is perturbed, TMK1 significantly affects gravitropism, hinting for that TMK1 possibly mediates TIR1/AFB-executed gravitropism.

## *4.10 Feedback: TMK1 regulation on TIR1/AFB1*

Previous studies showed that the intensity of auxin signaling reporter DR5 was attenuated in *tmk* mutants [1], indicating a role of TMK in regulation of canonical auxin signaling. As we discovered the interaction between TIR1/AFB and TMK1, we further test if TMK1 regulates TIR1/AFB to modulate TIR1/AFB canonical signaling. We crossed *tmk1-1 or tmk4-1* with *pTIR1::TIR1-VENUS* or *pAFB1::AFB1-VENUS* and checked the intensity of TIR1 or AFB1 in *tmk* mutants. We found that lacking of TMK1 led to a slight but significant decrease in the intensity of TIR1-VENUS, independent of auxin (Figure 14a-b). This suggests that TMK1 positively regulates TIR1 level. Similarly, TMK4 might also positively regulates TIR1 level (Figure 14c-d). However, lacking of TMK4 resulted in a slight increase in AFB1 level (Figure 14e-f), suggesting that TMK4 negatively regulates AFB1 level.

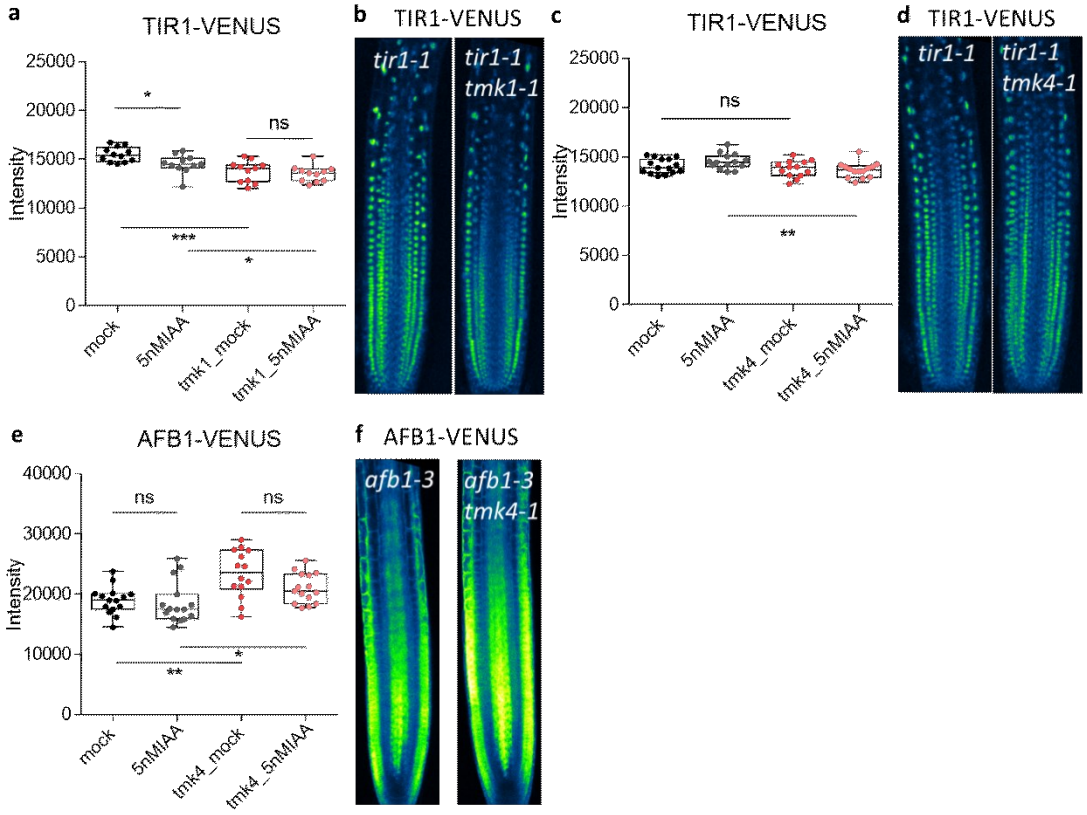


**Figure 14.** TMK1/4 regulate TIR1/AFB1 level.

**a-f**, Visualization (**b, d, f**) and quantification (**a, c, e**) of the fluorescence intensity in TIR1-VENUS (**a-d**) and AFB1-VENUS (**e-f**) in *tmk1-1* (**a-b**) and *tmk4-1* (**c-f**) roots compared to that in WT. The intensity was measured on the whole root tip area from the Z projected images. 5 nM IAA application for 1 hour.

Given that TMK may regulate TIR1/AFB level (Figure 14) and their downstream signaling [1], and that TMK1 is a kinase, we hypothesis that TMK1 may phosphorylate TIR1/AFB and regulate it stability. First, we predicted the potential phosphorylation sites in the sequences of TIR1/AFB family members and detected S434 conserved among TIR1, AFB1, AFB2 and AFB3 using an online website (Figure 15), suggesting that TIR1/AFB could be potentially phosphorylated at a Serine site.

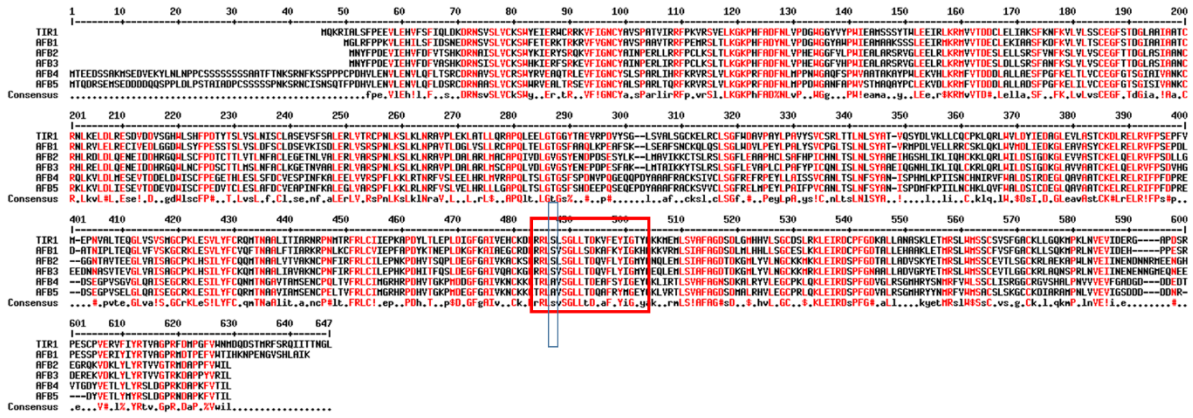

**Figure 15.** Predicted phosphorylation site in the sequences of TIR1/AFB proteins.
The sequences of TIR1/AFB were aligned with conserved sites marked in red. The blue window marked the Serine site conserved among TIR1, AFB1, AFB2 and AFB3, and this site is potentially phosphorylated following the prediction on the website scansite4.mit.edu.

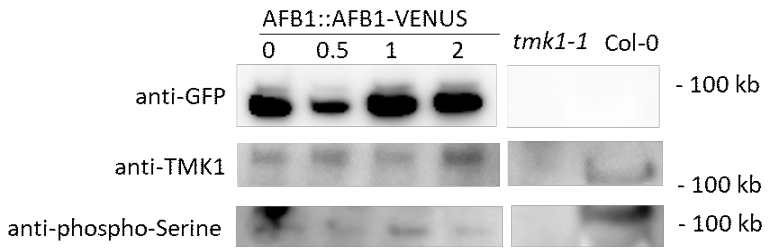


**Figure 16.** AFB1 is phosphorylated at Serine site(s).
CoIP AFB1-VENUS using GFP beads detected phosphorylated Serine using anti-phospho-Serine antibody at similar size to AFB1-VENUS. Treatment of 5 nM IAA was applied to 4-day-old seedlings for 0, 0.5, 1, and 2 hours and roots were harvested. The AFB1 phosphorylation was decreased after treatment of 5 nM IAA for 2 hours, correlating with an increased interaction with TMK1.

To verify if AFB1 is phosphorylated and how TMK1 interaction affects it, we Co-IP the AFB1-VENUS from the root extracts and detected phosphorylated Serine using Phosphoserine antibody (Figure 16) but did not detect phosphorylated Threonine (not shown). This confirms that AFB1 can be phosphorylated at Serine site(s). Inexplicably, Serine-phosphorylation on AFB1 was decreased in 2 hour when more TMK1 was associated to AFB1. This indicates that AFB1 is phosphorylated in the steady state, and auxin treatment decreases its phosphorylation which is correlated to an increased interaction with TMK1. A possible scenario is that AFB1 is phosphorylated by other kinases which is competing with and replaced by TMK1 in presence of high auxin. And the following open questions are what biological meaning for the phosphorylation of AFB1 and does it regulates the stability of AFB1.

## *4.11 Conclusions*

In this chapter, we showed that TIR1/AFB and TMK1 act antagonistically in the auxin-regulated growth in shoots and roots (Figure 1). Especially, both of them have opposite growth regulation in shoots and roots. Biochemically, we found that they both positively regulate PM $H^+$-ATPase AHA2 in the steady state and in presence of high auxin (Figure 2 and 3). Using ccvTIR1-cvxIAA system, we triggered TIR1-specific pathway and found lacking of TMK1 still makes root growth hypersensitive to cvxIAA application, confirming that TMK1 and TIR1/AFB are in the same pathway for pH and growth regulation (Figure 5). Furthermore, auxin-induced TMK1 increase requires TIR1/AFB (Figure 4), indicating TIR1/AFB is upstream of TMK1. This, together with the Chapter 3, forms a model where TIR1/AFB conduct the main pathway through $H^+$-influx and canonical auxin pathway to inhibit root growth, while TIR1 branches out through TMK1-AHA2 to counteract the main effect, for a fine-tuned growth regulation.

Significantly, we showed that TIR1/AFB and TMK1 can interact using CoIP with plant root extracts (Figure 6) and BiFC with tobacco leaves (Figure 7 and 8). The interaction might take place at the interface between PM and cytosol where TMK1 and TIR1/AFB are localized, respectively (Figure 9, 10). This potential interacting location is supported by the notion that TIR1/AFB are able to bind to membrane lipids (Figure 11). Additionally, another component of SCF, CUL1 can also associates with TMK1, and the interaction requires TMK1 kinase activity and is enhanced by auxin (figure 12).

This interaction between TMK1 and TIR1/AFB can lead to regulation on the protein level of each other. We found that auxin can induce TMK1 protein level and it requires TIR1/AFB (Figure 4). Considered that auxin increases the interaction of these two, it is possible that auxin induces TMK1-TIR/AFB interaction leading to accumulation of TMK1 protein, and that TIR1 maintains TMK stability in presence of auxin, which provide a molecular mechanism for TIR1-TMK-AHA pathway in Chapter 3.

On the other hand, TMK1 also regulate TIR1/AFB protein level in the steady state (Figure 14), which potentially underlies its regulation on auxin-induced TIR1 canonical signaling [2]. Notably, AFB1 was phosphorylated on Serine site(s) in the steady state, while the Serine phosphorylation was reduced correlating to an increased TMK1 association (Figure 15 and 16). This suggests that TMK1 competes with (an) unknown kinase(s) phosphorylating AFB1 upon interaction.

Additionally, we observed that TMK1 may function in the TIR1/AFB-mediated root gravitropism, as blocking TIR1/AFB using PEO-IAA leads to agravitropic response in WT roots but not in *tmk1-1* roots.

Open questions for the future to pursue as following.

1) Do TIR/AFB-TMK interact and regulate each other in shoots?
2) Does TIR1/AFB alone or with the whole SCF machinery interact with TMK1, and how TIR1/AFB regulate the stability of TMK1?
3) What is the biological meaning of the phosphorylation of TIR1/AFB, which sites are phosphorylated, can it be phosphorylated by TMK1, and does the phosphorylation regulate the stability of TIR1/AFB?

## *4.12 References*

1 Prigge, M.J.*, et al.* Genetic analysis of the Arabidopsis TIR1/AFB auxin receptors reveals both overlapping and specialized functions. *Elife* 9, e54740 (2020).

2 Dai, N., Wang, W., Patterson, S. E. & Bleecker, A. B. The TMK subfamily of receptor-like kinases in Arabidopsis display an essential role in growth and a reduced sensitivity to auxin. *PloS one* **8**, e60990 (2013).

# Chapter 5

## RALF1 triggers biphasic root growth inhibition involving auxin signaling

Lanxin Li[1], Huihuang Chen[1], Saqer S. Alotaibi[2], Aleš Pěnčík[3,4], Maciek Adamowski[1], Ondřej Novák[2,3], Matyáš Fendrych[5] and Jiří Friml[1]*

[1]Institute of Science and Technology (IST) Austria, 3400 Klosterneuburg, Austria

[2]Department of Biotechnology, College of Science, Taif University, P.O.BOX 11099, Taif 21944, Saudi Arabia.

[3]Institute of Experimental Botany, Czech Academy of Sciences, 78371 Olomouc, Czech Republic

[4]Department of Metabolomics, Centre of the Region Haná for Biotechnological and Agricultural Research, Faculty of Science, Palacký University, 78371 Olomouc, Czech Republic

[5]Department of Experimental Plant Biology, Charles University, Vinicna 5, 12800, Prague, Czech Republic

*Correspondence to: jiri.friml@ist.ac.at

## *5.1 Abstract*

Plant cell growth responds rapidly to various stimuli, adapting plant architecture to environmental changes. Two fast growth regulators are the secreted peptide rapid alkalinization factor (RALF) and the phytohormone auxin. Both trigger rapid cellular responses and exert long-term effects (1, 2). However, the way in which these distinct signaling pathways converge to regulate growth remains unknown. Using vertical confocal microscopy combined with a microfluidic chip, we examined the correlation between RALF1-induced rapid *Arabidopsis thaliana* root growth inhibition and apoplast alkalinization during the initial phase of the response. Furthermore, we investigated the crosstalk between RALF1 and the auxin signaling pathways during root growth regulation using time-lapse imaging. The results showed that RALF1 rapidly and reversibly inhibited primary root growth through apoplast alkalinization within one minute. This rapid apoplast alkalinization was the result of RALF1-induced $H^+$ influx and was mediated by the receptor FERONIA (FER). Moreover, RALF-FER signaling triggered auxin signaling in approximately one hour by upregulating auxin biosynthesis, thus contributing to sustained growth inhibition. This biphasic growth regulation allows plants to respond rapidly to environmental stimuli and reprogram growth and development in the long term.

**Keywords**: RALF1, auxin, crosstalk, root growth inhibition, apoplast alkalinization, biphasic regulation

## *5.2 Introduction*

Plant motions exhibit a wide range of speeds, from seed bursting in milliseconds to stomata opening in minutes to long-term architecture adaptation. One of the fastest underlying cellular motions is water-driven cell growth, such as root cell expansion under abiotic or biotic stress during gravitropism. Cell growth is directly regulated by the apoplastic pH, according to the Acid Growth Theory (3), which states that a low pH activates enzymatic reactions to modify the extensibility of cell walls and promote cell growth. Among numerous plant growth substances, two recognized rapid cell growth regulators are rapid alkalinization factor (RALF) peptides and the phytohormone auxin, which represent short- and long-range endogenous signals, respectively.

The RALF1 polypeptide can dramatically arrest root growth and alkalinize the cell medium (4, 5). It belongs to a family of over 37 members in *Arabidopsis thaliana* (6, 7). The presence of RALFs throughout the plant kingdom (as well as in fungi and bacteria) indicates their importance in the fundamental regulatory processes of plant growth and development (8, 9). The first discovered RALF receptor, FERONIA (FER), belongs to the *Catharanthus roseus* RLK1-like (crRLK1L) family in *A. thaliana*, with 17 members (10, 11). FER is located in the plasma membrane (PM) and consists of an extracellular domain with two malectin-like domains, a transmembrane domain, and an intracellular kinase domain (12). The kinase domain partially contributes to RALF1-induced root growth inhibition (13, 14).

RALF1-induced extracellular alkalinization coincides with RALF1-triggered phosphorylation of the PM $H^+$-ATPase 2 (AHA2) at Ser899 (10). Phosphomimetic mutation AHA2 S899D in yeast causes yeast cell growth inhibition (10). Thus, AHA $H^+$ pumps are thought to mediate RALF1-induced growth inhibition. However, whether $H^+$ pump activity is reduced by RALF1 and how this contributes to RALF1-FER-mediated alkalinization remain largely unknown (2). Moreover, several studies have shown that some RALF1-elicited growth inhibition might be independent of alkalinization (15, 16), leaving the biological roles of the RALF1-induced pH increase and other downstream effects of RALF1 signaling an open question (2).

Unlike RALFs, auxin is a long-range endogenous signal. Natural auxin, indole-3-acetic acid (IAA), is synthesized in both shoots and roots (17). It is mainly derived from the amino acid tryptophan (Trp) after sequential catalysis by the tryptophan aminotransferase of Arabidopsis (TAA) family and the YUCCA (YUC) family (18). Auxin can then be directionally transported from cell to cell via PIN, AUX1/LAX, and ABCB transporters (19). Finally, auxin participates in several signaling pathways. The TIR1/AFB receptors mediate the nuclear auxin signaling pathway together with the co-receptors Aux/IAA for transcriptional regulation (20). The TIR1/AFB receptors have also been shown to mediate a rapid, non-transcriptional $H^+$ influx across the PM for rapid growth inhibition (21-23). Moreover, the transmembrane kinase (TMK) family (auxin signaling components on the cell surface) plays versatile roles in growth regulation. TMK1 regulates gene transcription in the apical hook (24) and phosphorylates and activates PM $H^+$-ATPases, leading to apoplast acidification and growth promotion in shoots and roots (23, 25). TMK4 suppresses auxin biosynthesis (26). Auxin biosynthesis, transport, and signaling collectively contribute to the regulation of cell growth.

Both RALF and auxin trigger rapid responses, including extracellular alkalinization and growth inhibition. The crosstalk between these two growth regulators is of great interest. FER

possibly plays a role in auxin-regulated root growth inhibition (27). Conversely, RALF1-FER signaling regulates auxin transport. For instance, *fer-4* mutants have aberrant PIN2 and AUX1 polarity during gravitropism and root nutation growth (28, 29). Moreover, RALF1 has been found to trigger PIN2 internalization (30). Despite their connections, how these two growth regulators could converge on the immediate responses of extracellular alkalinization and primary root growth inhibition and their long-term effects remain largely unknown.

In this study, we revisited RALF1-induced rapid growth inhibition by analyzing the early kinetics of growth and apoplastic pH using microfluidics and time-lapse imaging of seedling growth in semi-normal growing conditions. We found that RALF1 triggers biphasic growth regulation, including a rapid phase taking place in one minute and another phase occurring within one hour, during which auxin is upregulated, facilitating auxin signaling to reprogram the growth and developmental state.

## *5.3 Both RALF1 and auxin alkalinize the apoplast to inhibit root growth rapidly and reversibly*

RALF1 induces rhizosphere alkalinization (31) and dramatically inhibits root growth (2). The rapid action of RALF1 resembles that of auxin, which also triggers apoplast alkalinization, leading to root growth inhibition within 30 seconds (23). To examine the temporal dynamics of RALF1-regulated root growth and the causal relationship between RALF1-induced alkalinization and growth inhibition, we used a microfluidic vRootchip (21, 23) combined with vertical confocal microscopy (32) for live imaging and applied a membrane-impermeable ratio-metric pH dye, 8-hydroxypyrene-1,3,6-trisulfonic acid (HPTS) (27) to investigate changes in the apoplastic pH. We tracked root tip growth as a sensitive readout for the accumulative effects of the elongation of individual cells and simultaneously monitored the apoplastic pH in elongating cells. We found that externally applied RALF1 at 10 μM dramatically inhibited root tip growth (Fig. 1 *A*) and alkalinized the apoplast in elongating cells (Fig. 1 *B*) within one minute of application (Fig. 1 *C*), indicating a close correlation between apoplast alkalinization and root growth inhibition induced by RALF1. As a complementary approach, we analyzed the cytosolic pH in the elongating epidermal cells using a *PM-Cyto* reporter (33). The cytosolic pH adjacent to the PM decreased rapidly after RALF1 application (Fig. 1 *D*). The pH increase outside the PM and the decrease inside it suggest that RALF1 triggers a rapid $H^+$ influx into

the cell, in line with previous observations of RALF33- and RALF36-induced increase in $H^+$ net flux measured by a noninvasive microelectrode (34).

Rapid growth responses to auxin occur without transcriptional regulation (21, 23). We thus examined whether this applies to RALF1 as well. We applied the protein translation inhibitor cycloheximide (CHX) for three minutes in vRootchip to block protein synthesis (21). We found that the addition of RALF1 still led to rapid root growth inhibition and apoplast alkalinization (Fig. S1 *A*), suggesting that RALF1 non-transcriptionally regulates a rapid $H^+$ influx and root growth inhibition. Furthermore, we examined whether RALF1-induced growth inhibition is reversible, like the response to auxin (21). We attempted to wash out the RALF1 effect using the basal medium in vRootchip; however, there was no growth recovery, and RALF1 precipitation blocked the medium flow in vRootchip within hours. Employing an alternative method, we transferred RALF1-pretreated seedlings to a fresh agar block containing a basic medium and observed a complete recovery of growth in 20 minutes (Fig. S1 *B*). This suggests that RALF1 inhibits root growth and alkalinizes the apoplast rapidly and reversibly.

To examine whether FER, the receptor of RALF1 on the PM (30), mediates the RALF1-triggered rapid responses, we analyzed *fer-4* mutants in vRootchip. After the application of 5 μM of RALF1, we observed slight root growth inhibition and slightly but significantly less apoplast alkalinization in *fer-4* compared to the complemented line *pFER::FER-GFP* in *fer*-4 (Fig. 1 *E* and *F*). This suggests that FER contributes to RALF1-triggered rapid responses, consistent with previous studies showing that FER mediates the rapid $H^+$ influx induced by RALF33 (34) and the long-term medium pH changes triggered by RALF1 (10). To track the long-term growth response, we recorded seedlings transferred to media containing various concentrations of RALF1 on a high-throughput vertical scanner (35). We found that the *fer-4* mutants were completely insensitive to 0.1–10 μM of RALF1 (Fig. S1 *C* and *D*) from the first to the fifth hour, indicating that receptor FER mediates long-term growth responses. To examine whether other crRLK paralogs contribute to RALF1-mediated long-term growth inhibition, we analyzed the root growth of *the1-1* and *herk* mutants after RALF1 treatment at various concentrations. We found that all of them exhibited a normal growth response over time (Fig. S1 *C–F*). Overall, FER dominantly mediates RALF1-triggered rapid and long-term growth inhibition.

RALF1-triggered rapid root growth inhibition and apoplast alkalinization closely correlate over time (Fig. 1 *A–C*). As we showed previously, in the context of auxin-triggered root growth, manipulation with the medium's pH has a direct impact on root growth (23). We observed that an alkaline medium inhibited root growth, while an acidic medium promoted

growth immediately and reversibly (Fig. 1 *G* and *H*), supporting that RALF1-triggered apoplastic alkalinization can cause rapid root growth inhibition. Importantly, *fer-4* and the complemented line had similar responses to external pH manipulation (Fig. 1 *G* and *H*), indicating that FER does not sense or respond to pH fluctuations but mediates RALF1-induced rapid apoplastic alkalinization and root growth inhibition.

## *5.4 TIR1/AFB auxin signaling is downstream of RALF-FER pathway during sustained root growth inhibition*

The RALF-FER and auxin-TIR1/AFB signaling mechanisms (23) have very similar rapid effects on PM $H^+$ influx and root growth inhibition. To investigate the possible interdependence of these mechanisms, we reciprocally examined the root growth reactions of the mutant of one receptor to the ligand of another. In vRootchip, *fer-4* showed rapid and normal growth inhibition after treatment with 5 nM of IAA (Fig. S2 *A*). Using the vertical scanner, we also observed that IAA inhibited the root growth of *fer-4*, *the1-1*, and *herk* mutants similarly to the wild type (WT) over a period of six hours (Fig. S2 *B*). Only when we used a high dose of IAA (100 nM) did we observe a transient and slight growth resistance of *fer-4* mutants, and only between the first and fifth hours (Fig. S2 *C*), in line with a previous study reporting *fer-4* resistance to 250 nM of IAA after eight hours of incubation (27). Considering the transient nature of decreased sensitivity and the high level of auxin required, we do not consider this observation evidence of direct FER activity in auxin-mediated growth regulation. Mutants may exhibit this slight resistance due to their reduced ability to take up exogenous auxin caused by defective PIN2 polarity (28, 29). Overall, we did not find evidence of a direct role of FER and its paralogs in auxin-mediated rapid root growth inhibition.

Reciprocally, we examined how impaired auxin signaling affects RALF1-triggered growth inhibition. We analyzed the contributions of two main types of auxin signaling: (i) the cell surface auxin signaling components TMK and (ii) the intracellular auxin signaling receptors TIR1/AFB and co-receptors Aux/IAA. The *tmk1-1*, *tmk4-1*, and *tmk1,4* double mutants responded to treatment with RALF1 at different concentrations similarly to the WT (Fig. S2 *D*), suggesting that this branch of auxin signaling is not involved in RALF1-mediated root growth inhibition. Notably, previous studies have shown that *tmk1,4* mutants have a significantly reduced abundance of AHA2 and general $H^+$-ATPase activity (23, 25). Given that *tmk1,4* mutants exhibit a normal response to RALF1, this suggests that $H^+$-ATPases may not

contribute to RALF1-induced growth inhibition. We tested this directly by assessing growth responses to RALF1 in *aha1-6* and *aha2-4* mutants, transgenic line *AtTAS1c-AHA* expressing synthetic trans-acting siRNA (36) targeting *AHA1/2/7/11* under the *PIN2* promoter in the outer root tissues (23), *ost2-3D* mutants with hyperactive AHA1, and *35S::SAUR19-GFP* with constitutively active AHAs (37). The single mutants *aha1-6* and *aha2-4* showed normal responses to 5 μM of RALF1 in terms of growth inhibition (Fig. S2 *E*), while the knockdown *AtTAS1c-AHA* lines showed hypersensitivity to 5 μM of RALF1 (Fig. S2 *F*), thus providing no indication that RALF1-induced growth inhibition was mediated by AHAs. The hyperactive *ost2-3D* mutants and *35S::SAUR19-GFP* lines also responded normally to 5 μM of RALF1 (Fig. S2 *G*). These observations suggest the possibility that, instead of AHA $H^+$-ATPases, an unknown $H^+$ channel or transporter contributes to the RALF-triggered $H^+$ influx across the PM, which has recently been suggested for auxin-induced $H^+$ influx (23).

Next, we investigated the involvement of the TIR1 auxin signaling pathway in RALF1-induced root growth inhibition. We employed the synthetic compound PEO-IAA, which acts as an auxin antagonist and blocks TIR1/AFB-mediated signaling by binding to the TIR1/AFB receptors (38). The application of 10 μM of PEO-IAA rescued root growth inhibition caused by 5 μM of RALF1, with the effect becoming stronger after approximately one hour (Fig. 2 *A* and *B*). Additionally, we employed a dominant negative variant of the Aux/IAA protein IAA17, expressed conditionally in the *HS::axr3-1* line. After heat-shock induction, *HS::axr3-1* seedlings exhibited reduced sensitivity to root growth inhibition at 5 μM of RALF1 after one hour (Fig. 2 *C*). These results indicate that TIR1/AFB-mediated auxin signaling participates in RALF1-induced long-term root growth inhibition.

As previously mentioned, blocking the TIR pathway made roots resistant to RALF1-triggered root growth inhibition after approximately one hour, while they seemed to be less affected during the first hour, as recorded by the vertical scanner. To examine the early time points, we first used vRootchip and observed that after RALF1 application, *tir1-1afb2-1afb3-1 (tir triple)* responded normally in both the short and long term (data not shown). The absence of long-term effects appeared inconsistent with the observations described above (Fig. 2 *A–C*). Therefore, we used an alternative method. We performed confocal imaging after transferring samples to agar blocks containing treatments and automatically tracked the root tip over time using TipTracker – a MATLAB-based program (32). We observed that the *tir triple* mutant showed normal growth reduction after treatment with 2 μM of RALF1 in the first hour (Fig. 2 *D*) but subsequently started to increase the growth rate, recovering to more than 80% of the initial rate after five hours (Fig. 2 *D*). Consistently, after treatment with 2 μM of RALF1, the

apoplast pH in the WT and *tir triple* increased to a similar extent in the first hour, after which the pH kept increasing in the WT but not in *tir triple* (Fig. 2 *E*). This indicates that the auxin signaling mutant *tir triple* exhibits a biphasic response to RALF1 treatment: its initial response is as sensitive as that of the WT, but its sensitivity decreases in the long term. This suggests a role of TIR/AFB signaling in the latter phase of the RALF1 response. We next examined whether the biphasic RALF1 response depended on the RALF1 dosage. We analyzed the growth responses to RALF1 at concentrations ranging from 1 to 5 μM on the vertical scanner. We observed a biphasic growth response in *tir triple* at 3 and 5 μM of RALF1, whereas 1 and 2 μM were not effective (Fig. S2 *H*). The growth rate of the mutant started to recover from 40 minutes onward, in line with the confocal imaging result (Fig. 2 *D*). The fact that we did not observe this recovery in vRootchip may have been because the constant flow of liquid medium changed the composition of root secretion or because the liquid growing condition differs from the agar growing condition. Finally, we tested mutants deficient in auxin response factors 10 and 16 (ARF10 and ARF16), which are transcription factors involved in canonical auxin signaling. We found that *arf10,16* responded to 10 μM of RALF1 normally at first, but their growth became resistant from the second hour onward (Figs. 2 *F* and S1 *D*). The recovery time was longer than in *tir triple* mutants, indicating that ARF10 and ARF16 participate in downstream regulation.

Taken together, RALF1-mediated biphasic growth responses in auxin signaling–deficient roots, either in mutants or after pharmaceutical manipulations, indicate that RALF1 plays a bimodal growth regulatory role and that auxin signaling mediates the sustained growth reduction after the initial, FER-mediated, response.

## *5.5 RALF1-FER signaling triggers auxin signaling*

To independently verify that the auxin-TIR1/AFB signaling pathway is downstream of RALF1-FER during root growth inhibition, we tracked the output of canonical auxin signaling using the reporter *R2DII*, which is based on the degradation of the auxin-responsive DII domain of Aux/IAA (39). Treatment with RALF1 at 10 μM led to DII degradation similarly to the effect of auxin at 10 nM, but with slower kinetics (Fig. 3 *A*). This indicates that RALF1 triggers nuclear auxin signaling. This RALF1-induced DII degradation was rescued by pretreatment with 10 μM of PEO-IAA (Fig. 3 *B* and *C*). In addition, we compared the kinetics of auxin signaling activation induced by RALF1 and IAA using the *DR5::LUC* line (40), in which the synthetic auxin-responsive promoter DR5 drives the expression of a fast folded/active

luciferase enzyme. We found that 10 μM of RALF1 triggered significant auxin signaling with a delay of approximately 10 minutes compared to treatment with 5 nM of IAA (Fig. 3 *D* and *E*). These observations suggest that RALF1 indirectly induces auxin canonical TIR1/AFB signaling and that the canonical TIR1/AFB auxin signaling pathway mediates RALF1-FER-induced sustained root growth inhibition.

We next examined whether the canonical TIR1/AFB auxin signaling pathway is also involved in root growth inhibition mediated by other RALF peptides. We analyzed RALF22, which, like RALF1, belongs to clade I of the RALF peptides (6). RALF22 inhibited root growth from the first hour onward and exerted a dosage-dependent effect similar to that of RALF1 (Fig. S3 *A*). The application of 10 μM of RALF22 led to DII degradation (Fig. S3 *B*) and an increase in DR5rev::GFP (Fig. S3 *C*) and DR5::LUC with a delay of approximately 10 minutes compared to 5 nM of IAA (Fig. S3 *D*). Furthermore, auxin signaling mutant *tir triple* became resistant to growth inhibition at 10 μM of RALF22 after one hour (Fig. S3 *E*). Also, *tmk1-1* mutants exhibited a normal growth response (Fig. S3 *D*). These observations indicate that auxin signaling is broadly involved in root growth inhibition induced by RALF peptides.

## *5.6 RALF1 promotes auxin biosynthesis*

Auxin signaling participates in RALF1-induced sustained root growth inhibition. Two possible scenarios may explain how RALF1-FER signaling triggers auxin signaling with a characteristic delay: the regulation of auxin transport and the regulation of auxin biosynthesis. To explore these two scenarios, we used pharmacological and genetic approaches. We pretreated seedlings with auxin transport inhibitors N-1-naphthylphthalamic acid (NPA) and 2,3,5-triiodobenzoic acid (TIBA) (41) at 10 μM for 80 minutes, and then applied 5 μM of RALF1 in a co-treatment with these inhibitors. We observed no rescue of RALF1-induced root growth inhibition (Fig. S4 A and B). We also tested the effect of RALF1 on mutants of PIN auxin efflux transporters pin2 and pin3,4,7 (42). Both mutants reacted normally to treatment with RALF1 at different concentrations (Fig. S4 C). These observations indicate that the modulation of auxin transport is unlikely to be the mechanism by which RALF1 triggers auxin signaling for root growth inhibition.

To examine whether RALF1 signaling regulates auxin biosynthesis, we preincubated seedlings in auxin biosynthesis inhibitors L-kynurenine (KYN; 20 μM) and yucasin (YUCA; 25 μM) (43, 44) for 80 minutes and then evaluated root growth on the surface of media additionally supplemented with 5 μM of RALF1. We observed that KYN completely rescued

RALF1-mediated root growth inhibition after four hours (Fig. 4 A), while YUCA resulted in partial rescue (Fig. 4 B). Similarly, KYN fully rescued RALF1-induced DII degradation, while YUCA had a partial effect (Fig. S4 D and E). Additionally, we tested the mutants of auxin biosynthesis genes TAA1, TAR1, TAR2, and YUCCAs, including wei8-1tar2-2, wei8-3tar2-2, wei8-3tar2-1, wei8-3tar1-1, and yuc2,5,7,8, and found that they were partially resistant to root growth inhibition at 5 μM of RALF1 (Fig. 4 C and D). These observations strongly suggest that auxin biosynthesis is involved in RALF1-triggered sustained root growth inhibition. As elevated auxin levels inhibit root growth (23), RALF1 may induce an increase in auxin levels that contributes to root growth inhibition.

To examine how RALF1 induces auxin biosynthesis, we employed reporter lines expressing eGFP under YUC native promoters. We observed an increased signal in the epidermal cells and/or stele of the late elongation zone of roots expressing pYUC5::eGFP-GUS, pYUC6::eGFP-GUS, and pYUC11::eGFP-GUS after treatment with 5 μM of RALF1 for three hours (Fig. 4 E and F). This suggests that RALF1 induces auxin biosynthesis by upregulating the transcription of YUCs. To examine whether RALF1 indeed increases the auxin levels and whether FER is required, we performed mass spectrometry analysis of auxin metabolites in root tips of the WT and fer-4 treated with 5 μM of RALF1 or mock for three hours. We found that RALF1 increased the levels of IAA, the major IAA catabolite oxIAA, and the conjugates IAA-aspartate (IAAsp) and IAA-glutamate (IAGlu) (Fig. 4 G) in WT roots but less or not at all in fer-4 mutants (Fig. 4 G). On the other hand, the direct IAA precursors indole-3-pyruvic acid (IPyA), indole-3-acetamide (IAM), and indole-3-acetonitrile (IAN) were slightly decreased, while the precursors in the earlier steps anthranilate (ANT) and tryptophan (TrpRP) increased, and tryptamine (TRA) decreased after RALF1 treatment for three hours in WT roots but less or not at all in fer-4 mutants (Fig. 4 H). This confirms that RALF1 leads to a shift in auxin homeostasis from precursors to IAA to its catabolites and conjugates and that the receptor FER is involved. Taken together, these observations suggest that RALF1-FER triggers auxin biosynthesis upregulation, contributing to sustained root growth inhibition.

Overall, the findings suggest that RALF1 triggers a biphasic FER-mediated root growth regulation, including (i) a phase of rapid and reversible growth inhibition through an H+ influx across the PM and (ii) a phase of sustained growth inhibition contributed mediated by canonical TIR1 auxin signaling via upregulation of auxin biosynthesis (Fig. 5).

## *5.7 Discussion*

RALF peptides are known to trigger extracellular alkalinization and arrest root growth (5, 10). Despite the correlation between alkalinization and growth inhibition, their causal relationship and molecular mechanisms remain largely unknown. In this study, we used a microfluidic chip and vertical confocal microscopy to achieve simultaneous live imaging of root growth and apoplastic/cytosolic pH. We showed that in one minute, RALF1-FER triggers rapid growth inhibition (Fig. 1 *C*) that is non-transcriptionally regulated (Fig. S1 *A*) and reversible (Fig. S1 *B*). Through external pH manipulation, we found that RALF1-FER-induced apoplast alkalinization leads to rapid and reversible growth inhibition. This resembles, but does not depend on, the rapid auxin regulation of root growth (Fig. 2 *D* and *E*) (23). In turn, through an analysis of auxin signaling mutants, especially *tir triple*, we uncovered a second, mechanistically different, stage of the RALF response, which is characterized by upregulation of auxin biosynthesis.

**RALF1-triggered root growth inhibition is not majorly mediated by PM $H^+$-ATPase**

We discovered that RALF1 induces an immediate $H^+$ influx across the PM (Fig. 1 *B–D*), like RALF33 and RALF36 (34). Regarding the mediation of this $H^+$ influx by RALF1-FER, it has been suggested that RALF1 may lead to the deactivation of PM $H^+$-ATPase AHA2 based on phosphorylation at the Ser899 site (10). However, it is unclear whether PM $H^+$-ATPases in *A. thaliana* are indeed deactivated responding to RALF1 and how much this contributes to rapid alkalinization (2). To study the role of PM $H^+$-ATPase during RALF1-induced root growth inhibition, we examined the mutants in PM $H^+$-ATPases and the mutants that had different PM $H^+$-ATPase levels or activity (Fig. S2 *D–G*). Except for the *AtTAS1c-AHA* mutants, which were hypersensitive to RALF1 (Fig. S2 *F*), all other mutants showed normal growth reduction (Fig. S2 *E* and *G*). All these results suggest that, rather than PM $H^+$-ATPases, an unknown $H^+$ channel or transporter contributes to a RALF1-triggered rapid $H^+$ influx. Whether the RALF1-FER-triggered $H^+$ influx has the same regulation mechanisms as the auxin-TIR/AFB-induced $H^+$ influx requires further investigation.

**RALF1-triggered sustained growth inhibition involves auxin signaling**

Our study demonstrated a biphasic growth response in auxin signaling–deficient roots by tracking the kinetics of root growth after RALF1 application. These roots responded normally to RALF1 treatment within the first hour but then developed resistance (Figs. 2 *B–F* and S2 *H*).

This phenomenon resulted from delayed auxin signaling induction (Fig. 3) through RALF1-FER-induced upregulation of auxin biosynthesis (Fig. 4).

In summary, we discovered that RALF1-FER triggers a biphasic root growth regulation that includes (i) a phase of rapid and reversible growth inhibition caused by an $H^+$ influx and (ii) a phase of sustained growth inhibition mediated by auxin biosynthesis and auxin signaling (Fig. 5). This biphasic growth regulation by RALF1 enables both intermediate and reprogrammed growth and developmental regulation in response to environmental changes.

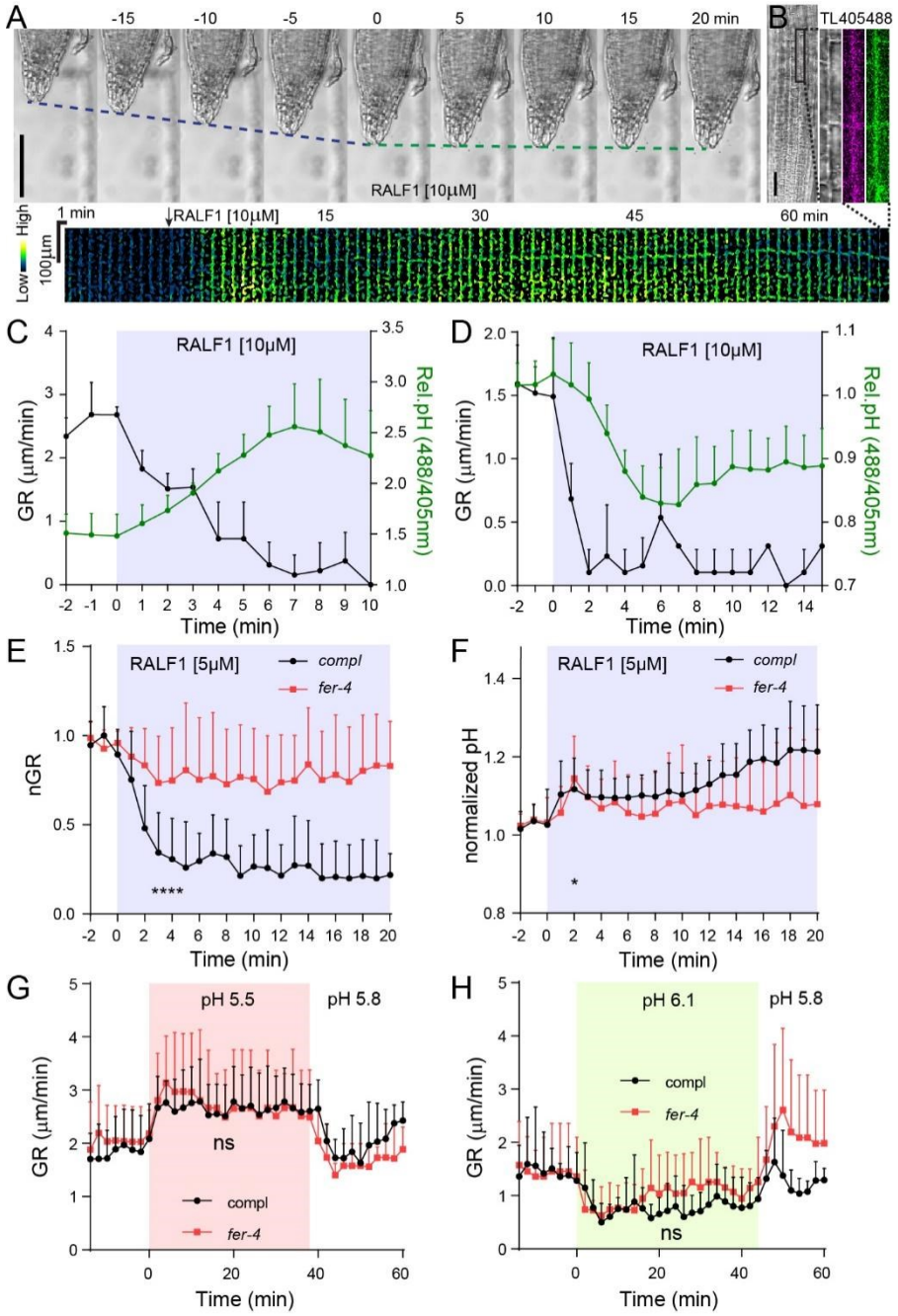

**Fig. 1. RALF1-FER signaling mediates rapid apoplast alkalinization correlating with rapid growth inhibition.**

(*A*) Time-lapse of root growth response to 10 μM RALF1 in vRootchip. The slope of blue and green dotted lines that track the root tip indicates the growth rate (GR) in basal medium and RALF1 medium, respectively. Scale bar, 100 μm.

(*B*) Time lapse of apoplastic pH response in root tip epidermal cells to 10 μM RALF1 in vRootchip. pH was monitored in the same region of interest (ROI) for 85 minutes by the ratiometric HPTS dye. The image represents the ratio of emissions upon excitation at 488 and 405 nm. ROI includes the cell wall of elongating cells. TL is transmitted light image.

(*C*) Quantification of root growth (a) and apoplastic pH in elongating cells (b) of WT plants with RALF1 treatment in vRootchip. Mean of 4 roots+SD.

(*D*) Root growth and cytosolic pH in elongating cells of WT plants with 10 μM RALF1 treatment in vRootchip. Mean of 3 roots+SD. Cytosolic pH was quantified using the PM-cyto marker.

(*E* and *F*) Normalized root growth rate (nGR) and apoplastic pH in *fer-4* and the complementary line (*compl*) *pFER::FER-GFP in fer-4* responding to 5 μM RALF1 treatment in vRootchip. nGR and apoplastic pH were normalized to the average value at time point 0 of the same genotype. Mean of 2 replicates, 7 roots for *compl* (*E*), 6 for *fer-4* (*F*)+SD. $^{****}p < 0.0001$, $^{*}p < 0.05$, two-way ANOVA.

(*G* and *H*) Root growth in *fer-4* and *compl* in response to a pulse of acidic (pH 5.5) (*G*) or alkaline (pH 6.1) (*H*) medium. Mean of 5 roots for *compl* and 3 for *fer-4* (*G*), and 5 roots for *compl* and 2 for *fer-4* (*H*)+SD. ns, $p > 0.05$, two-way ANOVA. The shaded areas represent the duration of the indicated treatments.

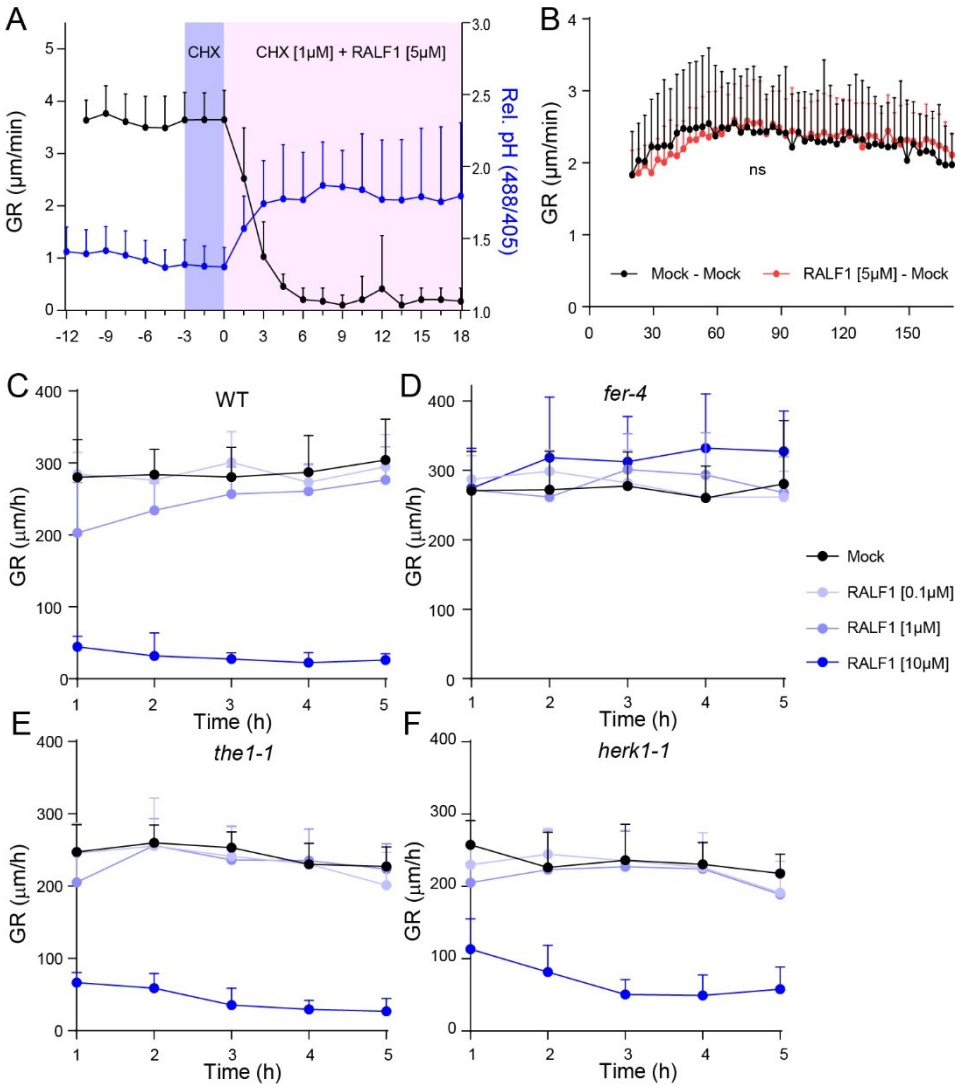


**Fig. S1. RALF1-FER mediates rapid and reversible root growth inhibition.**

(*A*) Root growth and apoplastic pH measured in WT plants in vRootchip with 3 minutes pre-treatment by 1 µM cycloheximide (CHX) followed by the addition of 5 µM RALF1. Mean of 8 roots+SD. The shaded areas represent the duration of the indicated treatments.

(*B*) Root growth of WT plants transferred to agar blot containing basal medium after 30 minutes pre-treatment of 5 µM RALF1 or Mock. Mean of 9 roots for each condition+SD. ns, $p > 0.05$, two-way ANOVA.

(*C-F*) Root growth of crRLK family mutants on different RALF1 concentrations. Root tips were recorded on vertical scanner. $n > 9$ for each condition, Mean+SD.

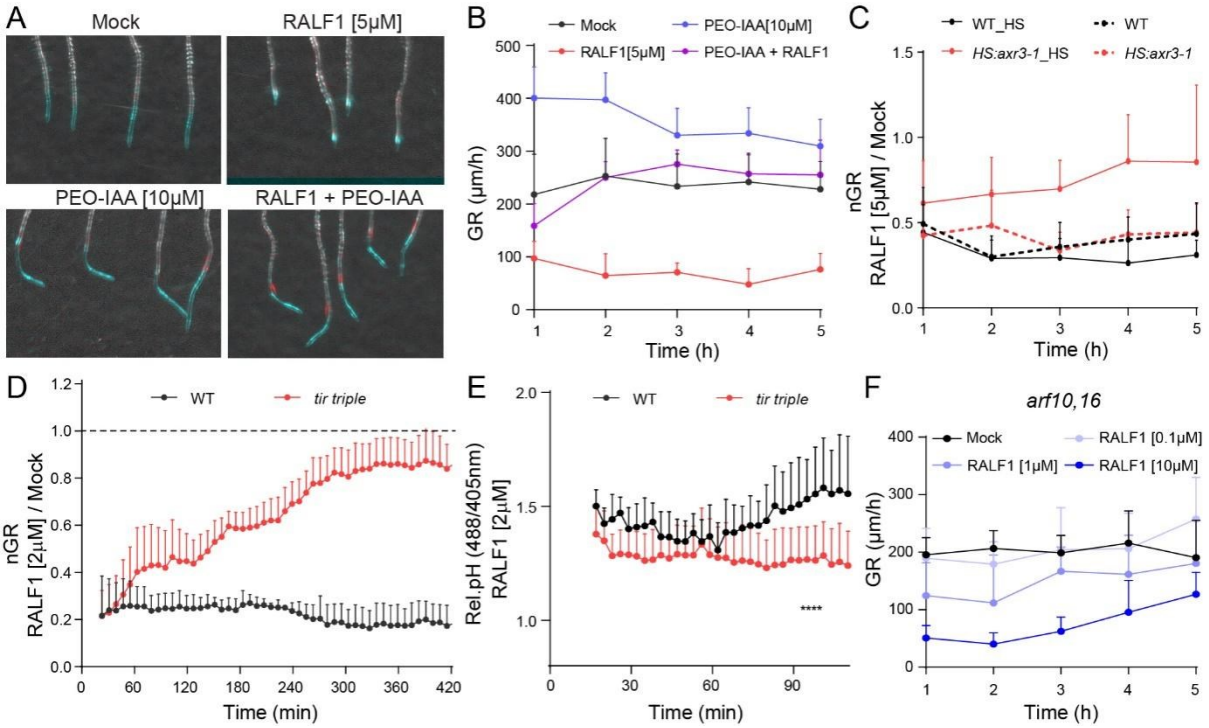


**Fig. 2. TIR1/AFB auxin signaling is downstream of RALF1-FER pathway during sustained root growth inhibition**

(*A* and *B*) Visualization (*A*) and quantification (*B*) of root growth in WT plants on vertical scanner after 5 µM RALF1 treatment with or without 10 µM PEO-IAA. Plants were pre-incubated in PEO-IAA or Mock treatment for 80 minutes. Images at 0 hours (red) and 5 hours (cyan) were merged; white pixels represent the coincided area of two time points, and cyan and red indicates the part which is absent in the other time point (*A*). n > 9, Mean+SD. $p < 0.0001$ between RALF1 and PEO-IAA+RALF1, two-way ANOVA (*B*).

(*C*) Normalized root growth rate (nGR) on vertical scanner in *HS::axr3-1* and WT. nGR is growth rate after 5 µM RALF1 normalized by that on Mock treatment corresponding to the same time points. Dotted lines are samples without heat shock induction. n > 11, Mean+SD. $p < 0.0001$ between heat-shocked *HS::axr3-1* and heat-shocked WT.

(*D* and *E*) nGR (*D*) and apoplastic pH in elongating cells (*E*) of *tir triple* and WT on a vertical microscope. Growth on 2 µM RALF1 was normalized by the growth on Mock corresponding to the same time points (*D*). n > 6, Mean+SD. $^{****}p < 0.0001$, two-way ANOVA for both graphs.

(*F*) Root growth of *arf10,16* on different concentrations of RALF1 on vertical scanner. Comparison should be made with WT response in Fig. 1 *D*. n = 5 for 10 µM RALF1 and n > 8 for other conditions, Mean+SD.

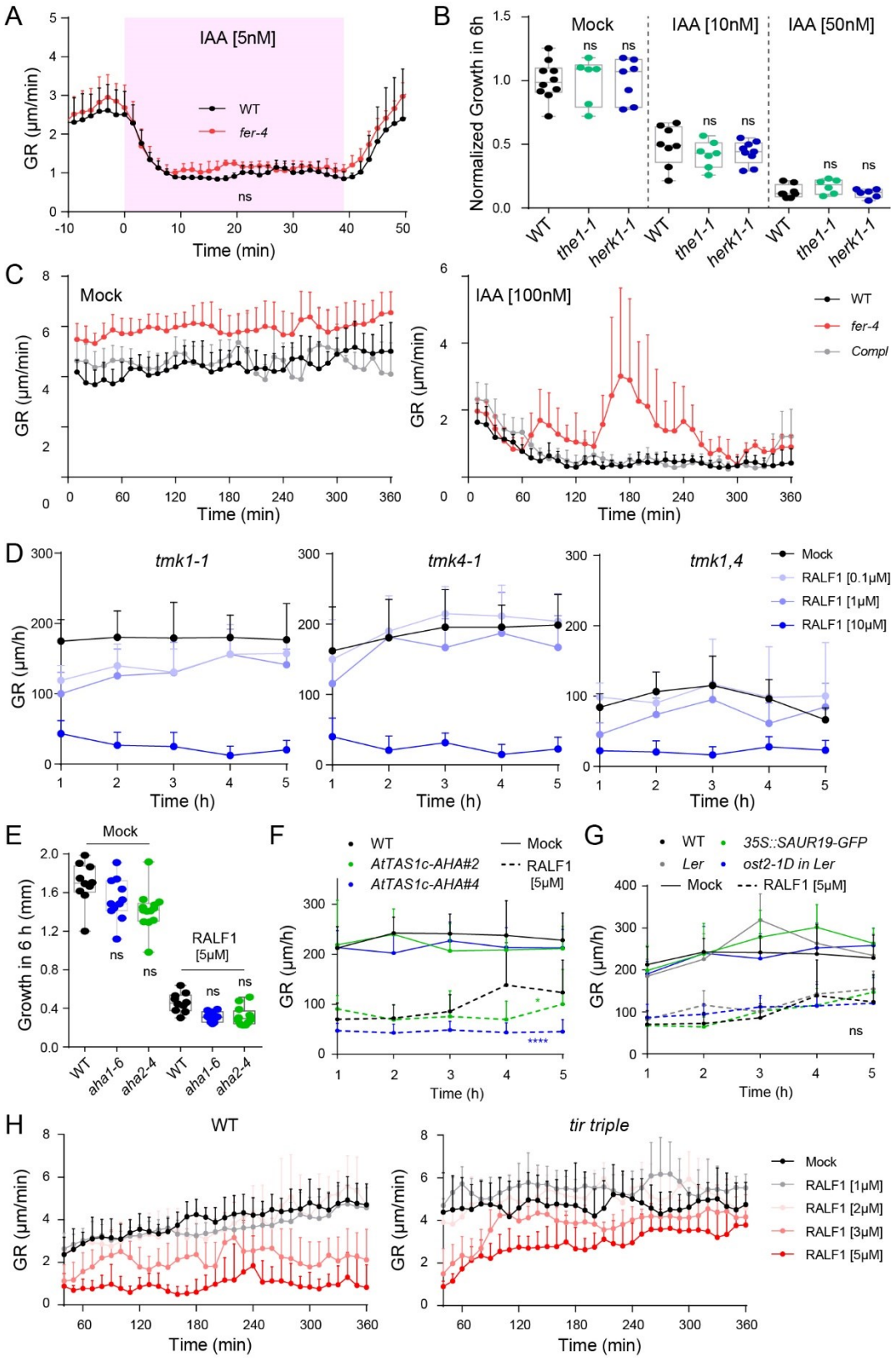


**Fig. S2. Crosstalk between auxin signaling and RALF1-FER signaling**

(*A*) Root growth of *fer-4* and WT responding to 5 nM IAA in vRootchip. Mean of 4 roots+SD. ns, p > 0.5, two-way ANOVA.

(*B*) Normalized root growth of *the1-1, herk1-1* and WT after 6-hour IAA treatments. Growth on IAA was normalized to growth on Mock of the same genotype. $n > 9$ for each condition. ns, $p > 0.5$ for the genotype variant, two-way ANOVA.

(*C*) Root growth of *fer-4*, of complementary line (*compl*) *pFER::FER-GFP in fer-4*, and of WT after Mock and 100 nM IAA treatments on vertical scanner. $n > 6$, Mean+SD. $p < 0.0001$ between *fer-4* and WT. $p < 0.001$ between *fer-4* and *compl*, two-way ANOVA.

(*D*) Root growth of *tmk1-1, tmk4-1* and the double mutant on different RALF1 concentrations. Comparison should be made with WT response in Fig. 1 *D*. $n > 3$ for *tmk1,4* and $n > 9$ for other conditions, Mean+SD.

(*E*) Root growth of *aha1-6* and *aha2-4* after Mock or 5 μM RALF1 treatment for 6 hours. Box plot bars show the min and max value. $n > 10$ for each condition. ns, $p > 0.5$ for the genotype variant, two-way ANOVA.

(*F*) Root growth of *AtTAS1c-AHA* #2 and #4 with Mock or 5 μM RALF1 treatment over time. Dotted lines represent RALF1-treated samples. $n > 10$ for each condition, Mean+SD. $^{*}p < 0.05$, $^{****}p < 0.0001$, two-way ANOVA.

(*G*) Root growth of *p35S::SAUR19-GFP* (control WT) and *ost2-1D* (control *Ler*) with Mock or 5 μM RALF1 treatment over time. Dotted lines represent RALF1-treated samples. $n > 10$ for each condition, Mean+SD. ns, $p > 0.5$ between all RALF1-treated samples, two-way ANOVA.

(*H*) Root growth of WT and *tir triple* on different RALF1 concentrations and Mock. $n > 6$ for each condition, Mean+SD.

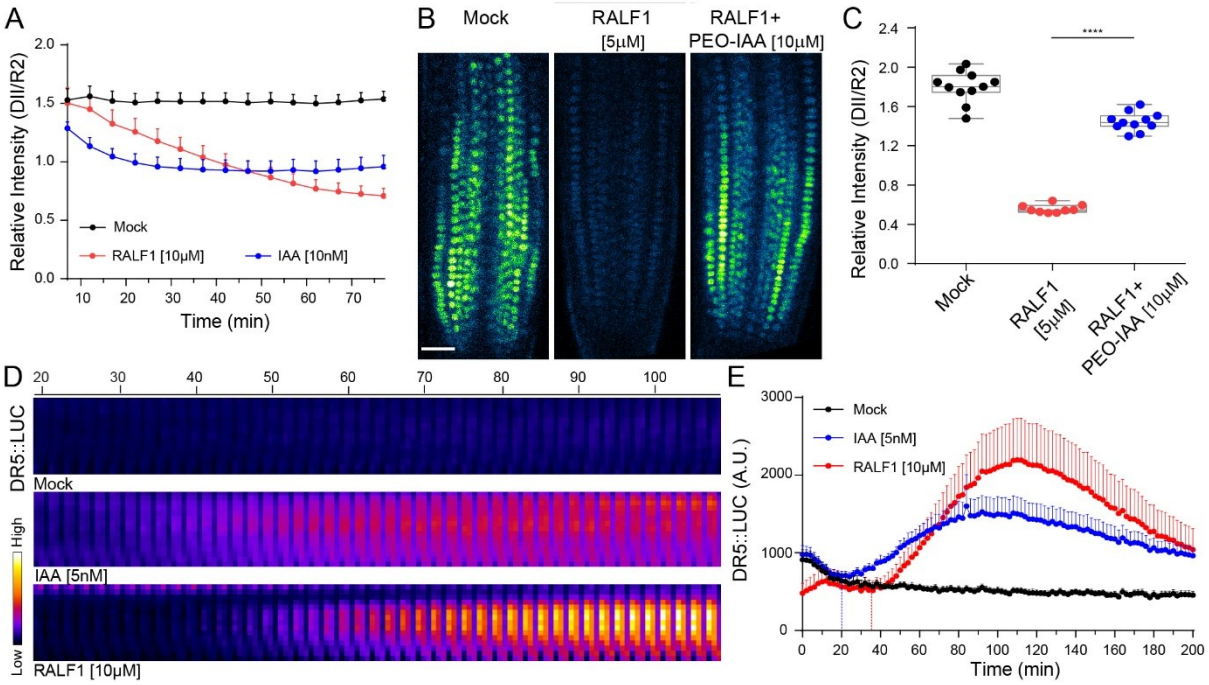


**Fig. 3. RALF1 triggers auxin signaling**

(*A*) Normalized fluorescence intensity of the AUX/IAA DII domain after treatment with 10 μM RALF1, 10 nM IAA, or Mock. n > 9, Mean+SD.

(*B* and *C*) Visualization of DII (*B*) and quantification of normalized DII intensity (*C*) after 5 μM RALF1 treatment for 160 minutes with pretreatment with 10 μM PEO-IAA or Mock for 80 minutes. Green-Fire-Blue LUT was applied. Scale bar, 30 μm (*B*). Box plot bars show the min and max value. n > 9 for each condition, $^{****}p<0.0001$, one-way ANOVA.

(*D* and *E*) Time lapse (*D*) and quantification (*E*) of DR5::LUC signal in root tip after treatment with 5 nM IAA, 10 μM RALF1 or Mock. Fire LUT was applied (*D*). Dotted lines indicate the time points at which signal intensity started to increase; n > 6 for each condition, Mean+SD (*E*).

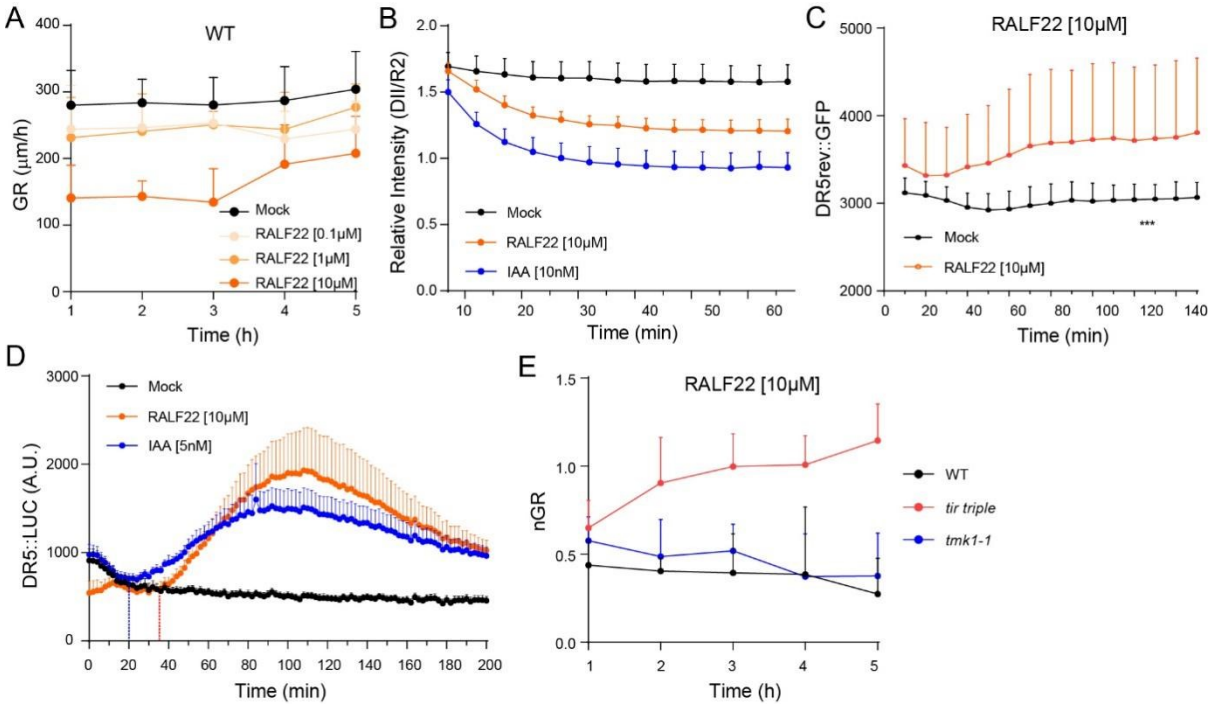


**Fig. S3. RALF22 triggers auxin signaling**

(*A*) Root growth of WT plants on different RALF22 concentrations. Root tips were captured on vertical scanner. n > 9 for each condition, Mean+SD.

(*B*) Normalized fluorescence intensity of DII after treatment with 10 µM RALF22, 10 nM IAA and Mock. n > 8 for each condition, Mean+SD.

(*C*) Fluorescence intensity of DR5rev::GFP on 10 µM RALF22 and Mock treatments. Mean of 4 roots for each condition+SD. $^{***}p<0.001$, two-way ANOVA.

(*D*) Luminescence intensity of DR5::LUC after treatment with 10 µM RALF22, 5 nM IAA and Mock. Dotted lines indicate the time points at which signal intensity started to increase. n > 6, Mean+SD.

(*E*) Normalized root growth (nGR) of *tir triple, tmk1-1,* and WT after 10 µM RALF22 treatment. nGR is growth after RALF22 normalized by that on Mock treatment at the same time point. n > 8, Mean+SD. $p < 0.0001$ between WT and *tir triple*; $p > 0.5$ between WT and *tmk1-1,* two-way ANOVA.

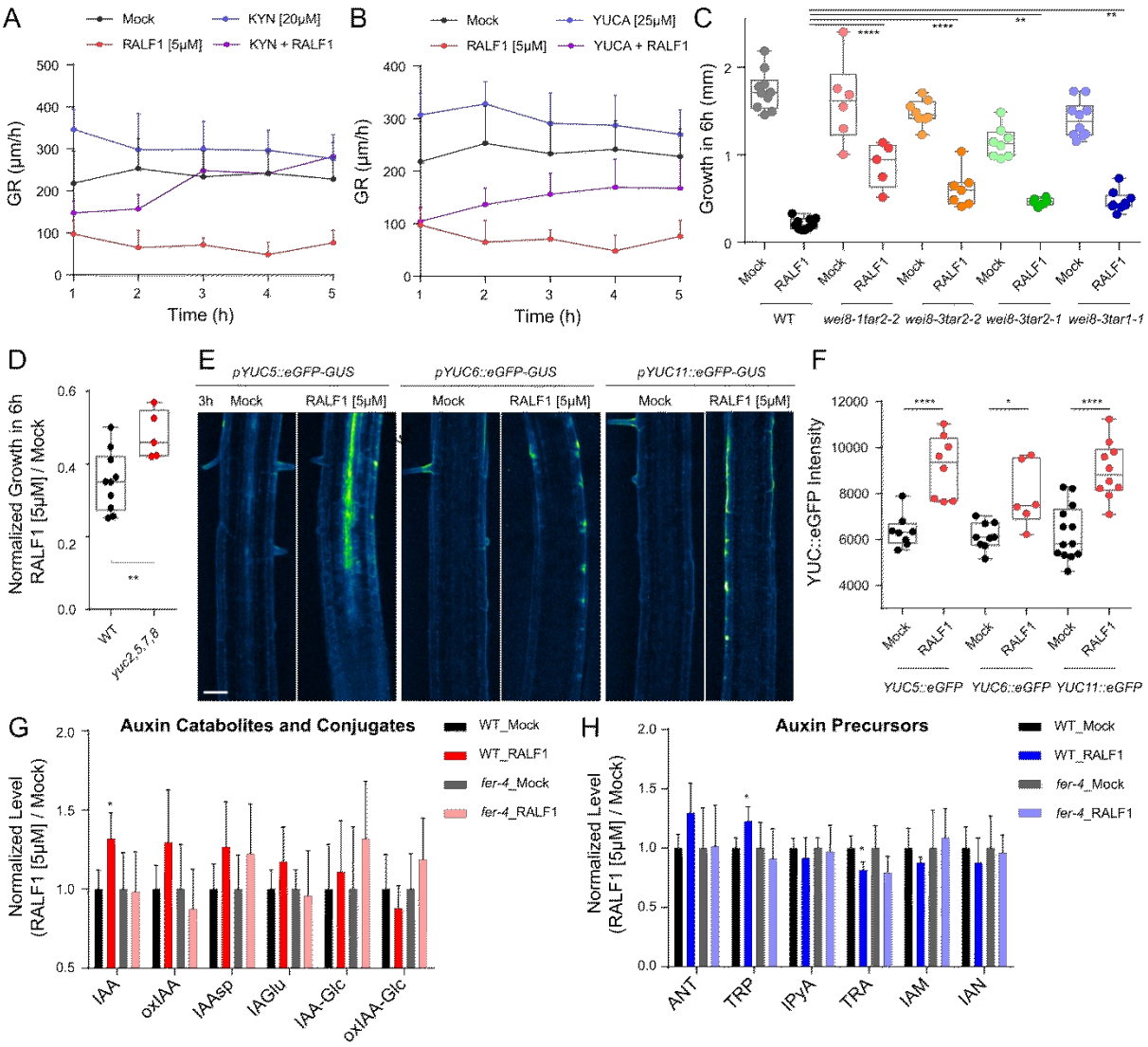


**Fig. 4. RALF1-FER axis promotes auxin biosynthesis**

(*A* and *B*) Root growth of WT after 5 μM RALF1 treatment with auxin biosynthesis inhibitors [20 μM KYN (*A*) or 25 μM YUCA (*B*)] or Mock on vertical scanner. Before RALF1 treatment, WT roots were pre-treated with inhibitors or Mock for 80 minutes. $n > 9$, Mean+SD. $p < 0.0001$ between RALF1 and RALF1+KYN, and $p < 0.001$ between RALF1 and RALF1+YUCA, two-way ANOVA.

(*C* and *D*) Root growth of auxin biosynthesis mutants *wei8-1tar2-2, wei8-3tar2-2, wei8-3tar2-1* and *wei8-3tar1-1* (*C*) and *yuc2,5,7,8* (*D*) after 5 μM RALF1 for 6 hours on vertical scanner. Box plot bars indicate the min and max value. $n > 5$. $^{****}p < 0.0001$; $^{***}p < 0.001$; $^{**}p<0.01$, one-way ANOVA.

(*E* and *F*) Visualization (*E*) and quantification (*F*) of eGFP expressed under YUC5, YUC6 and YUC11 promoters after Mock or 5 μM RALF1 treatment for 3 hours. Box plot bars indicate the min and max value. $n > 6$. $^{****}p < 0.0001$; $^{*}p < 0.05$, one-way ANOVA.

(*G* and *H*) Auxin metabolites including auxin catabolites and conjugates (*G*) as well as precursors (*H*) after Mock or 5 μM RALF1 treatment for 3 hours in WT or *fer-4* roots. Mean of 5 biological replicates with each containing 100 root tips+SD. $^{*}p<0.05$, one-way ANOVA.

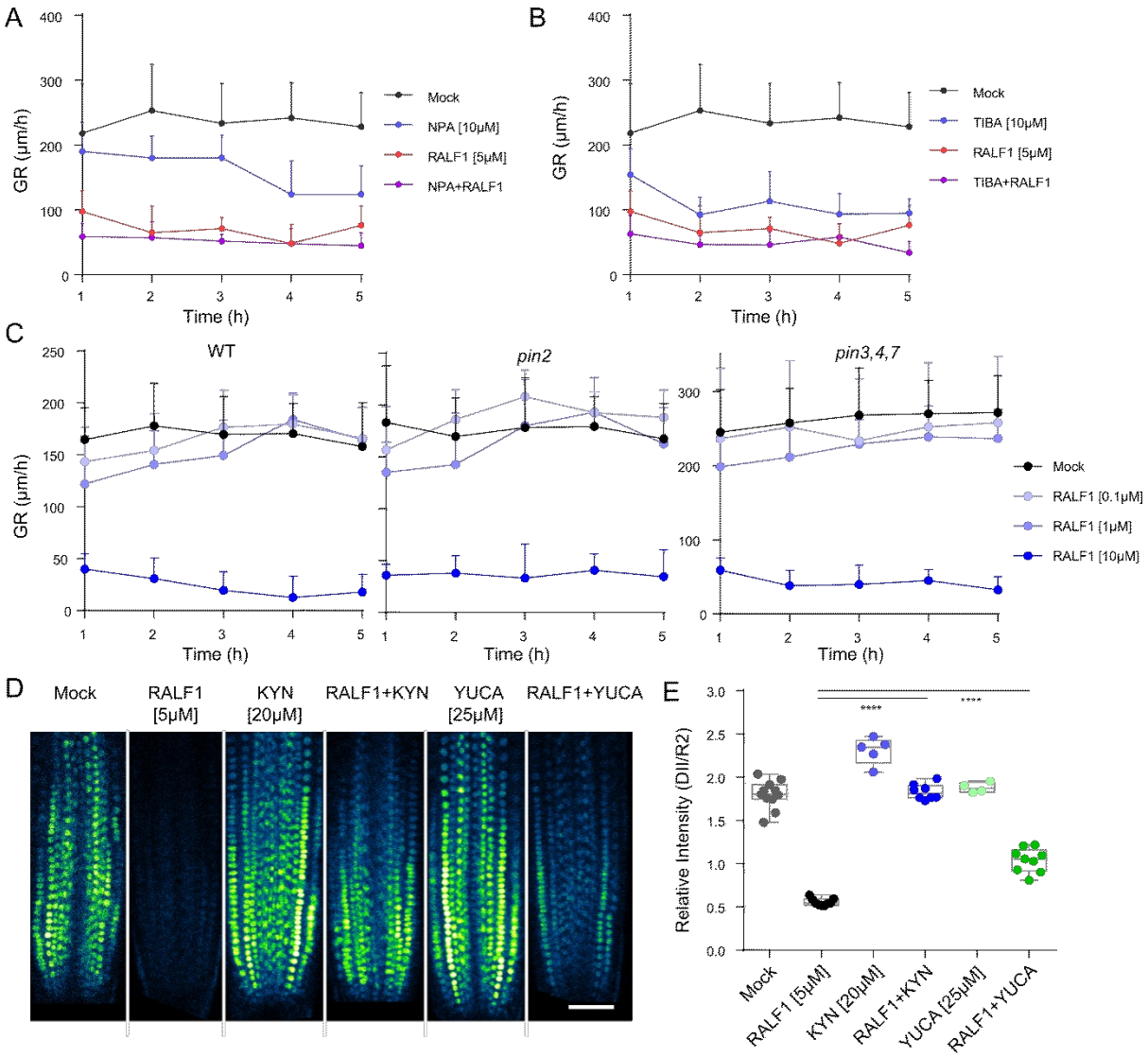


**Fig. S4. Auxin biosynthesis, but not auxin transport, plays a significant role in RALF1-induced root growth inhibition**

(*A* and *B*) Root growth of WT after 5 µM RALF1 with auxin transport inhibitors [10 µM NPA (*A*) or 10 µM TIBA (*B*)] or Mock on vertical scanner. Before RALF1 treatment, WT roots was pre-treated with inhibitors or Mock for 80 minutes. n > 8, Mean+SD. p > 0.05 between RALF1 and RALF1+NPA/TIBA, two-way ANOVA.

(*C*) Root growth of auxin transport mutants *pin2 (eir1-1)* and *pin3,4,7* on different RALF1 concentrations on vertical scanner. n > 9, Mean+SD.

(*D* and *E*) Visualization of DII (*D*) and quantification of normalized DII intensity (*E*) after 5 µM RALF1 treatment with pre-treatment by 20 µM KYN, 25 µM YUCA or Mock for 80 minutes. Green-Fire-Blue LUT was applied; scale bar, 50 µm (*D*). n > 8 for RALF1-treated samples and n > 5 for non-RALF1 samples. $^{****}p < 0.0001$, one-way ANOVA.

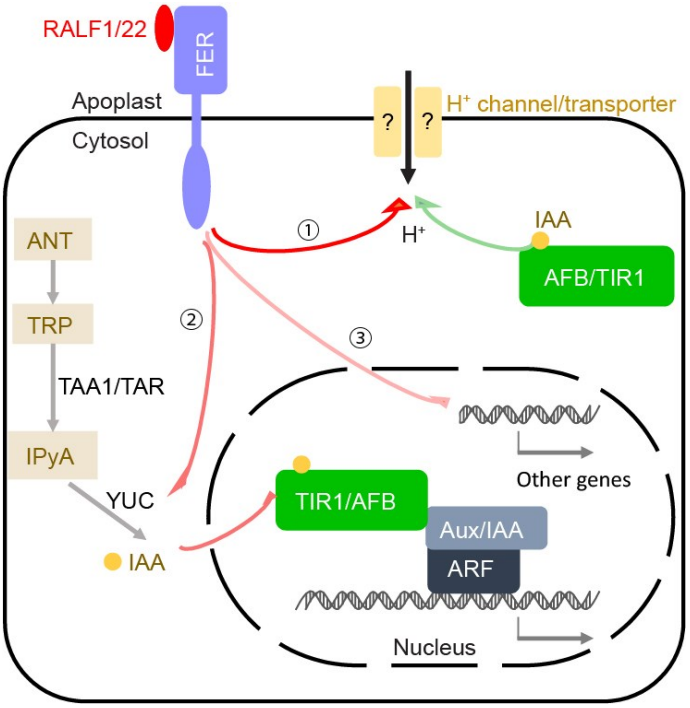


**Fig. 5. Model for RALF1-induced root growth inhibition.**

Path ①: RALF1-FER triggers a rapid $H^+$ influx across the plasma membrane (PM), independent of PM $H^+$-ATPases. The resulting apoplast alkalinization mediates a rapid and reversible root growth inhibition. This path shares high similarity with but is independent of auxin-TIR1/AFB-mediated rapid root growth inhibition. Path ②: within about 1 hour from stimulation, RALF1-FER promotes YUC expression and thus auxin biosynthesis to induce the canonical TIR1/AFB transcriptional pathway for sustained root growth inhibition. Path ③: other known transcriptional effects emanate from RALF1-FER.

## *5.8 Materials and Methods*

### Plant materials and growth conditions

All *A. thaliana* mutants and transgenic lines used are in Columbia-0 (Col-0) background. *PM-Cyto* marker line (33), *fer-4* (13), complemented line *pFER:FER-GFP* in *fer-4* (13), *the1-1* (31), *tir1-1afb2-1afb3-1* mutant (45), *HS::axr3-1* (46), *pYUC5::eGFP-GUS*, *pYUC6::eGFP-GUS*, *pYUC11::eGFP-GUS* (47), *R2DII* (39), *DR5rev::GFP* (48), *DR5::LUC* (40), *tmk1-1* (SALK_016360) (49), *tmk4-1* (GABI_348E01) (49), *tmk1-1tmk4-1* (49), *ost2-3D* (50) and *p35S::SAUR19-GFP* (37) were kindly shared by the authors. The *herk1-1* (SALK_008043), *aha2-4 (SALK_082786.46.35.x)*, and *aha1-7* (SALK_016325) were ordered from NASC. Two independent lines *AtTAS1c-AHA#2* and *#4* were generated as described previously (23).

Seeds were surface-sterilized by chlorine gas, sown on half-strength Murashige and Skoog (½ MS) medium supplemented with 1% (w/v) sucrose and 0.8% (w/v) phyto agar (pH 5.9), stratified in the dark at 4°C for 2 days and then grown vertically at 21°C with a long-day photoperiod (16 hours light/8 hours dark). Light sources used were Philips GreenPower LED production modules [in deep red (660 nm)/far-red (720 nm)/blue (455 nm) combination, Philips], with a photon density of 140.4 µmol/$m^2$/s ± 3%. 4-5 day-old seedlings were used.

**Microfluidics**

The microfluidic vRootchip was used to analyze rapid changes in root tip growth and apoplastic pH in real-time. The manufacturing of the chip, sample preparation procedure, and data analysis of root tip growth were performed as described previously (21) (23). ¼ MS + 0.1% sucrose was used as a basal medium during operation to avoid contamination. For one vRootchip, maximum 8 samples were used. When comparing two genotypes, 3-4 seedlings were used for each genotype and mounted in alternating channels to minimize the time difference between imaging the two genotypes. For each root, one ROI containing early elongating epidermal cells and the other ROI covering the root tip were imaged. As these two ROIs were captured sequentially, the apoplastic pH and the growth of the same root were imaged close to simultaneously with an in-house established vertical Zeiss LSM 800 confocal microscope (32). Note that RALF peptide in a longer time coats the channels and cannot be washed out in vRootchip, therefore, washout experiments were done by transferring RALF-incubated seedlings to fresh agar block containing basic medium.

**Tip Tracker assay**

Tip tracker assay was used as a complementary approach to perform confocal imaging for long time periods up to hours, as well as RALF washout experiments. ½ MS agar medium with indicated treatments or mock were prepared and solidified. A slice of this agar block was cut and 4-5 day-old seedlings placed on top before transferring to a Lab-Tek Chambered Coverglass. The chamber was mounted onto the vertical Zeiss LSM 800 confocal microscope (32). Imaging and analysis of root growth were done with the TipTracker scripts described previously (32).

**Vertical scanner growth assay**

As a high-throughput method of growth analysis, we used a vertical flatbed scanner (Epson perfection V370) (35) with slots for Petri dishes containing ½ MS medium with treatments as indicate. Automatic scanning at 1200 dpi every hour using the AutoIt script was described previously (51). The resulting image series were analyzed using StackReg stabilization and the Manual Tracking plugin in ImageJ.

**Imaging and measuring apoplastic pH with HPTS dye**

1 mM 8-hydroxypyrene-1,3,6-trisulfonic acid (HPTS) dye (Thermo Scientific 6358-69-6, dissolved in dd$H_2O$) was applied in Tip tracker and vRootchip assays. Imaging was performed on the vertical Zeiss LSM 800 confocal microscope (32). Fluorescent signals for protonated HPTS (excitation 405 nm, emission 514 nm, visualized in red) and deprotonated HPTS (excitation, 488 nm, emission 514 nm, visualized in green) were detected with a 20x/0.8 air objective. Image analysis was performed on a cropped region of elongating epidermis cells using a previously described ImageJ macro with batch processing modification (27). The relative pH value is calculated as the background-subtracted intensity of the deprotonated intensity divided by that of the protonated intensity to represent the relative pH. Note that the relative pH value was not transformed to the absolute pH values, which requires the generation of a calibration curve for each experiment.

**Imaging and measuring cytosolic pH with the *PM-Cyto* reporter line**

Real-time imaging of the cytosolic pH near the PM was done by using the *PM-Cyto* reporter in vRootchip on the vertical confocal microscope. Sequential illumination at 488 and 405 nm with emission 514 nm for both, corresponding to two absorption peaks of pHluorin, were taken with a 20x/0.8 air objective. For each root in vRootchip, two ROIs were tracked over time, with one containing the elongating epidermal cell for measuring cytosolic pH and one containing the root tip for measuring root growth rate. Image analysis was performed similarly to the HPTS analysis described above.

**Auxin signaling evaluation**

4 day-old seedlings of *R2DII*, *DR5rev::GFP*, or *DR5::LUC* line were used. The former two were transferred to agar blot containing treatments as indicated and immediately mounted on the vertical confocal microscope for live imaging. The *DR5::LUC* seedlings were transferred to agar blot medium containing treatments as indicated and immediately drops of 1 mM D-luciferin in ½ MS liquid medium were applied on top of roots. These samples were transferred

to a dark box (51), and luminescence was captured every two minutes using a Photometrics Evolve 512 EMCCD camera equipped with a 17 mm fixed lens/0.95 and an additional 125 mm lens. The EMCCD multiplier gain was 150 and the exposure time was 90 seconds.

**Imaging YUC reporter lines**

The reporter lines were incubated on the surface of ½ MS with 5 μM RALF1 or Mock for 3 hours. Afterward, the agar block with seedlings on top was cut and transferred to cover glass for imaging. The late elongation epidermal cells with eGFP signal were imaged at excitation 488 nm and emission 514 nm on a Zeiss LSM 800 inverted confocal microscope.

**Mass Spectrometry Analysis of Auxin Metabolites**

Concentrations of IAA and different IAA metabolites (precursors, conjugates, and catabolites) were measured using liquid chromatography-tandem mass spectrometry (Agilent Instruments) as described by (52). 4 day-old seedlings were treated with Mock or RALF1 (5 μM) for 2 hours. Afterward, 100 or 70 root tips were cut and flash-frozen in liquid nitrogen. The extraction procedure and the further analysis by using a Pegasus III gas chromatography/time-of-flight mass spectrometer (Leco) essentially follow (53). The chromatograms were processed with in-house developed scripts (54).

**Statistical analysis**

All graphs were generated using GraphPad Prism 6. For statistical analysis of vRootchip data, Two-way ANOVA was performed for the entire time of the x-axis. One-way ANOVA assays were used for others. Asterisks indicate significant differences on all graphs with ns for $p>0.05$, * for $p\leq0.05$, ** for $p\leq0.01$, *** for $p\leq0.001$ and **** for $p\leq0.0001$.

**Acknowledgments**

The authors thank Sarah M. Assmann, Kris Vissenberg, and Nadine Paris for kindly sharing homozygous seeds. This work was supported by the Austrian Science Fund (FWF) I 3630-B25 to Jiří Friml and the DOC Fellowship of the Austrian Academy of Sciences to Lanxin Li. Also authors appreciate Taif University Researchers Supporting Project number (TURSP-HC2021/02), Taif University, Taif, Saudi Arabia.

**Author Contributions**

L. L., M. F. and J. F. conceived the research. L. L. and J. F. designed the experiments and wrote the manuscript. L. L. and H. C. performed most experiments. O. N. and A. P. performed the auxin metabolites analysis. M. A. and S. A. revised the manuscript.

**Conflicts of Interest**

The authors declare no conflict of interest.

## *5.9 Reference*


1. M. Du, E. P. Spalding, W. M. Gray, Rapid auxin-mediated cell expansion. *Annu. Rev. Plant Biol.* 71:379-402 (2020).
2. M. R. Blackburn, M. Haruta, D. S. Moura, Twenty years of progress in physiological and biochemical investigation of RALF peptides. *Plant Physiol.* 182(4):1657-1666 (2020).
3. G. Arsuffi, S. A. Braybrook, Acid growth: an ongoing trip. *J. Exp. Bot.* 69(2):137-146 (2018).
4. G. Pearce, D. S. Moura, J. Stratmann, C. A. Ryan, RALF, a 5-kDa ubiquitous polypeptide in plants, arrests root growth and development. *Proc. Natl. Acad. Sci. U.S.A.* 98(22):12843-12847 (2001).
5. M. Haruta, G. Monshausen, S. Gilroy, M. R. Sussman, A cytoplasmic $Ca^{2+}$ functional assay for identifying and purifying endogenous cell signaling peptides in Arabidopsis seedlings: identification of AtRALF1 peptide. *Biochemistry* 47(24):6311-6321 (2008).
6. L. Campbell, S. R. Turner, A comprehensive analysis of RALF proteins in green plants suggests there are two distinct functional groups. *Front. Plant Sci.* 8:37 (2017).
7. J. Cao, F. Shi, Evolution of the RALF gene family in plants: gene duplication and selection patterns. *Evol. Bioinform.* 8:EBO. S9652 (2012).
8. S. Masachis*, et al.* A fungal pathogen secretes plant alkalinizing peptides to increase infection. *Nat. Microbiol.* 1(6):1-9 (2016).
9. E. Thynne*, et al.* Fungal phytopathogens encode functional homologues of plant rapid alkalinization factor (RALF) peptides. *Mol. Plant Pathol.* 18(6):811-824 (2017).
10. M. Haruta, G. Sabat, K. Stecker, B. B. Minkoff, M. R. Sussman, A peptide hormone and its receptor protein kinase regulate plant cell expansion, *Science* 343(6169):408-411 (2014).
11. A. Y. Cheung, H.-M. Wu, THESEUS 1, FERONIA and relatives: a family of cell wall-sensing receptor kinases? *Curr. Opin. Plant Biol.* 14(6):632-641 (2011).
12. P. Liu, M. Haruta, B. B. Minkoff, M. R. Sussman, Probing a plant plasma membrane receptor kinase's three-dimensional structure using mass spectrometry-based protein footprinting. *Biochemistry* 57(34):5159-5168 (2018).
13. D. Chakravorty, Y. Yu, S. M. Assmann, A kinase-dead version of FERONIA receptor-like kinase has dose-dependent impacts on rosette morphology and RALF 1-mediated stomatal movements. *FEBS Lett.* 592(20):3429-3437 (2018).

14. M. Haruta, V. Gaddameedi, H. Burch, D. Fernandez, M. R. Sussman, Comparison of the effects of a kinase-dead mutation of FERONIA on ovule fertilization and root growth of Arabidopsis. *FEBS Lett.* 592(14):2395-2402 (2018).
15. K. Dressano*, et al.* BAK1 is involved in AtRALF1-induced inhibition of root cell expansion. *PLoS Genet.* 13(10):e1007053 (2017).
16. W. F. Campos*, et al.* Arabidopsis thaliana rapid alkalinization factor 1–mediated root growth inhibition is dependent on calmodulin-like protein 38. *J. Biol. Chem.* 293(6):2159-2171 (2018).
17. C. Won*, et al.* Conversion of tryptophan to indole-3-acetic acid by TRYPTOPHAN AMINOTRANSFERASES OF ARABIDOPSIS and YUCCAs in Arabidopsis. *Proc. Natl. Acad. Sci. U.S.A.* 108(45):18518-18523 (2011).
18. K. Mashiguchi*, et al.* The main auxin biosynthesis pathway in Arabidopsis. *Proc. Natl. Acad. Sci. U.S.A.* 108(45):18512-18517 (2011).
19. J. Petrášek, J. Friml, Auxin transport routes in plant development. *Development* 136(16):2675-2688 (2009).
20. M. Lavy, M. Estelle, Mechanisms of auxin signaling. *Development* 143(18):3226-3229 (2016).
21. M. Fendrych*, et al.* Rapid and reversible root growth inhibition by TIR1 auxin signalling. *Nat. Plants* 4(7):453 (2018).
22. S. M. Dubey, N. B. Serre, D. Oulehlová, P. Vittal, M. Fendrych, No time for transcription—rapid auxin responses in plants. *Cold Spring Harb. Perspect. Biol.*:a039891 (2021).
23. L. Li*, et al.* Cell surface and intracellular auxin signalling for $H^+$-fluxes in root growth. *Research Square* DOI: 10.21203/rs.3.rs-266395/v3 (2021).
24. M. Cao*, et al.* TMK1-mediated auxin signalling regulates differential growth of the apical hook. *Nature* 568(7751):240-243 (2019).
25. Z. Yang*, et al.* TMK-based cell surface auxin signaling activates cell wall acidification in Arabidopsis. *Research Square* DOI:10.21203/rs.3.rs-203621/v1 (2021).
26. Q. Wang*, et al.* A phosphorylation-based switch controls TAA1-mediated auxin biosynthesis in plants. *Nat. Commun.* 11(1):1-10 (2020).
27. E. Barbez, K. Dünser, A. Gaidora, T. Lendl, W. Busch, Auxin steers root cell expansion via apoplastic pH regulation in Arabidopsis thaliana. *Proc. Natl. Acad. Sci. U.S.A.* 114(24):E4884-E4893 (2017).
28. Q. Dong, Z. Zhang, Y. Liu, L. Z. Tao, H. Liu, FERONIA regulates auxin-mediated lateral root development and primary root gravitropism. *FEBS Lett.* 593(1):97-106 (2019).
29. E. Li, G. Wang, Y. L. Zhang, Z. Kong, S. Li, FERONIA mediates root nutating growth. *Plant J.* 104(4):1105-1116 (2020).
30. M. Yu*, et al.* The RALF1-FERONIA interaction modulates endocytosis to mediate control of root growth in Arabidopsis. *Development* 147(13) (2020).
31. M. Gonneau*, et al.* Receptor kinase THESEUS1 is a rapid alkalinization factor 34 receptor in Arabidopsis. *Curr. Biol.* 28(15):2452-2458. e2454 (2018).
32. D. Von Wangenheim*, et al.* Live tracking of moving samples in confocal microscopy for vertically grown roots. *Elife* 6:e26792 (2017).

33. A. Martinière, *et al.* Uncovering pH at both sides of the root plasma membrane interface using noninvasive imaging. *Proc. Natl. Acad. Sci. U.S.A.* 115(25):6488-6493 (2018).
34. S. K. Gjetting, *et al.* Evidence for multiple receptors mediating RALF-triggered $Ca^{2+}$ signaling and proton pump inhibition. *Plant J.* 104(2):433-446 (2020).
35. Y. Zhang, L. Li, and J. Friml, "Evaluation of Gravitropism in Non-Seed Plants" in Plant Gravitropism: Methods and Protocols, E. B. Blancaflor (Springer, 2021).
36. A. Carbonell, *et al.* New generation of artificial microRNA and synthetic trans-acting small interfering RNA vectors for efficient gene silencing in Arabidopsis. *Plant Physiol.* 165(1):15-29 (2014).
37. A. K. Spartz, *et al.* SAUR inhibition of PP2C-D phosphatases activates plasma membrane $H^+$-ATPases to promote cell expansion in Arabidopsis. *Plant Cell* 26(5):2129-2142 (2014).
38. K.-i. Hayashi, *et al.* Rational design of an auxin antagonist of the $SCF^{TIR1}$ auxin receptor complex. *ACS Chem. Biol.* 7(3):590-598 (2012).
39. C.-Y. Liao, *et al.* Reporters for sensitive and quantitative measurement of auxin response. *Nat. Methods* 12(3):207-210 (2015).
40. M. A. Moreno-Risueno, *et al.* Oscillating gene expression determines competence for periodic Arabidopsis root branching. *Science* 329(5997):1306-1311 (2010).
41. L. Abas, *et al.* Naphthylphthalamic acid associates with and inhibits PIN auxin transporters. *Proc. Natl. Acad. Sci. U.S.A.* 118(1) (2021).
42. Y. Zhang, L. Rodriguez, L. Li, X. Zhang, J. Friml, Functional innovations of PIN auxin transporters mark crucial evolutionary transitions during rise of flowering plants. *Sci. Adv.* 6(50):eabc8895 (2020).
43. W. He, *et al.* A small-molecule screen identifies L-kynurenine as a competitive inhibitor of TAA1/TAR activity in ethylene-directed auxin biosynthesis and root growth in Arabidopsis. *Plant Cell* 23(11):3944-3960 (2011).
44. T. Nishimura, *et al.* Yucasin is a potent inhibitor of YUCCA, a key enzyme in auxin biosynthesis. *Plant J.* 77(3):352-366 (2014).
45. N. Dharmasiri, *et al.* Plant development is regulated by a family of auxin receptor F box proteins. *Dev. Cell* 9(1):109-119 (2005).
46. K. Knox, C. S. Grierson, O. Leyser, AXR3 and SHY2 interact to regulate root hair development. *Development* 130(23):5769-5777 (2003).
47. H. S. Robert, *et al.* Local auxin sources orient the apical-basal axis in Arabidopsis embryos. *Curr. Biol.* 23(24):2506-2512 (2013).
48. J. Friml, *et al.* Efflux-dependent auxin gradients establish the apical–basal axis of Arabidopsis. *Nature* 426(6963):147-153 (2003).
49. R. Huang, *et al.* Noncanonical auxin signaling regulates cell division pattern during lateral root development. *Proc. Natl. Acad. Sci. U.S.A.* 116(42):21285-21290 (2019).
50. S. Yamauchi, *et al.* The plasma membrane $H^+$-ATPase AHA1 plays a major role in stomatal opening in response to blue light. *Plant Physiol.* 171(4):2731-2743 (2016).
51. L. Li, S. G. Krens, M. Fendrych, J. Friml, Real-time analysis of auxin response, cell wall pH and elongation in Arabidopsis thaliana Hypocotyls. *Bio Protoc.* 8(1) (2018).

52. O. Novák, *et al.* Tissue-specific profiling of the Arabidopsis thaliana auxin metabolome. *Plant J.* 72(3):523-536 (2012).

53. J. Gullberg, P. Jonsson, A. Nordström, M. Sjöström, T. Moritz, Design of experiments: an efficient strategy to identify factors influencing extraction and derivatization of Arabidopsis thaliana samples in metabolomic studies with gas chromatography/mass spectrometry. *Anal. Biochem.* 331(2):283-295 (2004).

54. P. Jonsson, *et al.* High-throughput data analysis for detecting and identifying differences between samples in GC/MS-based metabolomic analyses. *Anal. Chem.* 77(17):5635-5642 (2005).

# Chapter 6

## The role of Aux/IAA during auxin-induced rapid root growth inhibition

Lanxin Li, Behrokh Shojaie and Jiri Friml*

Institute of Science and Technology (IST) Austria – 3400 Klosterneuburg (Austria).

## 6.1 *Introduction*

Auxin receptors TIR1/AFB perceive auxin together with the co-receptor Aux/IAA, which releases the repression of Aux/IAA on the transcriptional factor Auxin Response Factor (ARF) and regulates gene transcription in canonical auxin signaling [1]. Besides, a non-canonical branch of TIR1/AFB was recently found to regulate auxin-induced rapid apoplast alkalinization and root growth inhibition [2, 3]. Therefore, whether Aux/IAA itself, its ubiquitination and degradation are involved in auxin-triggered apoplast alkalinization and root growth inhibition, are still unrevealed. Here, we examined the questions by analyzing apoplast pH and root growth using transgenic mutants and pharmaceutical tools.

## 6.2 *Aux/IAA are involved in auxin-induced rapid root growth inhibition*

To examine if Aux/IAA are involved in auxin-induced alkalinization and root growth inhibition, we analyzed IAA14 and IAA17 using the *HS::axr3-1* transgenic line [4] and various *HS::IAA14-VENUS* lines [5] that are inducibly expressing mutated version of IAA17 or IAA14, respectively, of different stabilities in response to auxin.

Regarding to IAA14, we first analyzed its steady state growth over 3 hours with or without heat shock induction at 37 °C for 40 minutes. The induced *HS::axr3-1* line showed a significant resistance to growth inhibition after 5 nM IAA treatment for 3 hours. Moreover, we examined their rapid auxin responses in apoplastic pH and root growth using vRootchip. *HS::axr3-1* was partially resistant to both apoplast alkalinization and growth inhibition after treatment of 5 nM IAA. These suggest that IAA17 plays a partial role during auxin-triggered rapid apoplast alkalinization and root growth inhibition.

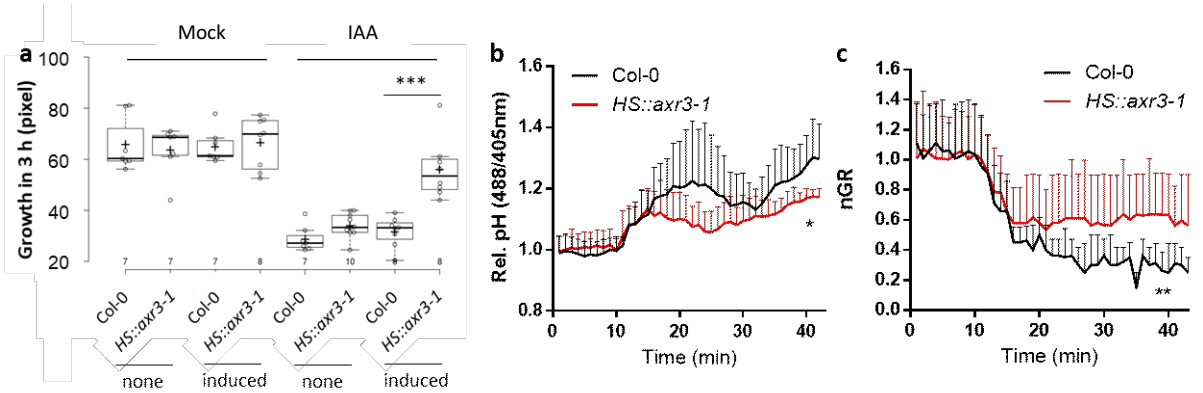


**Figure 1.** IAA17 is involved in auxin-induced rapid apoplast alkalinization and root growth inhibition.

**a,** Root growth amount in *HS::axr3-1* and Col-0 with or without heat shock induction after treatment of 5 nM IAA for 3 hours. Heat-shock induced *HS::axr3-1* line was more resistant to growth inhibition after treatment of 5 nM IAA for 3 hours. ***p<0.001, one way ANOVA.
**b-c,** Relative apoplastic pH (Rel. pH) and normalized root growth rate (nGR) in *HS::axr3-1* and Col-0 roots in vRootchip. Both Rel. pH and nGR are normalized to their average value before auxin treatment at 10 minutes. The heat shock was performed on both genotypes at 37°C for 40 minutes and the imaging starts 2 hours after induction. *p<0.05, **p<0.01, two way ANOVA.

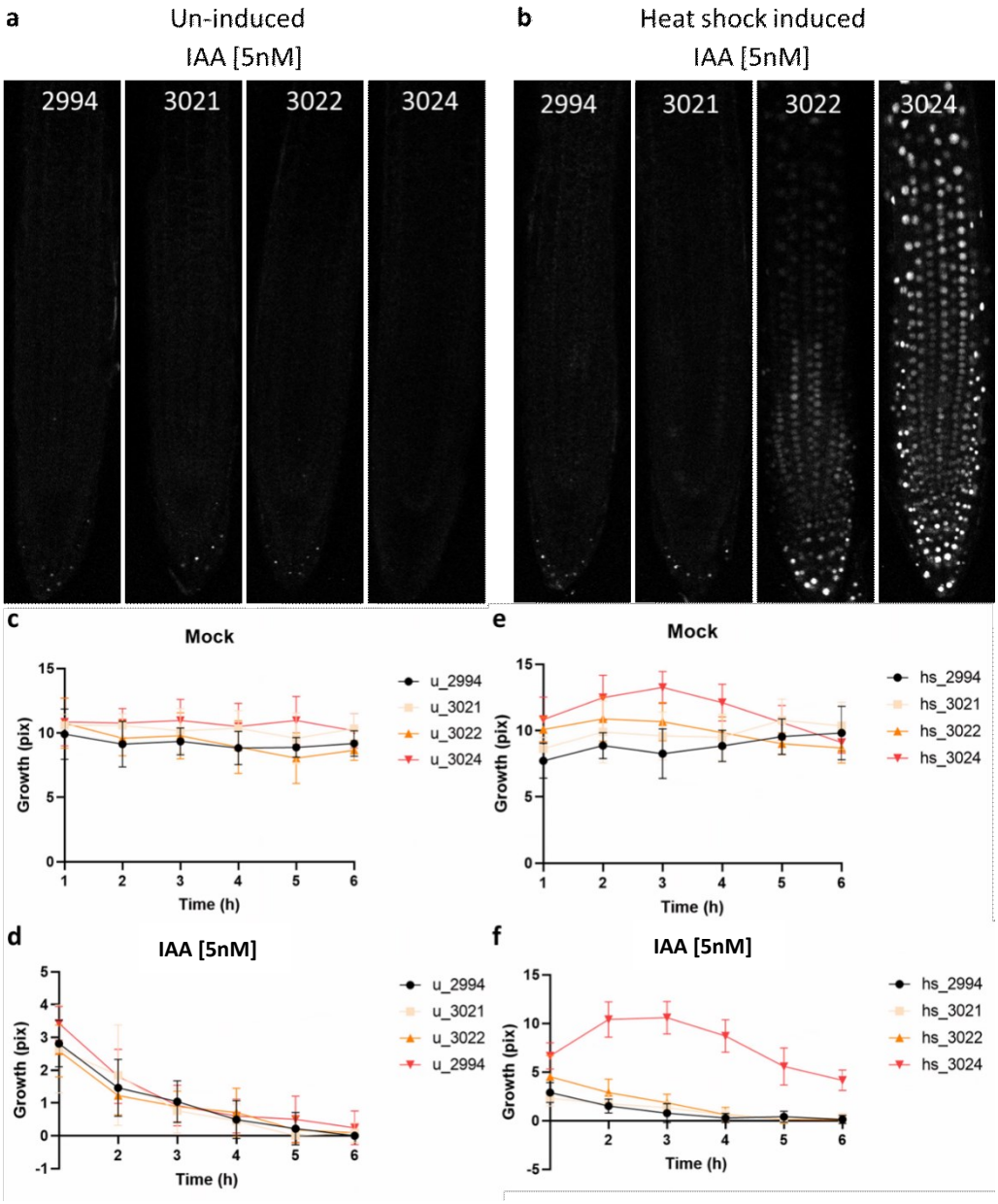


**Figure 2.** IAA14 is involved in auxin-induced root growth inhibition.

**a-b,** Fluorescence intensity of IAA14-VENUS after treatment of 5 nM IAA for 1 hour without (**a**) or with (**b**) heat shock induction. Lines 2994, 3021, 3022 and 3024 are expressing IAA14 with mutation on 3Ala for fast degradation, G79E for medium degradation, P81A for slow degradation and P81S for insensitive degradation in response to auxin, respectively.
**c-f,** Root growth rate in the un-induced (**c-d**) and induced (**e-f**) transgenic lines expressing variant IAA14 after treatment of mock (**c, e**) or 5 nM IAA (**d, f**). Without heat shock induction, all *HS::IAA14-VENUS* lines grew and responded similarly to auxin (**c, d**). After heat shock, 3024 line expressing insensitive IAA14 were partially resistant to auxin-induced growth inhibition (**f**). Heat shock was performed at 37°C for 2 hours and experiments started 1 hour after induction.

Regarding to IAA14, we tested their degradation and the resulting growth response in the steady state. The heat shocked induced line 3024 (expressing IAA14 with P81S mutation) was insensitive to auxin-induced degradation of IAA14-VENUS (Figure 2a-b). Accordingly, it was partially resistant to auxin-induced root growth inhibition and the resistance became stronger after 1 hour. These suggest that the role of IAA14 becomes important in the later phase of auxin-triggered root growth inhibition.

## *6.3 Degradation of Aux/IAA is not required for auxin-induced rapid root growth inhibition*

To study if the degradation of Aux/IAA is required for auxin-induced rapid root growth inhibition, we prevented Aux/IAA degradation by applying a 26S proteasome reversible inhibitor, Bortezomib (BZM) [6] and test if it affects the auxin-induced growth response. After pre-incubation of 10 μM BZM for 80 minutes (Figure 3a-b), DII intensity was enhanced. Importantly, pretreatment of BZM completely blocked IAA (10 nM for 30 minutes) induced DII degradation (Figure 3a-b). Besides, to examine if BZM treatment can sufficiently inhibit the expression of auxin-responsive genes, we comparing DR5::LUC intensity in roots with or without BZM treatment. 10 μM BZM application significantly inhibited auxin-induced gene transcription. Finally, we examined rapid root growth response to 5 nM IAA after pretreatment of 10 μM BZM for 80 minutes in vRootchip. Despite that the application of BZM and Mock caused a sudden, transient movement in the root tip (due to DMSO), auxin inhibited root

growth in the BZM pre-treated roots like in Mock-treated ones. This indicates that Aux/IAA degradation is not required for auxin-induced rapid root growth inhibition.

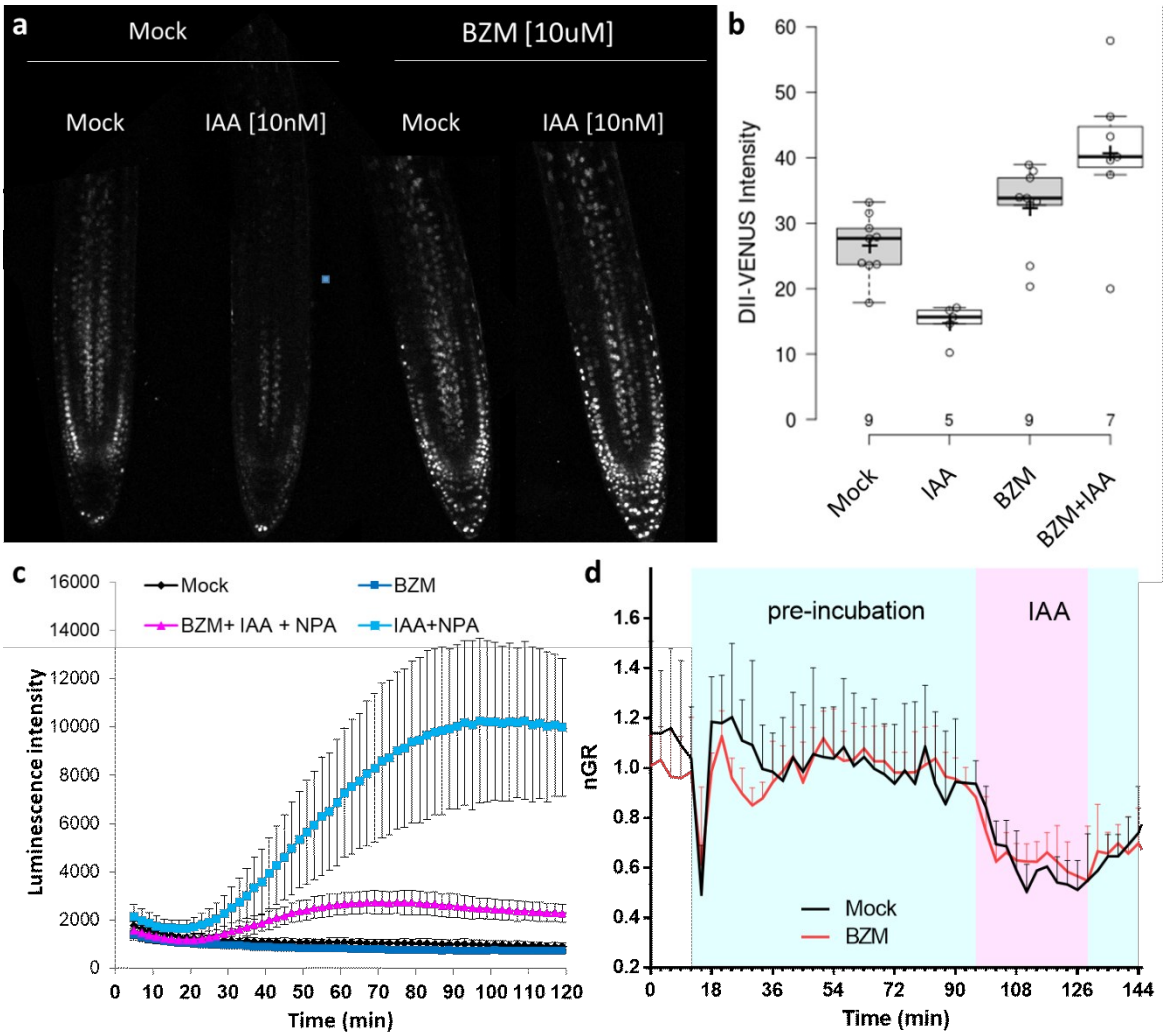


**Figure 3.** Degradation of Aux/IAA is not required for auxin-induced rapid root growth inhibition.

**a-b,** visualization (**a**) and quantification (**b**) of DII intensity after 10 nM IAA for 30 minutes following a pretreatment of mock or 10 µM BZM for 80 minutes. BZM pre-treatment blocked IAA-induced DII degradation. Box plot shows the minimum, maximum and mean value.

**c,** quantification of DR5::LUC intensity. Seedlings were pre-treated with 10 µM BZM or mock for 15 minutes, transferred to treatments of mock, 100 nM IAA+ 5 µM NPA, IAA+NPA+BZM or 10 µM BZM alone, followed by the application of substrate D-luciferin. NPA was used to enhance IAA effect. The luminescence intensity was quantified in ImageJ on a manual cropped region of root tips. Mean±SD.

**d,** Normalized root growth rate (nGR) of Col-0 in vRootchip. nGR was normalized to the average value between 0 to 96 minutes. Roots were pre-treated with 10 µM BZM (indicated in red line) or mock (indicated in black line) for 84 minutes (shaded in cyan), then treated with 5 nM IAA+ BZM or IAA (shaded in pink) for 33 minutes, followed by washout with BZM or mock (shaded in cyan), respectively. BZM treated roots still showed normal growth inhibition after auxin. Mean+SD.

## *6.4 The role of Aux/IAA ubiquitination during auxin-induced rapid root growth inhibition*

To study if Aux/IAA ubiquitination is required for auxin-induced rapid root growth inhibition, we applied a cereblon E3 ligase modulator Avadomide (AVA) [7] and examined the DII intensity and root growth response after 5 nM IAA. Auxin still inhibited root growth normally despite of 100 µM AVA pre-treatment for 90 minutes, however, the DII degradation was only partially inhibited by AVA. Therefore, we cannot exclude the possibility that the hampered Aux/IAA ubiquitination still allow the auxin-induced root growth inhibition.

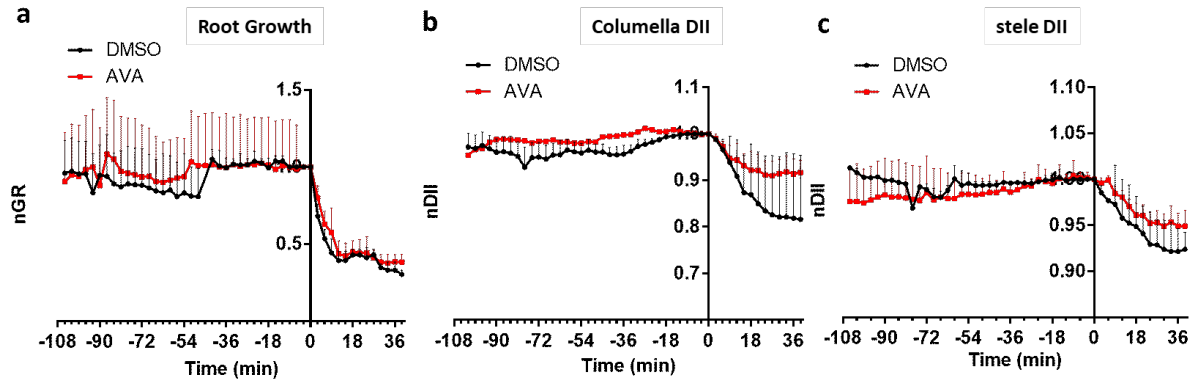


**Figure 4.** Analysis on the role of Aux/IAA ubiquitination by pre-treatment of Avadomide in vRootchip.

**a-c,** quantification of root growth rate (**a**) and DII intensity in columella (**b**) and stele (**c**) of the same roots in vRootchip. Normalized growth rate (nGR) and normalized DII (nDII) are normalized to the value at time 0. Red line indicates 100 µM AVA pretreatment for 90 minutes, and black represents mock pretreatment. Time point 0 started 5 nM IAA treatment. Mean+SD.

## 6.5 Conclusions

TIR1/AFB non-transcriptionally regulate auxin-induced rapid apoplast alkalinization and root growth inhibition [2, 3], however, the molecular mechanism is still largely unknown. Here, we analyzed transgenic lines inducibly expressing dominant negative mutated Aux/IAA and found these lines partially resistant to auxin-induced rapid apoplast alkalinization and root growth inhibition or long-term growth inhibition. Furthermore, completely blocking auxin-induced DII degradation using BZM treatment did not affect auxin-induced rapid root growth inhibition. These indicate that Aux/IAA may partially contribute to auxin-induced rapid responses regardless of its degradation upon auxin.

## 6.6 References


1. Lavy, M. & Estelle, M. Mechanisms of auxin signaling. *Development* **143**, 3226-3229 (2016).
2. Fendrych, M. *et al.* Rapid and reversible root growth inhibition by TIR1 auxin signaling. *Nat. Plants* **4**, 453 (2018).
3. Li, L. *et al.* Cell surface and intracellular auxin signalling for $H^+$-fluxes in root growth. *Research Square* DOI: 10.21203/rs.3.rs-266395/v3 (2021).
4. Knox, K., Grierson, C. S. & Leyser, O. AXR3 and SHY2 interact to regulate root hair development. *Development* **130**, 5769-5777 (2003).
5. Guseman, J. M. *et al.* Auxin-induced degradation dynamics set the pace for lateral root development. *Development* **142**, 905-909 (2015).
6. Chen, D., Frezza, M., Schmitt, S., Kanwar, J. & P Dou, Q. Bortezomib as the first proteasome inhibitor anticancer drug: current status and future perspectives. *Curr. Cancer Drug targets* **11**, 239-253 (2011).
7. Ito, T. & Handa, H. Cereblon and its downstream substrates as molecular targets of immunomodulatory drugs. *Int. J. Hemato.* **104**, 293-299 (2016).